Preparation and Applications of Catalytic Magnetic Nanoparticles

by

Huan Zhang

B.S. Chem. Eng., Tsinghua University, Beijing, China (2000)

M.S. Chem. Eng., Tsinghua University, Beijing, China (2002)

M.S.C.E.P. Chem. Eng., Massachusetts Institute of Technology, Cambridge, MA (2005)

Submitted to the Department of Chemical Engineering in partial fulfillment of the requirements for the degree of

Doctor of Philosophy in Chemical Engineering

at the
Massachusetts Institute of Technology
September, 2008

Signature of Author.....
Department of Chemical Engineering
September 22, 2008

Certified by.....
T. Alan Hatton
Ralph Landau Professor of Chemical Engineering Practice
Thesis Supervisor

Certified by.....
Kenneth A. Smith
Gilliland Professor of Chemical Engineering
Thesis Supervisor

Accepted by.....
William M. Deen
Professor of Chemical Engineering
Chairman, Committee for Graduate Students

Preparation and Applications of Catalytic Magnetic Nanoparticles

by

Huan Zhang

Submitted to the Department of Chemical Engineering in September, 2008,
in partial fulfillment of the requirements for the degree of
Doctor of Philosophy in Chemical Engineering

Abstract

It is critical to decontaminate organophosphate compounds in large scale economically, including OP pesticides in groundwater system and chemical nerve agents on the battle field. Homogeneous or micellar decomposition systems with various nucleophiles improve reaction rates significantly without affording the recovery and reuse of the nucleophiles. This research focuses on developing functional magnetic particles to carry strong α–nucleophilic groups, which are able to catalyze the decomposition reaction and can be recycled and reused.

The amidoxime modified magnetic particles were prepared first. The original particles were synthesized with the two-step procedure to obtain average particle size of around 80nm for effective capture by high gradient magnetic separation (HGMS). The precursor molecule cyanoacetohydrazide reacted with the free carboxyl groups on the particle surfaces and subsequently the nitrile groups were transformed into amidoxime groups. The modified particles were of similar average hydrodynamic diameter as the original ones and colloidally stable over a wide range of solutin pH. The amidoxime-modified particles accelerated the hydrolysis reaction of *p*-nitrophenyl acetate (PNPA). They were easily recycled by HGMS without loss of reactivity. Higher reactivity of the particle system than homogenous amidoxime systems was attributed to the increased concentration of the substrate on the particle surface due to the presence of hydrophobic centers using pseudo-phase exchange model.

Stronger nucleophilic groups, hydroxamic acid, were then attached on the particle surfaces. Original particles were prepared with unsaturated carboxylic acid as the second coating in the two-step procedure. The acrylamide monomers were copolymerized with the second coating and the attached amide groups were converted into the hydroxamic acid groups. The reaction was very efficient. Crosslinking increased the particle size to 200nm and therefore the particles were effectively captured by HGMS. The modified particles significantly accelerated the hydrolysis reaction of PNPA. They were five times more reactive than the amidoxime modified particles based on the same weight of materials. The acetylated particles were only partially regenerated due to the Lossen rearrangement of the acetylated hydroxamic acid groups.

During the hydrolysis of OP substrates, including diisopropyl fluorophosphate, methyl-paraoxon and ethyl-paraoxon, the added α-nucleophiles, 2-PAM and acetohydroxamic acid, only attacked the phosphorus atom to substitute the *p*-nitrophenol groups in methyl- and ethyl- paraoxon and the fluoride ions in DFP through second order nucleophilic substitution. Reactions between all three substrates and both nucleophiles yielded the same hydrolysis products as the spontaneous hydrolysis with no detected intermediates, indicating the unstable nature of any intermediates that may be formed. The hydroxamic acid modified particles accelerated the hydrolysis of methyl- and ethyl- paraoxon with relatively modest reactivity. Similar to polyhydroxamic acid, the reactivity was much lower than that of monomeric hydroxamic acid due to the steric hindrance from the polymer chains. The particles lost their reactivity after the reaction due to Lossen rearrangement of the phosphoryl hydroxamic acid.

Thesis Supervisor: T. Alan Hatton
Title: Ralph Landau Professor of Chemical Engineering Practice

Thesis Supervisor: Kenneth A. Smith
Title: Gilliland Professor of Chemical Engineering

Acknowledgements

It's been a long and difficult journey to complete the Ph.D. program. A lot of people have been very generous and supportive along the way. First and foremost, I would like to thank my advisors, Professors T. Alan Hatton and Kenneth A. Smith. The guidance, support, and interest throughout the project were critical to the final success. You have taught me all about scientific research and made me a much better researcher. Equally important is the freedom you gave to me during the process, which allowed me to explore interesting ideas. Except for knowledge and research ability I have learned in the lab, the whole process has been full of fun memories with the group activities and interesting comments during the group meetings. I would also like to thank my thesis committee members, Professors Robert Cohen and Daniel Blankschtein for their help and continuous support in and out of committee meetings.

I also want to thank the many people who have helped me so much through the years with my research. Tiangang Shang was the first person I have worked with closely in this lab on the first project. He had taught me a lot about chemical synthesis and the general lab procedures. Dr. Lev Bromberg was extremely helpful along the way. He started the general direction of this project, provided me many ideas and helped me a lot with some of experimental details. Ms. Elizabeth Finn helped a lot with some of the experiments during her UROP time in the lab. I want to thank Andre Ditsch for showing me the particle synthesis and more importantly for sharing with me his experience in the lab as well as career advices. It was a lot of fun to sit in the office with Smeet for five years and have a variety of conversations about life, research, and career. I want to thank all other people in the Hatton lab for showing me around, helping me with various instruments, and constructing such a supportive and fun environment. Beth Tuths was very helpful with respect to everything, from providing office supplies to ordering water, from taking care of the bills to bringing us mails. I also want to thank Claude Lupis and his wife for all the support and help to my family during the practice school and made that such an interesting and fruitful experience.

I wish to express my special thanks to my friends, Minggang She, Wei Chai, Wenchao Sheng, Yunpeng Yin, Hong He, Yu Pu, and many others for being with me together all these years. Thank you for all the encouragement, support, and fun.

Most importantly, I owe all this to my parents Tingxiang Zhang and Zhiying Wang for their love, guidance, and freedom they gave me throughout my life. I want to thank my three brothers back in China for taking care of the family. Lastly, I want to thank my wife, Tao Ni. You are always with me for all the ups and downs. I love you.

Table of Contents

List of Figures

List of Tables

Chapter 1

Introduction

Organophosphate compounds (OP) represent a major class of pesticides and are used widely as chemical warfare nerve agents. [1] OP pesticides are typically sprayed onto the target fields as small droplets and can contaminate ground water systems through air drift of the droplets, surface runoff, and leaching from the field. [2, 3] OP compounds inhibit acetocholinesterase (AChE), an essential enzyme for the breakdown of acetocholine needed to maintain normal function of the nervous system. Some OP compounds are fairly persistent in the natural environment, posing a cumulative threat to human and wild animals if consumed without proper treatment. For example, the typical half-life for the degradation of fenitrothion was found to be approximately 50 days at environmental pH 5-8, showing that fenitrothion has the capacity for environmental persistence. [4] Furthermore, threat from chemical weapons has increased significantly from both local application and wide dispersal toward military and civilian targets. [5] Therefore, an economical strategy is necessary to cope with this contamination challenge from both OP pesticides as well as chemical agents.

1.1 Organophosphate Compounds

Organophosphate (OP) is the general name for esters of phosphoric acid, including a diverse family of organic compounds. Apart being present in all biological systems in the form of DNA, RNA, and some cofactors, organophosphates are widely used as pesticides and nerve gases as chemical warfare agents. [1]

1.1.1 Organophosphate Usage

The typical chemical structure is shown in Scheme 1-1. They are esters, amides, or thiol derivatives of phosphoric, phosphonic, phosphorothioic, or phosphonothioic acids depending on the substituent groups on the phosphorus center. [1]

Scheme 1-1. General chemical structures of organophosphate compounds.

Pesticides are widely used in agriculture, medicine, industry, and the household to control insects in all developmental forms. In 2001, the overall pesticide market worldwide was $32 billion and the US market accounted for 34% of the world market. Insecticide sale was $3.1 billion in 2001, representing 25% of all US pesticide sales. Organophosphates represented 70% of the 100 million pounds of insecticides applied in various fields. [6]

Another major group of organophosphate compounds are chemical warfare agents, more specifically nerve agents. [7] As the most toxic of the known chemical agents, they can cause death in minutes after exposure. Nerve agents are considered major military threat agents. There are two major classes of nerve agents, the G-series, including tabun (GA), sarin (GB), soman (GD), and cyclosarin (GF), etc., and the V-series, with VX representing. The V-series agents are ten times more toxic than the G-series agents. The chemical structures of the above chemical agents are listed in Scheme 1-2.

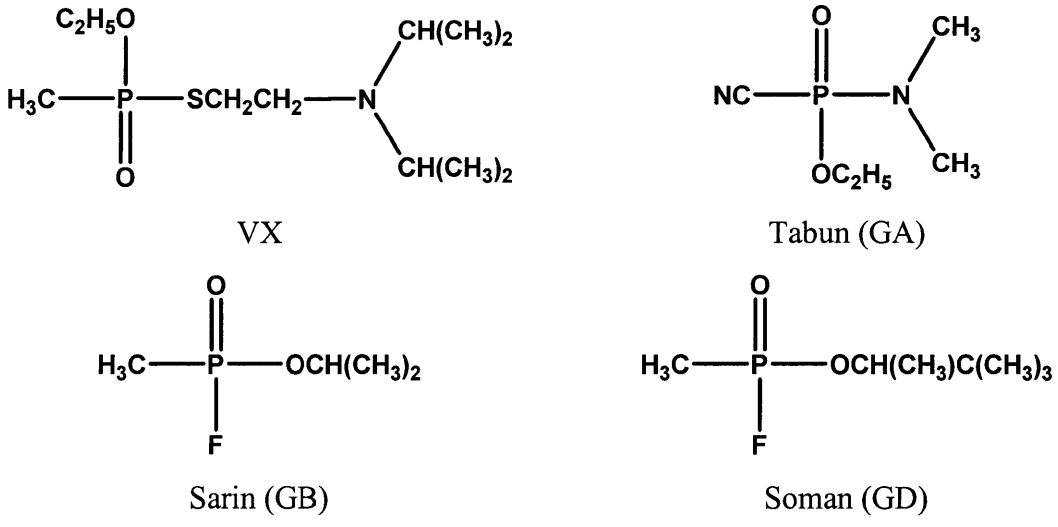

Scheme 1-2. Chemical structures of common nerve agents

1.1.2 Organophosphate Toxicity

Organophosphate compounds interrupt the electrochemical process that nerves utilize to communicate with muscles and with one another. [8-12] A key chemical in communication between cholinergic synapses is the neurotransmitter, acetylcholine. This chemical is responsible of sending signals to neurons in order to control the muscles to perform desired actions. In the neuro-transmitting process, acetylcholine is decomposed into inactive metabolite choline and acetate by an enzyme called acetylcholinesterase (AChE), which is concentrated in the extracellular synaptic cleft, where acetylcholine is secreted. The active site of AChE consists of a catalytic triad of serine, histidine, and glutamic acid residues. There is a gorge connecting the active site with the protein surface and a peripheral anionic site. [13, 14] This decomposition process allows the nerves to rest, thereby maintaining the normal functions of both the nerves and muscles. The reaction is shown in Scheme 1-3.

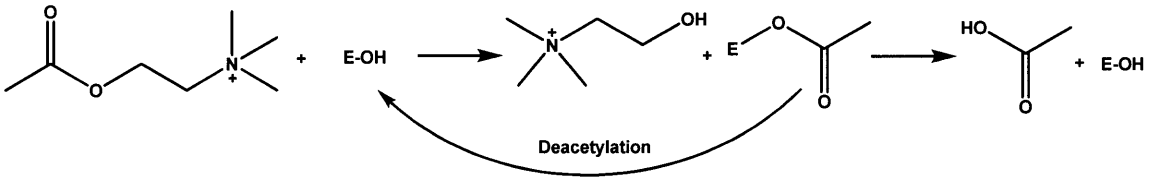

Scheme 1-3. Decomposition reaction of acetocholine by acetocholinesterase (AChE)

OP compounds are known for their acute toxicity. As strong cholinesterase inhibitors, OP compounds form stable covalent phosphoryl-intermediates with acetylcholinesterase through phosphorylation of the hydroxyl group of serine of the active site and thus prevent AChE from degrading acetylcholine. [8-10, 15, 16] As acetylcholine builds up, body muscles become over-stimulated, leading to paralysis and death in a very short period of time, typically minutes after nerve agent exposure. [9, 17] The spontaneous reversal of inhibition to regenerate AChE is a slow process. During the early stage of inhibition, it is possible to reactivate the phosphoryl enzyme with strong nucleophiles, such as pralidoxime (2-PAM), obidoxime, HI 6, and HLo 7. The formed phosphoryl oximes from the reactivation reaction are very unstable in water solutions and undergo decomposition or hydrolytic regeneration depending on the properties of OP substrates, nucleophiles, and solution conditions. [7, 10, 17-19] At later stages of inhibition, however, the phosphoryl

enzymes undergo an aging process wherein an alkyl group is lost from the phosphoryl moiety through a carbocation mechanism, rendering the intermediates resistant to oxime attack and the enzyme completely non-functional. [11, 20] The overall phosphorylation, reversal of inhibition, aging, and reactivation processes are shown in Scheme 1-4. A kinetic model was established to incorporate all the above processes to evaluate the reactivation efficiency of oximes. [21]

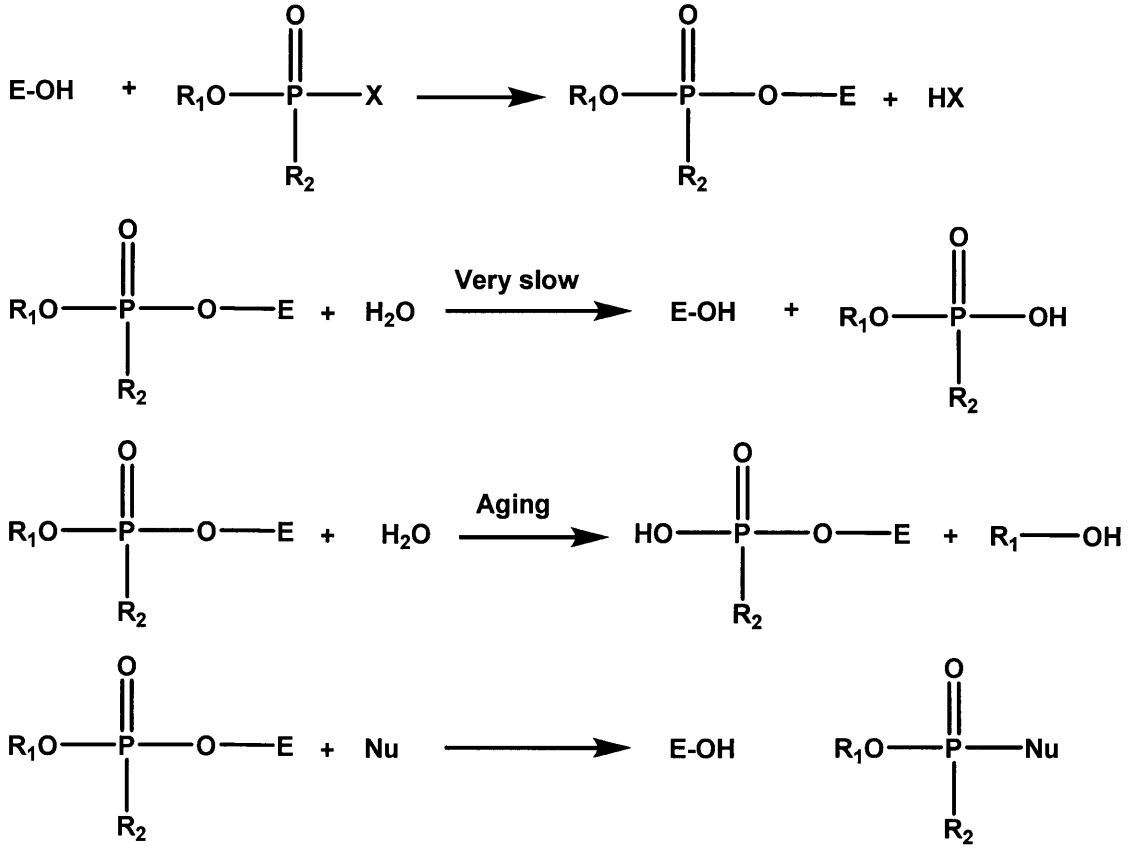

Scheme 1-4. Phosphorylation reaction of acetocholinesterase (E-OH), spontaneous hydrolysis reaction of the phosphoryl AChE, aging, and the reactivation of phosphoryl-AChE by strong nucleophiles (Nu). Further reactions of the phosphoryl nucleophiles are common and not discussed in the scheme.

Although there is debate about the extent, evidence has shown there are adverse health effects when exposed to repeated OP intoxication at a level not able to cause acute intoxication of the nervous system. Most research has focused on animal studies, though some literature has reported the effects of OP insecticides on human behavior. [7, 22-25] Bajgar et. al. found persistent effects on a few behavioral parameters of guinea pigs following a single inhalation exposure of soman. [26] Significant changes were found in

another study on rats when they were exposed to low-level sarin in a number of parameters, such as depression of red cell acetocholinesterase, gait disorder, and mobility, etc. [27] Sleep disruption was also seen in mice when exposed to soman. [28] Long term exposure to low levels of organophosphates can produce persistent and additive inhibition of acetylcholinesterase resulting in delayed cholinergic toxicity and delayed neuropathy. [29, 30] However, the detailed mechanism in regards to low-level exposure is not very clear at present.

1.1.3 Organophosphate Contamination

When nerve agents are applied on the battlefield, it is critical for military personnel to recover quickly from the intoxication through medical means. Equally important is the decontamination of military equipment for immediate reuse and to eliminate future hazards. Current decontamination technologies utilize large equipment, which poses serious logistic burdens, and harsh decontamination agents, which are hazardous to military hardware as well as to operators and the environment. Therefore, new technologies to decontaminate military equipment are desired. [31] Other than the battlefield, this new era is facing increasing threat from nerve agent application toward civilian targets by terrorist attacks, as shown by the release of the nerve gas sarin in the Tokyo subway system by members of the Aum Shinrikyo sect in 1995. [32] Water sources are potential high-risk targets. Decontamination of large bodies of surface and ground water poses special challenges.

When OP pesticides are applied for agricultural or home and garden use, these pesticides can contaminate water through a variety of means. As shown in Figure 1-1, pesticides enter water through surface runoff, leaching, air drifting, and/or erosion. When flowing across the field surface, newly applied pesticides could be washed off the field. Even though soil is able to bind a certain portion of pesticides, they will eventually enter into the water body. Wind and water can erode soil that contain pesticide residues and carry them into nearby bodies of water. Even comparatively insoluble pesticides and pesticides with high soil adsorption properties can move with eroded soil. The pesticide droplets can also be air-drifted into close-by water systems during application. [33, 34]

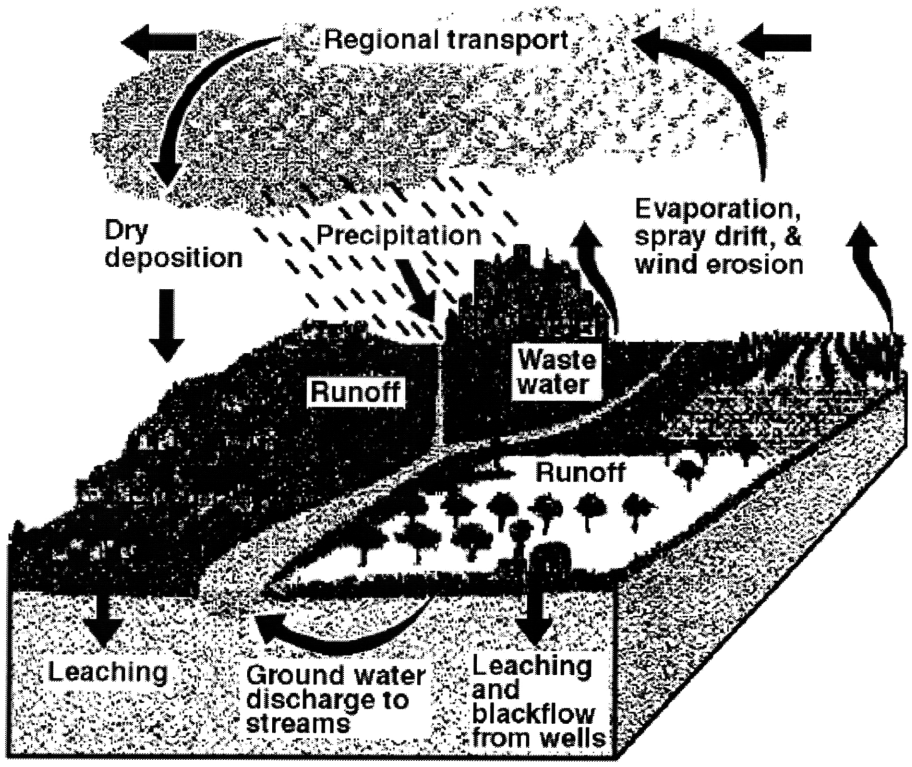

Figure 1-1. Pathways of pesticide movement in the environment [34]

1.1.4 Current Technologies and Their Problems

Various technologies have been utilized to purify water contaminated by organic chemicals, including OP compounds. Physical absorption, incineration, chemical treatment, and membrane technology are among the most widely applied methods to eliminate many organic hazardous chemicals.

Carbon black is the most widely used adsorbent in the physical process because of low cost and high adsorption capability. However, hazardous chemicals are only concentrated without being transformed into harmless products through the process and further treatments necessary. In addition, the adsorption materials have limited capacity and need to be recycled and regenerated frequently.

Incineration is a waste treatment technology that involves the combustion of organic materials and this process is very effective against OP materials. However the incineration facilities are notoriously expensive. All contaminated materials are required

to be sent to the central facility and dealt with there and this makes the process very inflexible. Furthermore, the OP compounds need to be removed from the water stream in order to be dealt with by the incineration technologies. [35]

Chemical processes apply bleaches, alkaline solution, or other strong oxidants to decompose OP compounds. The stoichiometric nature of the interaction between OP compounds and reactive chemicals requires a large quantity of material to achieve reasonable decomposition, especially for low OP concentration solutions with large volumes. As a result, this treatment actually adds more waste to the water body and makes the final clean-up more complex. [36]

A considerable amount of research has been also focused on membrane technologies for cleaning up water resources. A large number of membranes have been tested to purify water streams contaminated by OP materials in the reverse osmosis process, some of which have shown good separation efficiency. However, this process requires large pressure driving forces, which make this technology inflexible. Secondly, the selectivity of the membranes is still problematic. They may be selective for one OP compound, but not for others. This requires uses of multiple specific membranes because of the complexity of the groundwater system. Finally, membrane fouling is a serious issue because of the organic nature of OP chemicals and therefore increases operational costs dramatically. [33]

1.1.5 Catalytic Decomposition

When accumulated in natural water systems or attached to soil, OP compounds will decompose through spontaneous hydrolysis. Other natural processes may occur as well, such as microbial degradation, photolysis and phytolysis. However, these natural processes could be very lengthy. Furthermore, the decomposition products can be unpredictable and even more toxic than the original OP compounds. [9]

To accelerate the decomposition process and steer the reaction into desired products, catalytic decomposition has been tested widely for decomposing OP compounds because

of high specificity and dramatically enhanced reaction rates. [5, 37-47] Three types of catalysts have been focused upon for OP decomposition. The first is the highly reactive α-nucleophiles, such as oximates, [11, 37, 38, 48] hydroxamates, [41, 49-51] hydrogen peroxide anions, [52, 53] iodosobenzoate and its derivatives, [54-56] etc. The molecular structures of these functional groups are shown in Scheme 1-5. Ultra-Kleen™ 102P is a commercial decontamination system utilizing alkali peroxide. In these α-nucleophilic groups, the electron lone pair from the catalytic atom collaborates with another lone pair of electrons on the α-atom, thereby increasing the nucleophilicity dramatically. The second group is metal complexes and metallomicelles. [42, 57, 58] The third group are the biological catalysts. For example, organophosphorus hydrolase (OPH) is an enzyme isolated from the soil-dwelling bacterium *Pseudomonas diminuta* and is able to hydrolyze a wide variety of organophosphate compounds, including the chemical nerve agents such as sarin, soman, tabun, and VX, as well as the pesticides parathion, and paraoxon. [59] Landguard™ uses proprietary enzyme technology for OP decomposition.

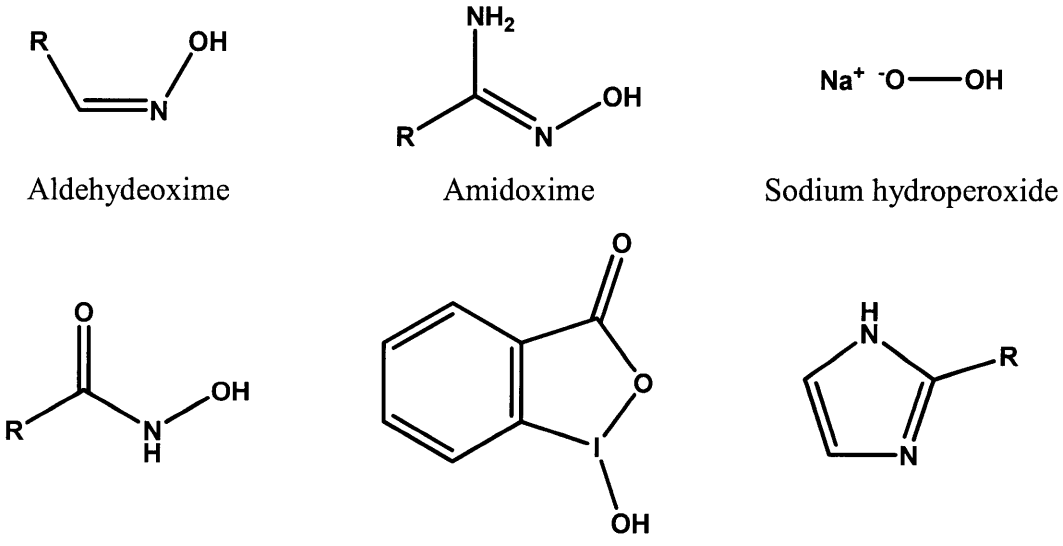

Aldehydeoxime | Amidoxime | Sodium hydroperoxide

Hydroxamic acid | Iodosobenzoate | Imidazole

Scheme 1-5. Chemical structures of α-nucleophiles

The typical mechanism of catalytic decomposition is shown in Scheme 1-6, in which methyl-paraoxon is catalytically decomposed by nucleophiles. Most studies on catalytic decomposition have concentrated on homogenous or micellar catalysis, which does not

afford recyclable systems that would allow reuses of the catalysts in order to reduce operational costs as well as the environmental footprint. [60-62]

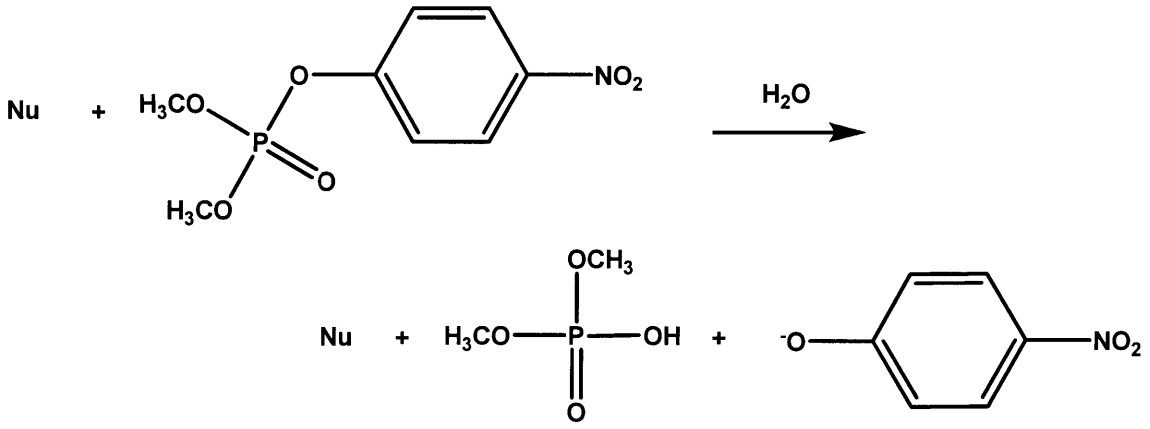

Scheme 1-6. Catalytic hydrolysis of methyl-paraoxon by nucleophiles

1.2 Magnetic Fluids and Particle Separation

Magnetic nanoparticles are attracting a great deal of interest from various research areas, including biological separation and biomedicine, [60, 63-65] magnetic resonance imaging (MRI),[66, 67] hyperthermia, [68] catalysis, [69, 70] and environmental remediation. [61, 71-74]

Magnetic fluids consist of magnetic nanoparticles with the typical sizes between 10-100nm suspended within a carrier fluid. [75] Because of the strong van der Waals interactions between particles, they tend to aggregate to form precipitates even with the strong Brownian motion characteristic of small particles. Electrostatic and/or steric interactions are often employed to stabilize the particles so that they can form stable suspensions within the carrier fluids for long term applications. This stabilization can be realized through coating the particle surfaces with small organic molecules or polymers, which depend on the specific applications and required carrier fluids. [75] The magnetic particles can be pure metals, such as iron, nickel and cobalt, [76-78] metal alloys, such as nickel-platinum, [79, 80] and metal oxides, such as magnetite and maghemite. [61, 63, 81] Among these magnetic materials, magnetite appears to be the most common for large-scale applications because it is relatively easy to prepare on a large scale with off-the-shelf raw materials, easily stabilized by ionic and/or steric interactions, and chemically stable with regard to subsequent chemical modifications, etc. [82] Magnetite particles could be

prepared in either organic or water carrier fluids. Because of the nature of water remediation, water will be used as the carrier fluid in this work and the corresponding magnetic fluids are discussed in the following review.

1.2.1 Particle Synthesis and Properties

Various methods have been used to prepare magnetite nanoparticles, including chemical co-precipitation, thermal decomposition and high-energy ball-milling, etc. Among these preparation methods, chemical co-precipitation provides many advantages over others for large-scale applications in water treatment.

Thermal decomposition of organometallic compounds is often employed to prepare mono-dispersed particles in the presence of stabilizing materials. [65, 83-88] The most widely used precursors are metal acetylacetonates and metal cupferronates. This method affords great control over the shape, size, and monodispersity due to the strong initial burst formation of crystal cores and slow controlled crystal growth stage. [83-86] However, this method requires usage of expensive raw materials. It affords magnetic fluids only in organic solvents due to the strict experimental conditions and therefore require complex chemical manipulations to be transferred into water medium. [87] This inhibits use of the method for large scale applications, particularly in aqueous media.

Chemical co-precipitation is convenient and flexible for preparation of magnetite nanoparticles from water solutions of Fe(II) and Fe(III) salts, in which an aqueous base is added at elevated or room temperature to precipitate magnetite or maghemite in the presence of stabilizing materials. The overall reaction is shown in Scheme 1-7.

$$2FeCl_3 + FeCl_2 + 8NH_4OH \rightarrow Fe_3O_4 + 4H_2O + 8NH_4Cl$$

Scheme 1-7. Reaction mechanism for magnetite formation in basic solution

In order to form crystalline magnetite with favorable magnetic properties, high pH and high temperature are required for the synthesis. The coating polymer is added either before or at the same time as the base solution. The prepared nanoparticles are

polydisperse and their shapes are not easily controlled during the preparation process due to the quick formation of whole magnetite crystals and lack of a controlled crystal growth phase. [66, 89, 90] However, this process is easy to reproduce and scale-up. All used raw materials are relatively easy and cheap to obtain. These properties make it an ideal candidate for large-scale applications. [82]

1.2.2 Stabilizing Polymer

Magnetic particles can be stabilized by electrostatic interactions or steric interactions, or both, by suitable coatings on the particle surfaces. Various coatings have been applied and tested, including surfactants, polyelectrolytes, etc. [61, 81, 90, 91] Bi-layer coatings are required for surfactant coated nanoparticles to be water dispersible and hydrophobic forces are needed to keep the second layer in place, making them labile to dissociation on dilution and attack from other organic polar compounds in water solution. [81, 92] Although the surfactant coating could be polymerized to increase the coating stability, it requires complex polymerization process. [89, 92] Therefore, polymer coatings have been the major focus because they can provide covalent attachment groups as well as stabilizing groups in the same molecule. This type of coating provides better stability and easier synthetic processes with off-the-shelf chemicals. [66, 90, 93]

Polymer attachment on the particle surfaces relies on the electrostatic interaction between anionic functional groups and surface cationic ions or chelating interactions between them. [94, 95] Unlike physical adsorption and ionic interactions, complexation affords strong bonds between the stabilizing polymer and the particle crystal cores and excellent stabilization and prevents interactions from being affected by ionic environment. Phosphate and carboxylic acid groups have been reported to form stable complexes with the magnetite surface. Since there is a much larger range of polymers and polymerizable materials containing carboxyl functional groups available, carboxylic acid groups have been used as a preferred choice when stabilizing the magnetite particles. [93]

Copolymerization and polymer branching have been used to incorporate various functionalities into polymer molecules in addition to the complexing carboxylic groups.

Acrylic acid is used to provide the carboxyl functional groups. Polymers branched with PEO were used to stabilize particles with steric interactions. [66, 71] When utilizing the electrostatic interactions, sulfonic acid groups were used to provide the constant ionic characteristics needed to increase the operational pH range of magnetic particles. Styrene sulfonic acid was used to provide hydrophobicity for better stability. [93]

1.2.3 Modified Functional Magnetic Particles

Not only do the coating materials on the magnetite surface provide stabilization against particle aggregation and gravitation, they also afford additional functionalities for desired applications or further modification. This provides much more flexibility and expands the application of magnetic particles dramatically. The coating materials can contain both the functional groups and chelation centers. As a result the prepared particles will provide the functional groups after chelation centers complexed with particle surface during synthesis. As mentioned above, styrene sulfonic acid was introduced onto the particle surface as part of the coating polymer to provide hydrophobicity to absorb proteins through hydrophobic interaction. [60] Chiral catalyst was attached to the surfaces of magnetite particles through covalent bonds with phosphonic acid as the particle chelating groups. These particles was used to catalyze asymmetric hydrogenation of aromatic ketones and recycled afterwards for reuse. [96] Oxime groups were chelated with the magnetite particles during synthesis for decomposition of the chemical warfare agent stimulant, diisopropyl fluorophosphate (DFP). [97, 98]

Functional groups have also been covalently bonded with functional groups on particle surfaces through chemical reactions after particle preparation. Enzymes or antibodies were attached on the particle surface to catalyze biological reactions or to separate target biological materials, such as proteins, nuleic acids, and cells, through specific affinity interactions. [64, 73, 99-101] The attachment commonly employed the chemistry between carboxylic acid and amine groups to form stable amide bonds with activation by 1-ethyl-3-(3-dimethylaminopropyl)-carbodiimide (EDC). [67] Gold nanoparticles and quantum dots have also been attached on magnetic particle surfaces through antibody-antigen interactions, covalent bonds, and electrostatic interactions. [102, 103]

Magnetic particles are also very useful for environmental applications. When not protected with polymer or other coating materials, magnetic hydrated iron oxide interacted strongly with and thus was effective in removing As(III) and As(V) traces or heavy metal ions, such as Cu(II) and Zn(II) ions from water media. [72] Magnetic oxides also functioned as heterogeneous catalysts for the Fenton reaction to decolorize wastewaters containing synthetic dyes or polycyclic aromatic hydrocarbons through catalyzing the decomposition of hydrogen peroxide to produce active hydroxyl radicals. [74] When coated with or embedded within chelating polymers, the formed functional particles were used for removing water contaminants. A cost-effective moving-bed process was developed for continuous removal of dissolved organic compounds from natural organic materials (NOM) with magnetic resins with the diameter around 10μm. [104] Processes using magnetic ion exchange resin (MIEX^{TM}) to remove dissolved organic carbon (DOC) were shown to be superior to standard coagulation processes. [105, 106] Magnetic polymethylmethacrylate microbeads (150-200μm in diameter) carrying amine functional groups were shown to remove Pb(II) ions from aqueous solutions. [107]

1.2.4 Magnetic Separation

Magnetic particles can be separated and recycled by exploiting magnetic fields. This enables repeated use of the functional particles and eliminates particle contamination of the final desired solution.

The magnetic particles of interest are superparamagnetic. Their magnetic dipoles are randomly distributed in the colloidal solution because the particle sizes are small and the energy required to change the direction of magnetization of the entire particle crystal is much less than the thermal energy. The net magnetic moment of the collective particles is zero at zero external magnetic fields, meaning no coercive field. However, the particles will align and produce a net magnetic moment when an external field is applied and reach saturation magnetization when the external field increases to a certain point. Remanence, the magnetization left behind in a medium after an external magnetic field is removed, is also zero for the superparamagnetic particles. A magnetic force is applied on the particles

when they are placed into a non-uniform field. The magnitude of the force is quantified by Equation 1-1.

$$F_M = \mu_0 V_{core} M_p \bullet \nabla H \qquad \textbf{Equation 1-1}$$

where

μ_0	=	permeability of the free space
V_{core}	=	volume of magnetic core
H	=	magnetic field
M_p	=	magnetization of the particles

The small size of nanoparticles affords small magnetite core volume. The particle magnetization is determined by the magnetite properties and the system often operates at the saturation magnetization conditions. Therefore, it requires larger gradient of magnetic field to exert enough force to counter the drag force by the flowing liquid and the diffusive force from the concentration gradient of particles in order to separate the magnetic particles from the carrier fluids. [71] This is realized by high gradient magnetic separation (HGMS), the schematic of which is shown in Figure 1-2.

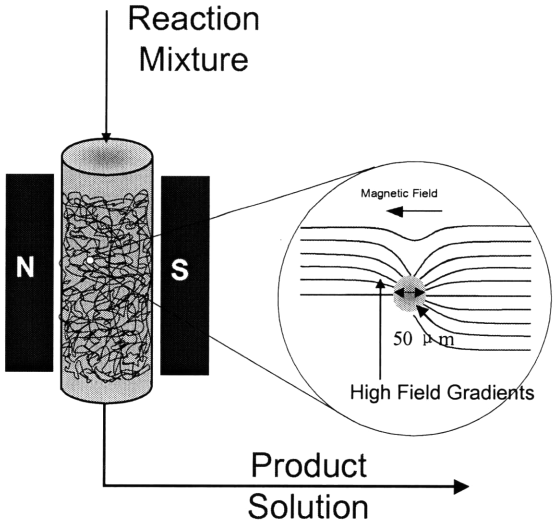

Figure 1-2. Illustration of high gradient magnetic separation

A column filled with small magnetizable metal meshes of wires on the order of tens of microns in diameter is placed in the gap between the magnetic fields to build up a typical HGMS device. This setup provides sufficiently large magnetic field gradients due to distortion of the magnetic fields by the mesh surfaces to capture the magnetic nanoparticles. Since the entire column is packed with the material, a high magnetic field capture zone is large enough to be overlapping among multiple wires to capture all particles. [108] Because of the superparamagnetic properties, nanoparticles can be captured when the magnetic field is applied and released readily into the solvent when the magnetic field is removed. [71]

However, it has been shown that only particles larger than 50nm would be captured efficiently by HGMS. The direct co-precipitation method is not able to produce particles of this size with good colloidal stability that are able to be captured efficiently. A two-step procedure has been developed to prepare particles stable against high ionic strength and larger than 50nm for efficient capture by HGMS. [108, 109] The prepared particles are aggregates of individual particles with multiple magnetic cores. The particle preparation mechanism is shown in Figure 1-3.

In this procedure, direct co-precipitation was employed to form the magnetite cores and the step of magnetite core formation and cluster aggregation was isolated from the stabilization step. During particle synthesis a certain amount of stabilizing polymer is initially added to the iron salt solution before the addition of base solution. However, the amount added was not enough to stabilize all the formed individual magnetite cores. They then formed aggregates because of the incomplete coating. The second addition of stabilizing polymer coated all of the possibly uncoated particle surfaces to fully stabilize the aggregates. The quantities and properties of the first and secondary polymer could be manipulated to produce the aggregates with desired sizes. The secondary polymer could be different from the first polymer so that the procedure is flexible enough to incorporate more functionality onto the particle surfaces. [93] Furthermore, molecular weight and polymer composition have been shown to influence the particle properties significantly and need to be optimized for appropriate sizes and best stabilization. [93] Hydrophobicity in

the copolymer increased the coating thickness and therefore enhanced the particle stability. [93, 110] The prepared clusters of individual particles remained superparamagnetic,. Therefore, they were readily captured by HGMS and subsequently recovered readily into a water solution when the external magnetic field was removed from the HGMS device.

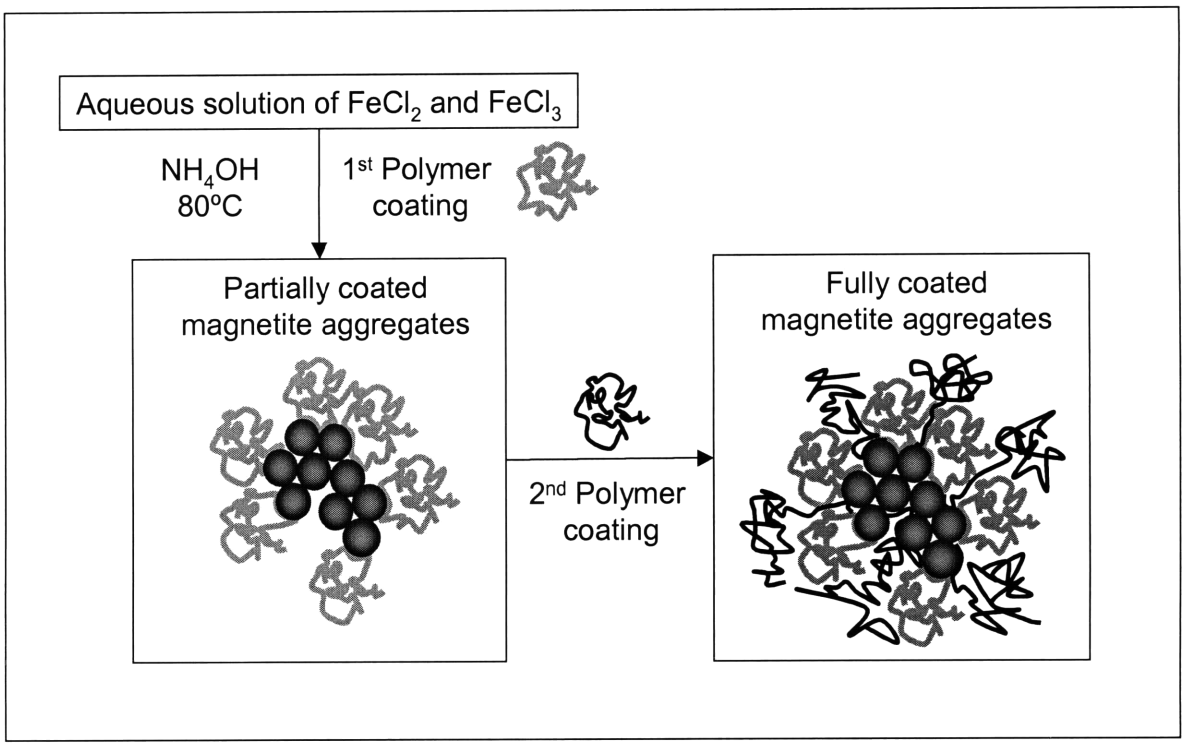

Figure 1-3. Two-step procedure to prepare magnetic particles larger than 50nm for efficient capture by HGMS [109]

1.3 Research Approach and Specific Aims

Based on the challenges posed by organophosphate contamination and the benefits provided by the catalytic decomposition and magnetic particles, we propose to utilize the following process to decompose OP contaminants, as shown in Figure 1-4. In this process, the contaminated water solution is mixed with magnetic particles with catalytic groups on their surfaces. The particles utilized are magnetite clusters prepared by the two-step procedure discussed above and then appropriately modified to carry the functional groups. The cluster size is controlled to be around 100nm for efficient capture by HGMS whereas the individual core size is around 8nm from the co-precipitation method. When the contaminants are fully decomposed, the mixture solution is passed through an HGMS device to capture the magnetic particles, which will be washed out of

the column and readily redispersed in water by removing the magnetic field after the column is filled up. The recycled particles will then be fed back into another batch of contaminated solution for catalytic reaction. The decomposed product will then go through the regular water treatment process for final use.

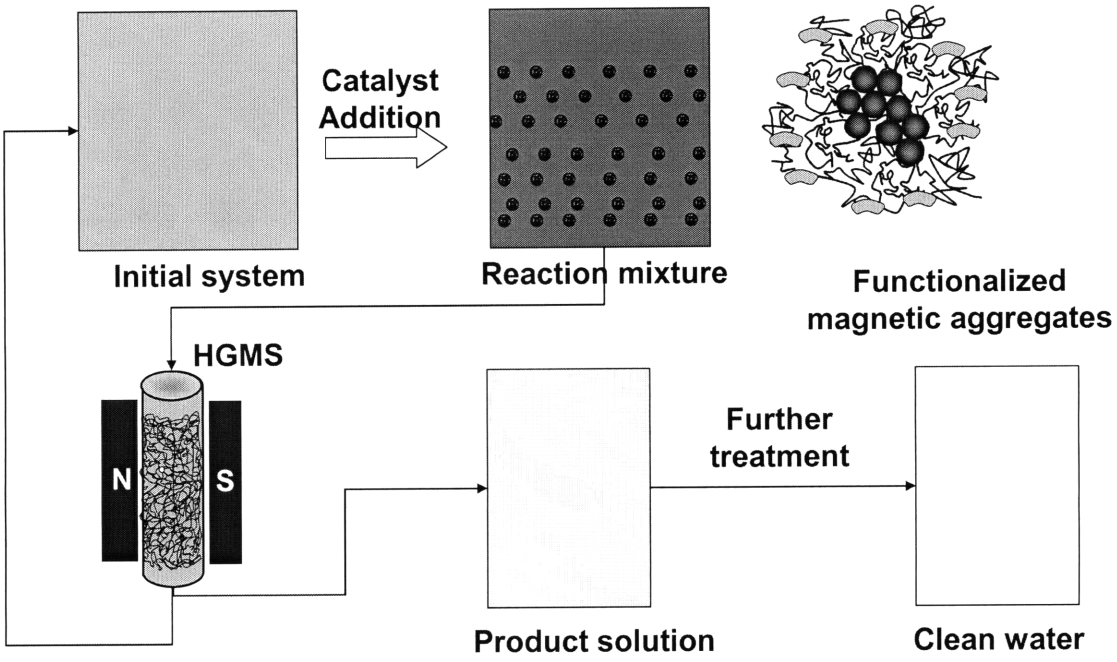

Figure 1-4. Proposed continuous process for OP decomposition by functional magnetic particles and their recovery by HGMS

The above process provides a variety of benefits. It is continuous and has the potential to be implemented on a large scale. Particles utilized are colloidally stable and active catalytic groups are attached on the particle surfaces to eliminate internal mass transfer resistance. Nanoparticles are used to increase the surface area and the density of carried functional groups to improve reaction efficiency with the same amount of material. Functional particles are recycled after usage to simplify the process, reduce cost, and minimize the environmental footprint.

The desired particles pose several requirements on the particle preparation process. First, the synthetic process for magnetic nanopartilces needs to be flexible in order to control the particle properties. Secondly, the particle synthesis has to be easy to scale up and therefore the raw materials have to be cheap and relatively easy to obtain in a large scale

in order to be economically possible. Thirdly, proper surface coating has to be introduced to ensure the colloidal stability of the nanoparticles and the availability of functional groups, and particle size larger than 50nm for efficient recovery of functional particles by HGMS. Finally, functional groups need to be attached on the particle surface through simple methods to provide strong reactivity and particles need to be stable even in relatively harsh environments during the modification as well as the application stage.

The overall objective of this research is to develop functionalized magnetic particles that can be used to catalyze decomposition of organophosphate compounds, including both pesticides and chemical nerve agents. Strong α–nucleophilic groups will be the major focus in that they are highly reactive toward the target applications, easily prepared with simple chemical modification steps, and stable under a wide range of environmental conditions, such as solution pH and significant presence of organic compounds, etc.

To accomplish the overall objective mentioned above, several specific research objectives will be investigated.

1. **Develop strategies to attach α–nucleophilic functional groups onto magnetic particles.** The two-step synthetic method is adopted to prepare the magnetic aggregates so that both colloidal stability and suitable aggregate size will be obtained. The following modification strategy will attach the functional groups onto particles surfaces while maintaining particle stability and particle size.
2. **Investigate the decomposition of model compounds with the particles.** Model compounds will be tested with the functionalized particles. The substrate partitioning between the bulk water phase and the particle surface phase will be paid special attention. The particles will be optimized to obtain the maximum reactivity against the model compound.
3. **Study the decomposition mechanism of OP compounds by the catalytic particles.** The chemical mechanism of OP hydrolysis by nucleophiles will be studied within homogeneous systems. The reactivity of the functionalized particles will be tested for the selected OP compounds.

1.4 Bibliography

1. Chambers, J. E.; Levi, P. E., *Organophosphates: chemistry, fate, and effects*. Academic Press: San Diego, 1992; p xviii, 443 p.
2. Coats, J. R.; Yamamoto, H.; American Chemical Society. Division of Agrochemicals., *Environmental fate and effects of pesticides*. American Chemical Society: Distributed by Oxford University Press: Washington, D.C., 2003; p xii, 300 p., 1 leaf of plates.
3. Vighi, M.; Funari, E., *Pesticide risk in groundwater*. Lewis Publishers: Boca Raton, 1995; p 275 p.
4. Greenhalgh, R.; Dhawan, K. L.; Weinberger, P., Hydrolysis Of Fenitrothion In Model And Natural Aquatic Systems. *Journal Of Agricultural And Food Chemistry* **1980,** 28, (1), 102-105.
5. Smith, B. M., Catalytic methods for the destruction of chemical warfare agents under ambient conditions. *Chemical Society Reviews* **2008,** 37, (3), 470-478.
6. Kiely, T.; Donaldson, D.; Grube, A. *Pesticides Industry Sales and Usage - 2000 and 2001 Market Estimates*; U.S. Environmental Protection Agency: Washington, DC, May, 2004.
7. Marrs, T. C.; Maynard, R. L.; Sidell, F., *Chemical Warfare Agents: Toxicology and Treatment*. 2nd ed.; Wiley: 2007; p 750.
8. Worek, F.; Thiermann, H.; Szinicz, L., Reactivation and aging kinetics of human acetylcholinesterase inhibited by organophosphonylcholines. *Archives Of Toxicology* **2004,** 78, (4), 212-217.
9. Munro, N. B.; Talmage, S. S.; Griffin, G. D.; Waters, L. C.; Watson, A. P.; King, J. F.; Hauschild, V., The sources, fate, and toxicity of chemical warfare agent degradation products. *Environmental Health Perspectives* **1999,** 107, (12), 933-974.
10. Kassa, J., Review of oximes in the antidotal treatment of poisoning by organophosphorus nerve agents. *Journal Of Toxicology-Clinical Toxicology* **2002,** 40, (6), 803-816.
11. Jiří Patočka, J. C., Kamil Kuča, Daniel Jun, Oxime reactivation of acetylcholinesterase inhibited by toxic phosphorus esters: in vitro kinetics and thermodynamics. *Journal of applied biomedicine* **2005**, (3), 91-99.
12. Chambers, J. E.; Oppenheimer, S. F., Organophosphates, serine esterase inhibition, and modeling of organophosphate toxicity. *Toxicological Sciences* **2004,** 77, (2), 185-187.
13. Kovarik, Z.; Radic, Z.; Berman, H. A.; Simeon-Rudolf, V.; Reiner, E.; Taylor, P., Mutant cholinesterases possessing enhanced capacity for reactivation of their phosphonylated conjugates. *Biochemistry* **2004,** 43, (11), 3222-3229.
14. Kapkova, P.; Stiefl, N.; Surig, U.; Engels, B.; Baumann, K.; Holzgrabe, U., Synthesis, biological activity, and docking studies of new acetylcholinesterase inhibitors of the bispyridinium type. *Archiv Der Pharmazie* **2003,** 336, (11), 523-540.
15. Marrs, T. C., Organophosphate Poisoning. *Pharmacology & Therapeutics* **1993,** 58, (1), 51-66.
16. Rang, H. P.; Dale, M. M.; Ritter, J. M.; Flower, R., *Rang & Dale's Pharmacology*. 6th ed.; Churchill Livingstone: 2007; p 844.

17. Bajgar, J., Organophosphates/nerve agent poisoning: Mechanism of action, diagnosis, prophylaxis, and treatment. In *Advances In Clinical Chemistry, Vol. 38*, Elsevier Academic Press Inc: San Diego, 2004; Vol. 38, pp 151-216.
18. Kim, T. H.; Kuca, K.; Jun, D.; Jung, Y. S., Design and synthesis of new bis-pyridinium oxime reactivators for acetyleholinesterase inhibited by organophosphorous nerve agents. *Bioorganic & Medicinal Chemistry Letters* **2005,** 15, (11), 2914-2917.
19. Worek, F.; Widmann, R.; Knopff, O.; Szinicz, L., Reactivating potency of obidoxime, pralidoxime, HI 6 and HLo 7 in human erythrocyte acetylcholinesterase inhibited by highly toxic organophosphorus compounds. *Archives Of Toxicology* **1998,** 72, (4), 237-243.
20. Masson, P.; Fortier, P. L.; Albaret, C.; Froment, M. T.; Bartels, C. F.; Lockridge, O., Aging of di-isopropyl-phosphorylated human butyrylcholinesterase. *Biochemical Journal* **1997,** 327, 601-607.
21. Worek, F.; Szinicz, L.; Eyer, P.; Thiermann, H., Evaluation of oxime efficacy in nerve agent poisoning: Development of a kinetic-based dynamic model. *Toxicology And Applied Pharmacology* **2005,** 209, (3), 193-202.
22. Brown, M. A.; Brix, K. A., Review of health consequences from high-, intermediate- and low-level exposure to organophosphorus nerve agents. *Journal Of Applied Toxicology* **1998,** 18, (6), 393-408.
23. Ray, D. E., Chronic effects of low level exposure to anticholinesterases - a mechanistic review. *Toxicology Letters* **1998,** 103, 527-533.
24. Somani, S. M.; Romano, J. A., *Chemical Warfare Agents: Toxicity at Low Levels*. CRC Press: 2000; p 447.
25. Ray, D. *Organophosphorus esters: An evaluation of chronic neurotoxic effects*; MRC INSTITUTE FOR ENVIRONMENT AND HEALTH: Leicester, UK.
26. Bajgar, J.; Sevelova, L.; Krejcova, G.; Fusek, J.; Vachek, J.; Kassa, J.; Herink, J.; de Jong, L. P. A.; Benschop, H. P., Biochemical and behavioral effects of soman vapors in low concentrations. *Inhalation Toxicology* **2004,** 16, (8), 497-507.
27. Kassa, J.; Krejcova, G.; Skopec, F.; Herink, J.; Bajgar, J.; Sevelova, L.; Tichy, M.; Pecka, M., The influence of sarin on various physiological functions in rats following single or repeated low-level inhalation exposure. *Inhalation Toxicology* **2004,** 16, (8), 517-530.
28. Crouzier, D.; Le Crom, V. B.; Four, E.; Lallement, G.; Testylier, G., Disruption of mice sleep stages induced by low doses of organophosphorus compound soman. *Toxicology* **2004,** 199, (1), 59-71.
29. Karalliedde, L.; Wheeler, H.; Maclehose, R.; Murray, V., Review article - Possible immediate and long-term health effects following exposure to chemical warfare agents. *Public Health* **2000,** 114, (4), 238-248.
30. Williams, F. M.; Charlton, C.; deBlaquiere, G. E.; Mutch, E.; Kelly, S. S.; Blain, P. G., The effects of multiple low doses of organophosphates on target enzymes in brain and diaphragm in the mouse. *Human & Experimental Toxicology* **1997,** 16, (2), 67-71.
31. Tiron, R., Decontamination Technology Still Outdated. *National Defense* **2003,** June.
32. Hood, E., Chemical and biological weapons: New questions, new answers. *Environmental Health Perspectives* **1999,** 107, (12), 931-932.

33. Bhattacharya, A., Remediation of Pesticide-Polluted Waters Through Membranes. *Separation & Purification Review* **2006,** 35, 1-38.
34. Stevenson, D. E.; Baumann, P.; Jackman, J. A. *Pesticide Properties That Affect Water Quality*; Texas Agricultural Extension Service: pp B-6050.
35. Shea, P. J.; Machacek, T. A.; Comfort, S. D., Accelerated remediation of pesticide-contaminated soil with zerovalent iron. *Environmental Pollution* **2004,** 132, (2), 183-188.
36. Walker, A. W.; Keasling, J. D., Metabolic engineering of Pseudomonas putida for the utilization of parathion as a carbon and energy source. *Biotechnology And Bioengineering* **2002,** 78, (7), 715-721.
37. Ghosh, K. K.; Kolay, S.; Satnami, M. L.; Moore, S.; Palepu, R. M.; Dafonte, P. R., Kinetics of reaction of oximate alpha-nucleophiles with p-nitrophenyl acetate in alkyltriphenyl phosphonium bromide micelles. *Journal Of Dispersion Science And Technology* **2007,** 28, (2), 213-218.
38. Chen, L.; Bromberg, L.; Hatton, T. A.; Rutledge, G. C., Catalytic hydrolysis of p-nitrophenyl acetate by electrospun polyacrylamidoxime nanofibers. *Polymer* **2007,** 48, (16), 4675-4682.
39. Abuin, E.; Lissi, E.; Biasutti, M. A.; Duarte, R., Kinetics of p-nitrophenyl acetate hydrolysis catalyzed by Mucor javanicus lipase in AOT reverse micellar solutions formulated in different organic solvents. *Protein Journal* **2007,** 26, (7), 475-479.
40. Ghosh, K. K.; Vaidya, J.; Satnami, M. L., The alpha-effect in micelles: Nucleophilic substitution reaction of p-nitrophenyl acetate with N-phenylbenzohydroxamate ion. *International Journal Of Chemical Kinetics* **2006,** 38, (1), 26-31.
41. Ghosh, K. K.; Satnami, M. L., Nucleophilic substitution reaction of carboxylate and phosphate esters with hydroxamate ions in microemulsions. *Colloids And Surfaces A-Physicochemical And Engineering Aspects* **2006,** 274, (1-3), 125-129.
42. Yatsimirsky, A. K., Metal ion catalysis in acyl and phosphoryl transfer: Transition states as ligands. *Coordination Chemistry Reviews* **2005,** 249, (17-18), 1997-2011.
43. Mancin, F.; Tecilla, P.; Tonellato, U., Metallomicelles made of Ni(II) and Zn(II) complexes of 2-pyridinealdoxime-based ligands as catalyst of the cleavage of carboxylic acid esters. *Langmuir* **2000,** 16, (1), 227-233.
44. Hampl, F.; Liska, F.; Mancin, F.; Tecilla, P.; Tonellato, U., Metallomicelles made of Ni(II) complexes of lipophilic 2-pyridineketoximes as powerful catalysts of the cleavage of carboxylic acid esters. *Langmuir* **1999,** 15, (2), 405-412.
45. Roa, A.; Goble, M. L.; Garcia, J. L.; Acebal, C.; Virden, R., Rapid burst kinetics in the hydrolysis of 4-nitrophenyl acetate by penicillin G acylase from Kluyvera citrophila. *Biochemical Journal* **1996,** 316, 409-412.
46. Martel, B.; Morcellet, M., Cyclodextrin-Poly(Vinylamine) Systems.2. Catalytic Hydrolysis Of P-Nitrophenyl Acetate. *European Polymer Journal* **1995,** 31, (11), 1089-1093.
47. Bender, M. L.; Marshall, T. H., Elastase-catalyzed hydrolysis of p-nitrophenyl trimethylacetate. *J. Am. Chem. Soc.* **1968,** 90, (1), 201-207.
48. Couderc, S.; Toullec, J., Catalysis of phosphate triester hydrolysis by micelles of hexadecyltrimethylammonium anti-pyruvaldehyde 1-oximate. *Langmuir* **2001,** 17, (13), 3819-3828.

49. Ghosh, K. K.; Bal, S.; Satnami, M. L.; Rodriguez-Dafonte, P.; Palepu, R. M., Studies of nucleophilic substitution reactions of p-nitrophenyl acetate with some dihydroxamate ions in cationic micellar media. *Journal Of Dispersion Science And Technology* **2006,** 27, (3), 349-355.
50. Swidler, R.; Steinberg, G. M., The Kinetics of the Reaction of Isopropyl Methylphosphonofluoridate (Sarin) with Benzohydroxamic Acid. *J. Am. Chem. Soc.* **1956,** 78, (15), 3594-3598.
51. Ghosh, K. K.; Sinha, D.; Satnami, M. L.; Dubey, D. K.; Shrivastava, A.; Palepu, R. M.; Dafonte, P. R., Enhanced nucleophilic reactivity of hydroxamate ions in some novel micellar systems for the cleavage of Parathion. *Journal Of Colloid And Interface Science* **2006,** 301, (2), 564-568.
52. Chanda, A.; Khetan, S. K.; Banerjee, D.; Ghosh, A.; Collins, T. J., Total degradation of fenitrothion and other organophosphorus pesticides by catalytic oxidation employing Fe-TAML peroxide activators. *Journal Of The American Chemical Society* **2006,** 128, (37), 12058-12059.
53. Balakrishnan, V. K.; Buncel, E.; Vanloon, G. W., Micellar catalyzed degradation of fenitrothion, an organophosphorus pesticide, in solution and soils. *Environmental Science & Technology* **2005,** 39, (15), 5824-5830.
54. Moss, R. A.; Kanamathareddy, S.; Vijayaraghavan, S., Kinetics of cleavage of paraoxon and parathion by cetyltrimethylammonium iodosobenzoate. *Langmuir* **2001,** 17, (20), 6108-6112.
55. Moss, R. A.; Kim, K. Y.; Swarup, S., Efficient Catalytic Cleavage Of Reactive Phosphates By An Ortho-Iodosobenzoate Functionalized Surfactant. *Journal Of The American Chemical Society* **1986,** 108, (4), 788-793.
56. Moss, R. A.; Alwis, K. W.; Shin, J. S., Catalytic Cleavage Of Active Phosphate And Ester Substrates By Iodoso-Benzoates And Iodoxybenzoates. *Journal Of The American Chemical Society* **1984,** 106, (9), 2651-2655.
57. Ge, Q. C.; Guo, Y. H.; Lin, H.; Gao, D. Z.; Lin, H. K.; Zhu, S. R., Role of trinuclear Zn(II) complexes in promoting the hydrolysis of 4-nitrophenyl acetate. *Canadian Journal Of Chemistry-Revue Canadienne De Chimie* **2004,** 82, (3), 409-417.
58. diTargiani, R. C.; Chang, S. C.; Salter, M. H.; Hancock, R. D.; Goldberg, D. P., Hydrolysis of 4-nitrophenyl acetate by a novel (N2S)zinc-hydroxide complex: A kinetic and thermodynamic study of a reactive peptide deformylase model. *Journal Of Inorganic Biochemistry* **2003,** 96, (1), 238-238.
59. Morales-Rojas, H.; Moss, R. A., Phosphorolytic reactivity of o-iodosylcarboxylates and related nucleophiles. *Chemical Reviews* **2002,** 102, (7), 2497-2521.
60. Ditsch, A.; Yin, J.; Laibinis, P. E.; Wang, D. I. C.; Hatton, T. A., Ion-exchange purification of proteins using magnetic nanoclusters. *Biotechnology Progress* **2006,** 22, (4), 1153-1162.
61. Moeser, G. D.; Roach, K. A.; Green, W. H.; Laibinis, P. E.; Hatton, T. A., Water-based magnetic fluids as extractants for synthetic organic compounds. *Industrial & Engineering Chemistry Research* **2002,** 41, (19), 4739-4749.
62. Moss, R. A.; Chung, Y. C., Immobilized Iodosobenzoate Catalysts For The Cleavage Of Reactive Phosphates. *Journal Of Organic Chemistry* **1990,** 55, (7), 2064-2069.

63. Bucak, S.; Jones, D. A.; Laibinis, P. E.; Hatton, T. A., Protein separations using colloidal magnetic nanoparticles. *Biotechnology Progress* **2003,** 19, (2), 477-484.
64. Li, X. H.; Sun, Z. G., Synthesis Of Magnetic Polymer Microspheres And Application For Immobilization Of Proteinase Of Balillus-Sublitis. *Journal Of Applied Polymer Science* **1995,** 58, (11), 1991-1997.
65. Zhang, Y.; Zhang, J., Surface modification of monodisperse magnetite nanoparticles for improved intracellular uptake to breast cancer cells. *Journal Of Colloid And Interface Science* **2005,** 283, (2), 352-357.
66. Lee, H.; Lee, E.; Kim, D. K.; Jang, N. K.; Jeong, Y. Y.; Jon, S., Antibiofouling polymer-coated superparamagnetic iron oxide nanoparticles as potential magnetic resonance contrast agents for in vivo cancer imaging. *Journal Of The American Chemical Society* **2006,** 128, (22), 7383-7389.
67. Gupta, A. K.; Gupta, M., Synthesis and surface engineering of iron oxide nanoparticles for biomedical applications. *Biomaterials* **2005,** 26, (18), 3995-4021.
68. Bonder, M. J.; Gallo, D.; Srinivasan, B.; Hadjipanayis, G. C., Size dependent in-vitro heating with polyethylene glycol coated magnetic nanoparticles. *Ieee Transactions On Magnetics* **2007,** 43, (6), 2457-2458.
69. Zheng, Y.; Duanmu, C.; Gao, Y., A magnetic biomimetic nanocatalyst for cleaving phosphoester and carboxylic ester bonds under mild conditions. *Organic Letters* **2006,** 8, (15), 3215-3217.
70. Wang, Z. F.; Shen, B.; Zou, A. H.; He, N. Y., Synthesis of Pd/Fe3O4 nanoparticle-based catalyst for the cross-coupling of acrylic acid with iodobenzene. *Chemical Engineering Journal* **2005,** 113, (1), 27-34.
71. Moeser, G. D.; Roach, K. A.; Green, W. H.; Hatton, T. A.; Laibinis, P. E., High-gradient magnetic separation of coated magnetic nanoparticles. *Aiche Journal* **2004,** 50, (11), 2835-2848.
72. Cumbal, L.; Greenleaf, J.; Leun, D.; SenGupta, A. K., Polymer supported inorganic nanoparticles: characterization and environmental applications. *Reactive & Functional Polymers* **2003,** 54, (1-3), 167-180.
73. Horak, D.; Babic, M.; Mackova, H.; Benes, M. J., Preparation and properties of magnetic nano- and microsized particles for biological and environmental separations. *Journal Of Separation Science* **2007,** 30, (11), 1751-1772.
74. Baldrian, P.; Merhautova, V.; Gabriel, J.; Nerud, F.; Stopka, P.; Hruby, M.; Benes, M. J., Decolorization of synthetic dyes by hydrogen peroxide with heterogeneous catalysis by mixed iron oxides. *Applied Catalysis B-Environmental* **2006,** 66, (3-4), 258-264.
75. Rosensweig, R. E., *Ferrohydrodynamics*. Cambridge University Press: Cambridge; New York, 1985; p xv, 344 p.
76. Huber, D. L., Synthesis, properties, and applications of iron nanoparticles. *Small* **2005,** 1, (5), 482-501.
77. Zhang, H. T.; Wu, G.; Chen, X. H.; Qiu, X. G., Synthesis and magnetic properties of nickel nanocrystals. *Materials Research Bulletin* **2006,** 41, (3), 495-501.
78. Grass, R. N.; Athanassiou, E. K.; Stark, W. J., Covalently functionalized cobalt nanoparticles as a platform for magnetic separations in organic synthesis. *Angewandte Chemie-International Edition* **2007,** 46, (26), 4909-4912.

79. Lu, P.; Teranishi, T.; Asakura, K.; Miyake, M.; Toshima, N., Polymer-protected Ni/Pd bimetallic nano-clusters: Preparation, characterization and catalysis for hydrogenation of nitrobenzene. *Journal Of Physical Chemistry B* **1999,** 103, (44), 9673-9682.
80. Behrens, S.; Bonnemann, H.; Matoussevitch, N.; Gorschinski, A.; Dinjus, E.; Habicht, W.; Bolle, J.; Zinoveva, S.; Palina, N.; Hormes, J.; Modrow, H.; Bahr, S.; Kempter, V., Surface engineering of Co and FeCo nanoparticles for biomedical application. *Journal Of Physics-Condensed Matter* **2006,** 18, (38), S2543-S2561.
81. Shen, L. F.; Laibinis, P. E.; Hatton, T. A., Bilayer surfactant stabilized magnetic fluids: Synthesis and interactions at interfaces. *Langmuir* **1999,** 15, (2), 447-453.
82. Lu, A. H.; Salabas, E. L.; Schuth, F., Magnetic nanoparticles: Synthesis, protection, functionalization, and application. *Angewandte Chemie-International Edition* **2007,** 46, (8), 1222-1244.
83. Sun, S. H.; Zeng, H., Size-controlled synthesis of magnetite nanoparticies. *Journal Of The American Chemical Society* **2002,** 124, (28), 8204-8205.
84. O'Brien, S.; Brus, L.; Murray, C. B., Synthesis of monodisperse nanoparticles of barium titanate: Toward a generalized strategy of oxide nanoparticle synthesis. *Journal Of The American Chemical Society* **2001,** 123, (48), 12085-12086.
85. Sun, S. H.; Murray, C. B.; Weller, D.; Folks, L.; Moser, A., Monodisperse FePt nanoparticles and ferromagnetic FePt nanocrystal superlattices. *Science* **2000,** 287, (5460), 1989-1992.
86. Murray, C. B.; Norris, D. J.; Bawendi, M. G., Synthesis And Characterization Of Nearly Monodisperse Cde (E = S, Se, Te) Semiconductor Nanocrystallites. *Journal Of The American Chemical Society* **1993,** 115, (19), 8706-8715.
87. Lattuada, M.; Hatton, T. A., Functionalization of monodisperse magnetic nanoparticles. *Langmuir* **2007,** 23, (4), 2158-2168.
88. Lee, S. Y.; Harris, M. T., Surface modification of magnetic nanoparticles capped by oleic acids: Characterization and colloidal stability in polar solvents. *Journal Of Colloid And Interface Science* **2006,** 293, (2), 401-408.
89. Shen, L. F.; Stachowiak, A.; Hatton, T. A.; Laibinis, P. E., Polymerization of olefin-terminated surfactant bilayers on magnetic fluid nanoparticles. *Langmuir* **2000,** 16, (25), 9907-9911.
90. Lutz, J. F.; Stiller, S.; Hoth, A.; Kaufner, L.; Pison, U.; Cartier, R., One-pot synthesis of PEGylated ultrasmall iron-oxide nanoparticles and their in vivo evaluation as magnetic resonance imaging contrast agents. *Biomacromolecules* **2006,** 7, (11), 3132-3138.
91. Williams, D. N.; Gold, K. A.; Holoman, T. R. P.; Ehrman, S. H.; Wilson, O. C., Surface modification of magnetic nanoparticles using gum arabic. *Journal Of Nanoparticle Research* **2006,** 8, (5), 749-753.
92. Olle, B.; Bucak, S.; Holmes, T. C.; Bromberg, L.; Hatton, T. A.; Wang, D. I. C., Enhancement of oxygen mass transfer using functionalized magnetic nanoparticles. *Industrial & Engineering Chemistry Research* **2006,** 45, (12), 4355-4363.
93. Ditsch, A.; Laibinis, P. E.; Wang, D. I. C.; Hatton, T. A., Controlled clustering and enhanced stability of polymer-coated magnetic nanoparticles. *Langmuir* **2005,** 21, (13), 6006-6018.

94. da Silva, S. W.; Soler, M. A. G.; Gansau, C.; Buske, N.; Morais, P. C., Study of the interactions between the surface chemisorbed layer and the surrounding media in magnetite-coated nanoparticles using Raman spectroscopy. *Journal Of Magnetism And Magnetic Materials* **2001,** 226, 1890-1892.
95. Mikhailik, O. M.; Povstugar, V. I.; Mikhailova, S. S.; Lyakhovich, A. M.; Fedorenko, O. M.; Kurbatova, G. T.; Shklovskaya, N. I.; Chuiko, A. A., Surface-Structure Of Finely Dispersed Iron Powders.1. Formation Of Stabilizing Coating. *Colloids And Surfaces* **1991,** 52, (3-4), 315-324.
96. Hu, A. G.; Yee, G. T.; Lin, W. B., Magnetically recoverable chiral catalysts immobilized on magnetite nanoparticles for asymmetric hydrogenation of aromatic ketones. *Journal Of The American Chemical Society* **2005,** 127, (36), 12486-12487.
97. Bromberg, L.; Hatton, T. A., Nerve agent destruction by recyclable catalytic magnetic nanoparticles. *Industrial & Engineering Chemistry Research* **2005,** 44, (21), 7991-7998.
98. Bromberg, L.; Hatton, T. A., Decomposition of toxic environmental contaminants by recyclable catalytic, superparamagnetic nanoparticles. *Industrial & Engineering Chemistry Research* **2007,** 46, (10), 3296-3303.
99. Shaw, S. Y.; Chen, Y. J.; Ou, J. J.; Ho, L., Preparation and characterization of Pseudomonas putida esterase immobilized on magnetic nanoparticles. *Enzyme And Microbial Technology* **2006,** 39, (5), 1089-1095.
100. Safarik, I.; Safarikova, M., Magnetic nanoparticles and biosciences. *Monatshefte Fur Chemie* **2002,** 133, (6), 737-759.
101. Osaka, T.; Matsunaga, T.; Nakanishi, T.; Arakaki, A.; Niwa, D.; Iida, H., Synthesis of magnetic nanoparticles and their application to bioassays. *Analytical And Bioanalytical Chemistry* **2006,** 384, (3), 593-600.
102. Wang, D. S.; He, J. B.; Rosenzweig, N.; Rosenzweig, Z., Superparamagnetic Fe2O3 Beads-CdSe/ZnS quantum dots core-shell nanocomposite particles for cell separation. *Nano Letters* **2004,** 4, (3), 409-413.
103. Caruntu, D.; Cushing, B. L.; Caruntu, G.; O'Connor, C. J., Attachment of gold nanograins onto colloidal magnetite nanocrystals. *Chemistry Of Materials* **2005,** 17, (13), 3398-3402.
104. Eldridge, R. J., Moving-Bed Ion-Exchange With Magnetic Resins. *Reviews In Chemical Engineering* **1995,** 11, (3), 185-228.
105. Boyer, T. H.; Singer, P. C., A pilot-scale evaluation of magnetic ion exchange treatment for removal of natural organic material and inorganic anions. *Water Research* **2006,** 40, (15), 2865-2876.
106. Boyer, T. H.; Singer, P. C., Bench-scale testing of a magnetic ion exchange resin. for removal of disinfection by-product precursors. *Water Research* **2005,** 39, (7), 1265-1276.
107. Denizli, A.; Satiroglu, N.; Patir, S.; Bektas, S.; Genc, O., Magnetic polymethylmethacrylate microbeads carrying amine functional groups for removal of Pb(II) from aqueous solutions. *Journal Of Macromolecular Science-Pure And Applied Chemistry* **2000,** 37, (12), 1647-1662.
108. Ditsch, A.; Lindenmann, S.; Laibinis, P. E.; Wang, D. I. C.; Hatton, T. A., High-gradient magnetic separation of magnetic nanoclusters. *Industrial & Engineering Chemistry Research* **2005,** 44, (17), 6824-6836.

109. Ditsch, A.; Massachusetts Institute of Technology. Dept. of Chemical Engineering. Purification of recombinant proteins with magnetic nanoclusters. Thesis Ph. D. --Massachusetts Institute of Technology Dept. of Chemical Engineering 2005., 2005.
110. O'Shaughnessy, B.; Vavylonis, D., Irreversibility and polymer adsorption. *Physical Review Letters* **2003,** 90, (5).

Chapter 2

Amidoxime Modified Magnetic Nanoparticles

2.1 Introduction

Hydrolysis of carboxyl esters and phosphate esters is a commercially important reaction in the field of organic synthesis and environmental treatment. [1] Catalytic hydrolysis utilizes various catalysts to accelerate the hydrolytic reaction. This has been tested with carboxyl esters and many insecticides and chemical warfare agents that are organophosphate compounds. It has shown to have high specificity and dramatically enhanced reaction rates relative to spontaneous hydrolysis. [2-12] Studies of catalytic hydrolysis of carboxyl ester, *p*-nitrophenyl acetate (PNPA), include the use of enzymes, [4, 12] metal oxides and metal ion complexes with different ligands, [7, 13, 14] and strong nucleophiles. [15] The strong nucleophilic catalysts include oximes, [2, 3, 16] hydroxamic acids, [17, 18] iodosobenzoates, [19, 20] and hydro peroxides, [21, 22] etc. Most studies have concentrated on homogenous or micellar catalysis, neither of which affords the advantages of easy catalyst recycle. [23-25]

Magnetic nanoparticles have attracted attention for possible applications in biological and environmental separations because they permit fast and economical removal of target compounds from complex media by use of magnetic fields. [23, 24, 26, 27] The particles are colloidally stabilized by electrostatic and/or steric interactions from surface coating and readily dispersed in water without sedimentation. Magnetite nanoparticles are most commonly utilized and often prepared by co-precipitation of Fe(II) and Fe(III) salts in water. [26] Magnetic nanoparticles may also be functionalized by reactive groups and used as catalysts. [28-32] Because the particles are small, the surface area per unit volume is high and mass transfer resistances are small.[33]

In this chapter, colloidally stable magnetic nanoparticles with an average diameter of about 80 nm were prepared through co-precipitation of iron (II) and iron (III) chlorides in

the presence of a random copolymer of acrylic, vinylsulfonic, and styrene sulfonic acids. After controlled aggregation of the nanoparticles to form aggregates with a diameter of about 80nm, the exposed carboxyl groups were reacted with cyanoacetohydrazide to form a carbodiimide with a terminal nitrile group. Oximation with hydroxylamine led to formation of the amidoxime. The amidoxime-presenting magnetic nanoparticles were colloidally stable over a broad pH range presumably because of the strong surface charge and the resulting electrostatic repulsion. The catalytic activity of the particles was tested by the hydrolysis of *p*-nitrophenyl acetate. The presence of the amidoxime-presenting particles accelerated the hydrolysis rate significantly. The particles were readily recovered from the aqueous milieu by high gradient magnetic separation (HGMS) and reused with no loss of reactivity. Comparison with hydrolysis catalyzed by free malonohydroxamamide showed that the particles are more effective. Based on the analysis with a two-phase model, it is hypothesized that the enhancement is due to solubilization of the *p*-nitrophenyl acetate within the polymeric coating of the particles.

2.2 Experimental Section

2.2.1 Materials

Ferric chloride hexahydrate (97%), ferrous chloride tetrahydrate (99%), acrylic acid (99%), vinylsulfonic acid sodium salt (technical grade, 25% in water), 4-styrenesulfonic acid sodium salt hydrate, sodium metabisulfite, potassium persulfate (99%), poly(acrylic acid) (M_w = 5,000), *N*-(3-Dimethylaminopropyl)-*N'*-ethylcarbodiimide hydrochloride (EDC), cyanoacetohydrazide, 4-morpholineethanesulfonic acid (MES), hydroxylamine hydrochloride, and *p*-nitrophenyl acetate (PNPA) were purchased from Sigma-Aldrich Chemical Company (Milwaukee, WI) and used as received. Methanol, ammonium hydroxide (30% in water), and sodium hydroxide were purchased from Mallinckrodt Baker Inc. (Phillipsburg, NJ) and used as received. Malonohydroxamamide (tech) was purchased from Ryan Scientific (Mt. Pleasant, SC) and used as received. Water was generated by the Milli-Q water system.

2.2.2 Particle Synthesis and Modification

Particle precipitation took place in the presence of a random copolymer of acrylic acid (AA), vinylsulfonic acid sodium salt (VSA), and 4-styrenesulfonic acid sodium salt hydrate (SSA) with the molar ratio of 2:1:1. The pKa is 4.25, 0.53, and 0.60 for AA, vinyl sulfonic acid and 4-styrenesulfonic acid respectively. The last two pKa values were calculated by SPARC online property calculator. The AA-VSA-SSA copolymer was prepared according to a published procedure. [34] In brief, 1.05g of AA, 3.79g of VSA solution, and 1.5g of SSA were mixed with 0.1g of potassium persulfate as initiator and 0.4g of sodium metabisulfite as chain transfer agent. The solution volume was adjusted to 22mL by addition of water. Reaction was kept at 80°C for 3 hr. The molecular weight of the polymer was measured by GPC. The polymer solution was used directly for the particle synthesis without further purification.

Magnetic nanoclusters of primary magnetite particles (~7.5nm in diameter) were synthesized according to the published two-step procedure. [34] In brief, 40mL of water was added into three-neck flask and deaerated by nitrogen bubbling for 30min. Then iron (II) chloride tetrahydrate (0.86g, 4.3mmol) and iron (III) chloride hexahydrate (2.36g, 8.6mmol) were dissolved into the deoxygenated water and the resulting solution was heated to 80°C. 2.5ml of the previously prepared AA-VSA-SSA terpolymer solution was mixed with 6mL of 28% aqueous ammonium hydroxide and the mixture was quickly added to the iron salt solution, at which point the solution immediately turned black due to the formation of magnetite particles. The dispersion was stirred for 15 min. Then 1 g of aqueous 50%wt poly(acrylic acid) solution was added to the magnetite dispersion as a secondary polymer and the resulting dispersion was kept at 80°C with stirring for another 15min. After cooling, the particle dispersion was mixed with 50mL of acetone. The particles were removed from the supernatant by attracting them to an electromagnet and decanting the solution. The particles were then re-dispersed into 50ml of water and decanted after mixing with 50ml of acetone. This was repeated for a total of three times. The particles were finally dried under vacuum until a constant weight was attained. Then the particles were re-dispersed in 50mL of deionized water and sonicated for 1min using a Branson Sonifier Model 450 at 40% power output. The particle concentration was

20mg/ml. These particles are referred to as the "original particles" in the following discussion.

The carboxyl groups on the particle surface were then functionalized by attaching nitrile groups. To the above mixture was added 0.49g of MES to form a particle dispersion in 50mM MES buffer, and the dispersion pH was adjusted to 5.3 by gradual addition of 1M hydrochloric acid. Activating agent EDC (0.6g, 3.1mmol) was then added to the particle dispersion. The particle/EDC dispersion was allowed to equilibrate for 5min. Then 1g of cyanoacetohydrazide was added and the reaction mixture was kept at room temperature overnight with stirring. The nitrile-modified particles were then washed by magnetic decantation with addition of 50ml of acetone. After drying under vacuum overnight, particles were dispersed in 50mL of methanol. Control experiments without addition of EDC were also performed to validate the nitrile attachment.

The nitrile groups were then converted to amidoxime groups through the oximation reaction. [3] Hydroxylamine hydrochloride (1.35g, 1.94mmol) and sodium hydroxide (0.78g, 1.94mmol) were added to the particle dispersion. The reaction mixture was refluxed at 65°C overnight. Particles were then repeatedly washed by excess water and magnetic decantation and finally dried under vacuum until a constant weight was attained. These particles are referred to as "modified particles" in the following discussion.

2.2.3 Characterization

The molecular weight of original 2:1:1 polymer was measured with gel permeation chromatography (GPC). The prepared 2:1:1 polymer was purified by repeated washing with water dissolution and acetone precipitation. The fully clean polymer was dried in a vacuum oven until constant weight. GPC studies were performed by injecting a 0.1% (mass) solution of the polymer dissolved in 10mM of phosphate buffered saline (PBS) solution at pH 7.4 into an Ultrahydrogel Linear column (Waters Co., Milford, MA) with a Waters 2414 RI detector and 1X PBS solution as the eluent.

A Nexus-870 FT-IR spectrometer (Thermo Nicolet Corp., Madison, WI) was used in absorbance mode to determine the chemical bonds present on the particle surfaces. All particle samples were ground, mixed with KBr, and then pressed to form pellets. The KBr background was subtracted from the sample spectrum.

Dynamic light scattering (DLS) was used to measure the hydrodynamic diameters of the particles before and after modification. DLS experiments were performed with a Brookhaven BI-200SM light scattering system at a measurement angle of 90°. Sample temperature was kept at 25°C. Particle dispersion was adjusted to 0.005%wt with 0.01M buffer to keep the solution pH constant. The buffers used were citrate buffer for pH 4 to 6, phosphate buffer for pH 7 to 8, borate buffer for pH 9, carbonate buffer for pH 10 and 11, and phosphate buffer for pH 12. Particle diameter was extracted from the measured autocorrelation function by using the vendor-supplied software to fit an exponential model. Quoted particles sizes are based on intensity-averaged size distributions and the number average of four independent measurements.

Zeta potentials were measured on a Brookhaven ZetaPals Zeta Potential Analyzer. Particles were diluted to 0.005%wt Fe_3O_4 within 10mM buffer solution and 0.1M sodium chloride prior to measurement. Buffers used were the same ones used in DLS measurements. The zeta potential was converted from the electrophoretic mobility (μ_e) of the particles measured over 25 cycles by fitting to the Smoluchowski equation, as shown in Equation 2-1, where η and ε are the viscosity and dielectric constant of the dispersion medium respectively. The Smoluchowski equation requires that the particle size be much larger than the Debye length of the electrical double layer. The Debye lengths in 0.1M of 1:1 and 2:1 electrolytes solution are 0.96nm and 0.56nm at 25°C respectively. Since particles were larger than 70nm, the Smoluchowski equation was always applicable. The quoted zeta potentials are number averages of five measurements.

$$\zeta = \frac{\eta}{\varepsilon}\mu_e \qquad \textbf{Equation 2-1}$$

Transmission electron microscopy (TEM) analysis was performed on a JEOL 200CX microscope (200kV) to analyze the cluster structures before and after the modification reaction. Samples were prepared by evaporating dilute particle solutions on carbon-coated films.

A thermo gravimetric analyzer (TGA) was utilized to measure the particle weight change with increasing temperature to determine the relative polymer content of the functionalized particles. The analysis was conducted on a TGA Q50 instrument (TA Instruments). Approximately 15mg of dried magnetic particles were loaded into the sample pan and the sample pan was then inserted into the furnace purged with nitrogen to prevent oxidation. The heating profile in the TGA was as follows: heat to 150°C at 5°C/min; hold at 150°C for 30min; heat to 900°C at 5°C/min. The sample weight was then recorded as a function of temperature.

Elemental analysis for nitrogen was performed at Atlantic Microlab, Inc. (Norcross, GA) to quantify the functional groups present after the particle modification.

2.2.4 Kinetics Measurement

Hydrolysis of *p*-nitrophenyl acetate was followed by using a Hewlett-Packard 8453 UV/Vis spectrophotometer. The hydrolysis product, *p*-nitrophenol ion, has a strong absorbance at 404nm. Samples were measured at 25°C and solution pH was kept at 8 in 50mM Tris buffer to prevent pH change during the hydrolysis. Reaction systems comprised of magnetic particles with concentrations of 1 to 4mg/ml, 0.25mM *p*-nitrophenyl acetate substrate, 0.2M NaCl, 50mM Tris buffer at pH 8, and 20%vol ethanol in water solution. The presence of ethanol was to facilitate PNPA solubilization and these concentrations were overall concentrations in the final reaction mixture. Samples of the reaction mixture were withdrawn at selected intervals and the magnetic particles were removed by a high gradient magnetic separation (HGMS) device and a 50mM Tris buffer at the same pH was used to wash out of the column any possibly trapped hydrolysis product. The HGMS device was an L-1CN Frantz canister separator supplied by S. G. Frantz Co., Inc. (Trenton, NJ). The system consisted of a cylindrical plastic column

packed with type 430 fine-grade stainless steel wool (40-66μm diameter) also supplied by S. G. Frantz Co., Inc. The packing fraction was 12%vol. A magnetic field was generated by an electromagnet with an intensity of 1.3 Tesla between the two plates, as measured by a handheld magnetometer. The flow rate through the column was 1ml/min. The liquid flow was controlled by a peristaltic pump. Recycling of the magnetic particles was performed by passing the previous reaction mixture through the column. The electromagnet was then turned off and the particles were fully washed out of the column with 20ml of deionized water. Particles were collected through magnetic decantation with addition of 20ml of acetone and dried at 50°C in oven until constant weight. Particles were then dispersed into water to form a solution with the same particle concentration as that before the recycle. The particle solution was then subjected to the same reaction procedure as discussed above.

PNPA hydrolysis catalyzed by free malonohydroxamamide, which has two amidoxime groups, was also performed with 1 to 4mM of amidoxime, 0.05mM *p*-nitrophenyl acetate substrate, 0.2M NaCl, and 50mM Tris buffer at pH 8 in the final reaction mixture. The kinetic parameters from this homogenous system were compared with those from the particle system.

2.2.5 PNPA Solubilization on Particle Surface

The hydrophobic absorption of *p*-nitrophenyl acetate on the surfaces of the modified magnetic particles was determined as follows. 2ml of 5%wt of the amidoxime modified particle dispersion in a 0.25M sodium chloride solution was mixed with 0.5ml of 0.4mM PNPA ethanol solution and kept at pH 7 to minimize hydrolysis. This mixture was similar to that used for kinetic measurements. The dispersion mixture was put into a Centriprep® YM-50 centrifugal filter unit and centrifuged at 1500g for 5min. Then 1ml of the obtained pure liquid was mixed with 1ml of 1M sodium hydroxide solution and the mixture was kept at room temperature for one hour to let PNPA be fully hydrolyzed. The *p*-nitrophenol ion concentration in the final mixture was determined on a UV/Vis spectrophotometer at an absorbance of 404nm. The above procedure was carried out again without addition of any particles to get the reference concentration under the same

conditions. The difference in the *p*-nitrophenol ion concentration was used to calculate the absorption of PNPA by the particles.

2.3 Results and Discussion

2.3.1 Particle Preparation and Characterization

Applications of magnetic particles in aqueous media require colloidal stability and recyclability of the particles. Particles can be stabilized colloidally by steric or electrostatic interactions or both. Small particles offer large surface areas and a resulting ability to present more functional groups than is possible with larger particles of the same total weight. However, individual magnetic particles with sizes less than 10 nm are not captured efficiently by HGMS because of the small magnetic forces acting on the particles and the relatively strong diffusive forces resulting from the particle concentration gradient. [35] However, it has been shown that magnetic nanoparticle clusters with a hydrodynamic diameter larger than 50 nm can be effectively captured by HGMS.[36]

Therefore, magnetic clusters of many primary magnetic particles were synthesized by co-precipitation of the iron chlorides in the presence of chelating polymers through a two-step procedure described previously. [34, 36] A terpolymer was prepared according to Scheme 2-1 with weighted average molecular weight of 6,000 and chelated to the particle surface as the first coating.

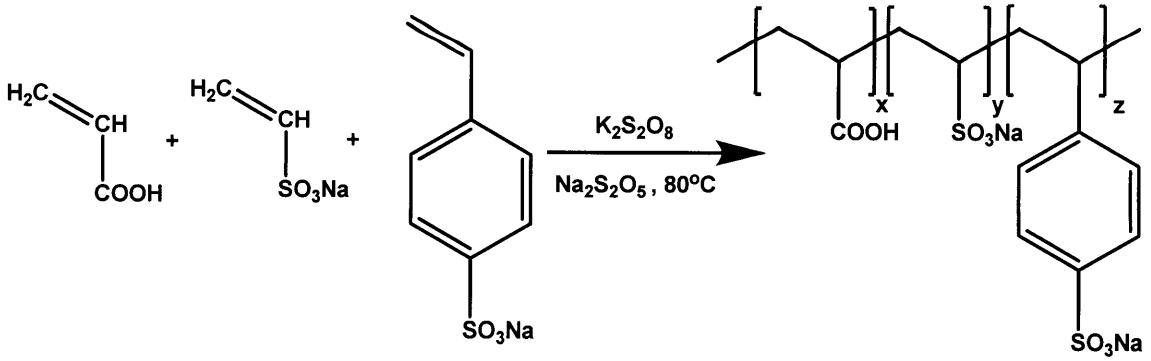

Scheme 2-1. Preparation of the first coating polymer of AA-VSA-SSA (2:1:1)

In this coating copolymer, acrylic acid provided carboxyl groups to chelate with magnetite surface, while vinyl sulfonic acid (VSA) and styrenesulfonic acid (SSA)

provided pH-independent negative charges over a broad range of solution pH, and SSA afforded hydrophobicity necessary to increase coating thickness and enhance particle stability. [34, 37] The prepared magnetic clusters were stabilized colloidally by electrostatic repulsion and withstood months in water without noticeable sedimentation even when dispersed in 1M sodium chloride solutions.

The precursor attachment is depicted in Scheme 2-2, in which the precursor molecules formed carbonyl hydrazide bonds with the free carboxyl groups on the particle surfaces.

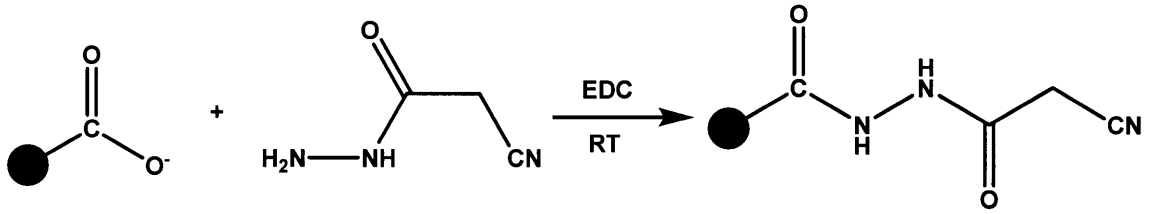

Scheme 2-2. Attachment of nitrile groups through carbodiimide chemistry

Cyanoacetohydrazide was utilized because it provided both a hydrazide group for carbonyl hydrazide bond formation and a nitrile group that could be converted subsequently into a nucleophilic amidoxime group. Nucleophilic properties of amidoxime in hydrolytic reactions of PNPA and organophosphates have been demonstrated. [3, 38] The modified particles were tested for the presence of nitrile groups by FT-IR and the results are shown in Figure 2-1. Major absorption bands were seen at 625, 1570, and 3440cm^{-1}, corresponding to vibrational frequencies of magnetite, carboxyl groups, and surface hydroxyl groups from the surface FeOH and chemisorbed water on the magnetite, respectively. [39-41] After the modification, two major absorption bands appeared at 1710cm^{-1} and 2250cm^{-1}, corresponding to the carbonyl amide and nitrile stretching, respectively. Analogous control procedures applied to the system without the activating agent (EDC) did not result in particles with any detectable presence of nitrile groups. This suggested that the above procedure successfully produce particles with nitrile groups chemically bonded to the particle surface.

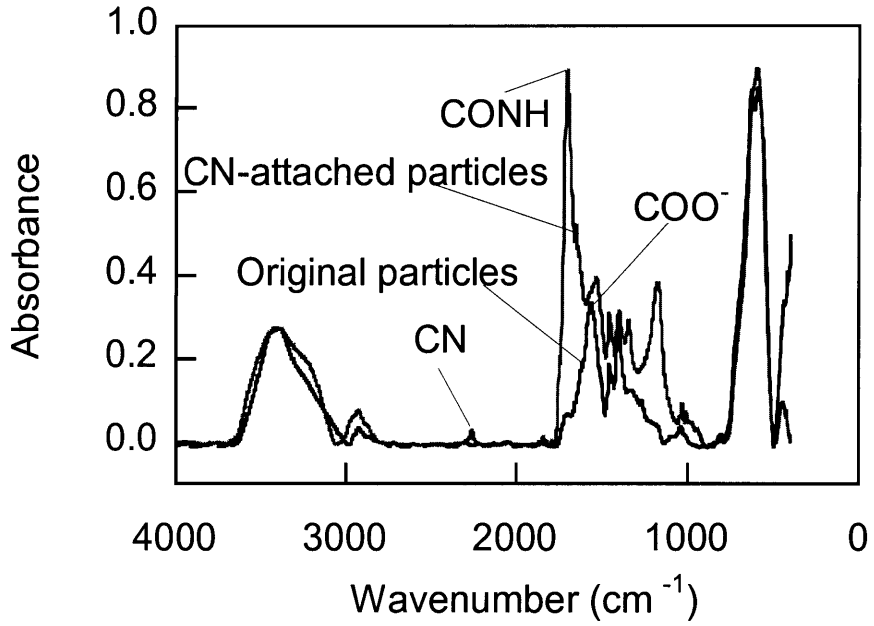

Figure 2-1. IR spectra of particles before and after nitrile attachment. Black line was from the original particles and the red line from the nitrile-attached particles.

Attached nitrile groups were then transformed into amidoxime groups through the oximation reaction shown in Scheme 2-3.

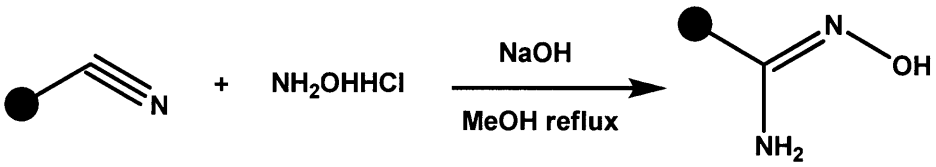

Scheme 2-3. Oximation of nitrile groups into amidoxime.groups

FT-IR test results of the oximated particles are shown in Figure 2-2. The appearance of an absorption peak at 1680cm^{-1}, corresponding to oxime groups, and the disappearance of nitrile groups suggest that the nitrile groups were successfully converted into amidoxime groups. It has been shown that carboxyl groups can be transformed into hydroxamic acid groups by hydroxylamine. [42] Control experiments were performed to check on the possibility by subjecting the original particles to the same conversion procedures as used for the modified particles. The control samples did not show any reactivity for PNPA hydrolysis, which suggests that carboxyl groups were not transformed into hydroxamic groups by this particular procedure.

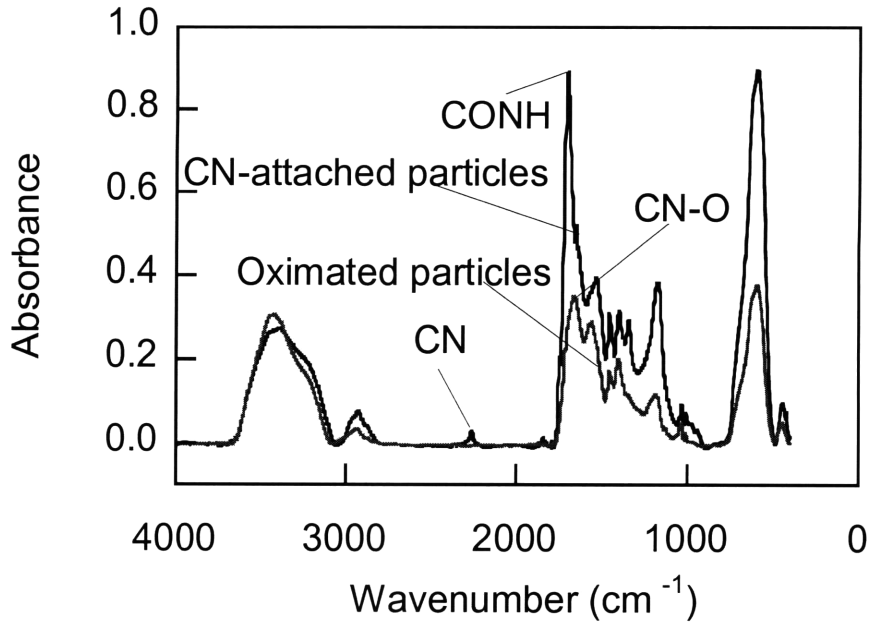

Figure 2-2. IR spectra of particles before and after oximation reaction. Black line was from the CN-attached particles and the red line from the oximated particles.

TEM pictures of the particle clusters before and after the reaction are shown in Figure 2-3. Very low particle concentrations were utilized in order to ensure that the results are depictions of clusters and not of artificial clustering of the particles during TEM preparation. As seen in Figure 2-3, particles after nitrile attachment and oximation reaction remained in the form of clusters. This indicated that the reactions did not change the particle morphology.

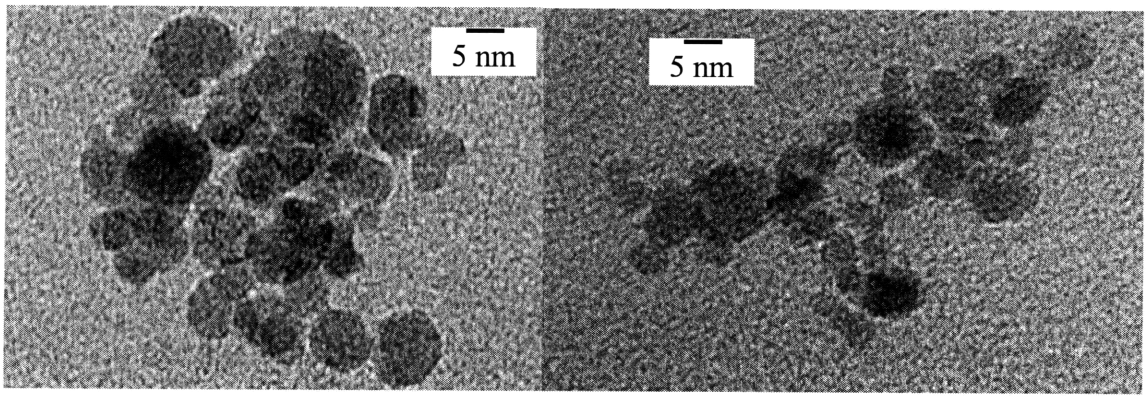

(a) (b)

Figure 2-3. Cluster structure before (a) and after (b) overall chemical modification. Samples were prepared by putting a water dispersion of particles at 0.005wt% on the TEM grid and evaporating water at room temperature.

Hydrodynamic diameters of prepared particles were determined by dynamic light scattering (DLS). As shown in Figure 2-4, particle size is very similar to that of the original particles over the pH range of 5 to 12. This indicated the absence of agglomeration and particle suitability for recovery by high gradient magnetic separation (HGMS) over the normal pH operational range. [36]

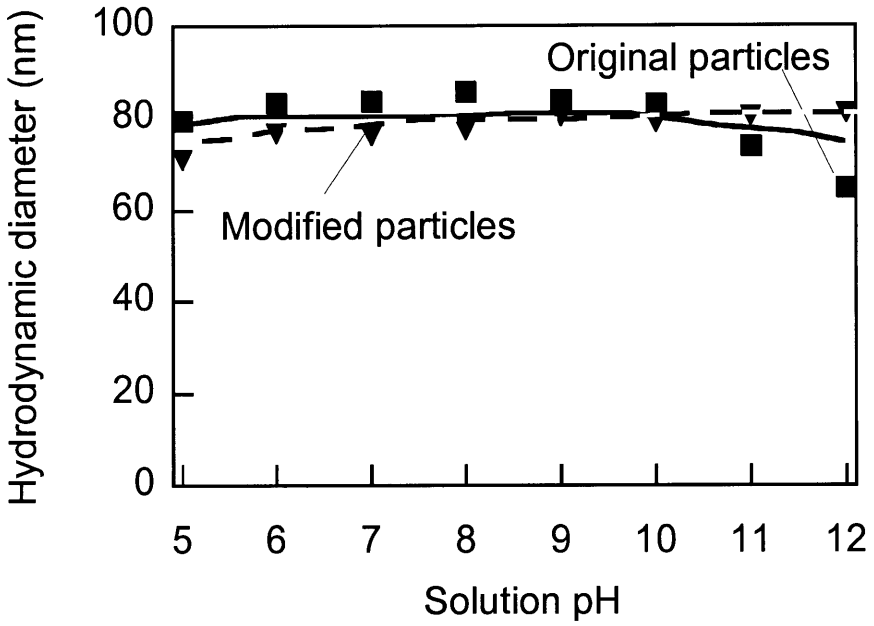

Figure 2-4. Size comparison before and after modification reaction at various solution pH. Original particles were particles from the two-step synthesis procedure and modified particles were those after the nitrile-attachment and oximation reaction. Particle concentration was kept at 0.005wt% for measurement. All samples were measured in 0.01M buffer, citrate buffer for pH 5 to 6, phosphate buffer for pH 7 to 8, borate buffer for pH 9, carbonate buffer for pH 10 and 11, and phosphate buffer for pH 12.

Zeta potential measurements were performed to analyze surface charges of the magnetic particles. Zeta potentials of particles at various pH values are shown in Figure 2-5. The original particles were strongly negatively charged over the whole pH range studied because of the presence of sulfonic and carboxyl groups. Since they have a pKa value of 4.25, the carboxyl groups start to become protonated at around pH 5 and therefore the negative charge decreases with decreasing solution pH. After the modification, particles were still strongly negatively charged due to the presence of the sulfonic groups, which have pKa values less than 1. However, the electrokinetic potential of the modified particles was less negative than that of the original particles, which can be attributed to

the fact that carboxyl groups reacted with amine groups and lost their negative charge. The amidoxime groups have a pKa value around 10.6 and this causes the gradual decrease of zeta potential in the high solution pH range. At relatively lower pH, the surface charges became similar in both cases, indicating that the sulfonic groups were playing the dominant role. Because of the strong surface charge, both particles were able to maintain excellent colloidal stability for months without observable sedimentation at neutral pH.

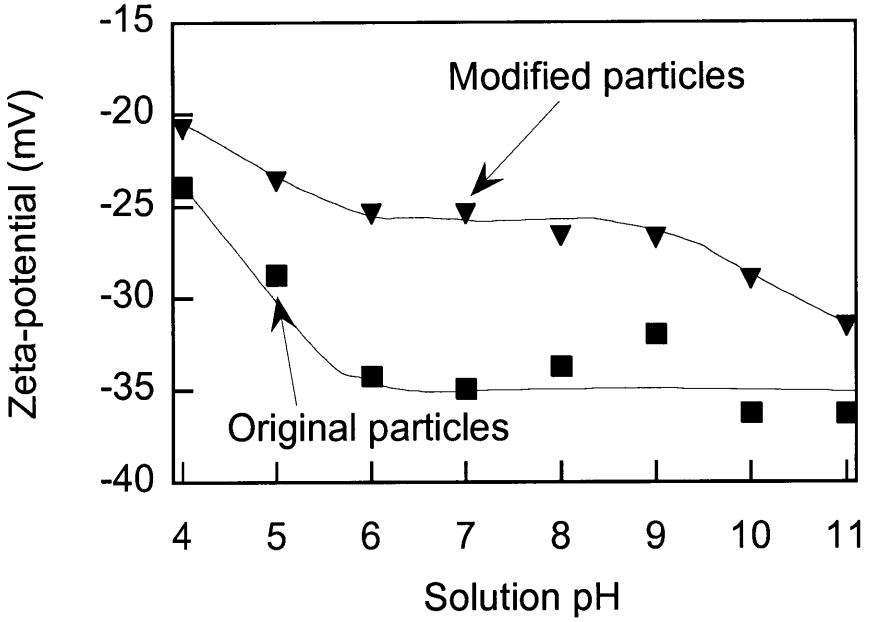

Figure 2-5. Zeta potential of particles before (square) and after (triangle) the modification procedure at various solution pH. Particle concentration was kept at 0.005%wt for measurement. All samples were measured in 0.01M buffer and 0.1M of NaCl, citrate buffer for pH 4 to 6, phosphate buffer for pH 7 to 8, borate buffer for pH 9, carbonate buffer for pH 10 and 11.

The magnetic particles before and after the chemical modification were analyzed with thermo gravimetric analyzer (TGA) to determine the amount of chemically bound material on the particles after they were purified and dried. The TGA results are shown in Figure 2-6, in which the residual mass percentage is plotted as a function of temperature. For the original particles, the attached polymer was decomposed in two separate phases. The first phase was probably due to decomposition of the side chains of the attached polymer. The second phase started at around 550°C as the chemically bound groups on the magnetite surface started to decompose. For the modified particles, the second phase

started around the same temperature as the first phase was finished. The initial weight loss of the modified particles was much more than that of the original particles, indicating that the attached functional groups were decomposed at this stage in addition to the previously mentioned polymer side chains. The residual magnetite weight percentage was used to compute the bound-polymer/magnetite mass ratios, which were found to be 0.60 and 0.78 before and after the chemical modification. The polymer/magnetite ratio was also measured through iron titration test to be around 0.70 and 0.85 respectively, consistent with the TGA measurements.

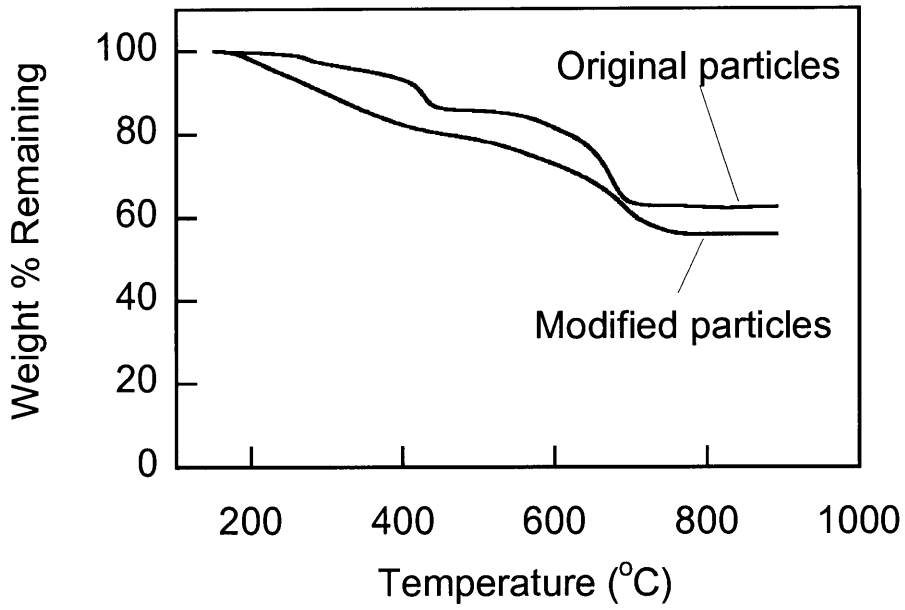

Figure 2-6. TGA analysis of magnetic particles before and after the chemical modification. The initial faster weight loss and final weight percentage difference were from the attachment of amidoxime groups.

Elemental analysis showed that the nitrogen content of the particles was 3.32%wt. This nitrogen weight content was converted into an average molar concentration by assuming that all EDC-activated carboxyl groups reacted with cyanoacetohydrazide and that all nitrile groups were completely converted into amidoxime groups. Based on the fact that one functional group contains four nitrogen atoms, 1mg/mL particle solution corresponded to 0.59mM functional amidoxime groups assuming that the functional groups are homogenously distributed in the solution.

2.3.2 Hydrolysis Kinetics of *p*-Nitrophenyl Acetate

Hydrolysis of *p*-nitrophenyl acetate has been studied extensively under a wide range of conditions in the presence of various homogenous catalysts. [2, 5-8, 12] The present work is unique in that we have been able to combine the advantages of both homogenous and heterogeneous systems. Because the particle size was very small and functional groups were located on the particle surface, mass transfer resistance was minimal and the particles functioned much like homogenous catalysts. [26] However, the functional groups were carried on magnetic particles, which made recycling and reuse of the catalyst by HGMS fairly straightforward.

In the presence of amidoxime groups, PNPA is hydrolyzed both spontaneously and by nucleophilic substitution as shown in Scheme 2-4. [3] The amidoxime groups on the particle surface attack the ester group, forming an intermediate complex and releasing *p*-nitrophenol. It has been shown that the substitution is a second order reaction. [12] The complex is then deacetylated by hydroxide ions and the original amidoxime groups are regenerated for further catalytic reaction.

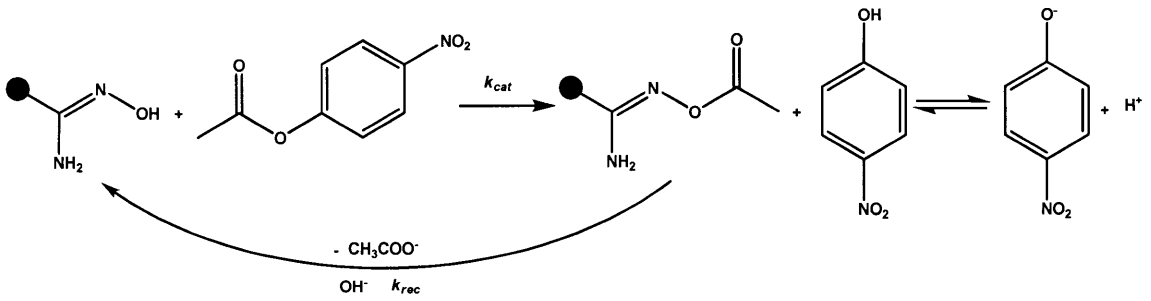

Scheme 2-4. Catalytic hydrolysis of PNPA by amidoxime groups on the particle surfaces

Since the pK_a of *p*-nitrophenol is 7.2 and the reaction solution was kept at pH 8, the hydrolyzed product was in the form of both *p*-nitrophenol and *p*-nitrophenol ions. The total concentration of hydrolyzed product was calculated from the measured concentration of *p*-nitrophenol ions through Equation 2-2.

$$[PNP]_{total} = [PNP^-]_{measure}\left(1+1/10^{pH-pK_a}\right) = 1.16[PNP^-]_{measure} \qquad \textbf{Equation 2-2}$$

Because the dissociation of *p*-nitrophenol releases protons, which can change the hydrolysis rate, 50mM Tris buffer was used to keep pH constant at 8.

Figure 2-7 shows the concentration change of the hydrolyzed product with time on the addition of different amounts of amidoxime modified particles. With unmodified particles, overall hydrolysis was no different than spontaneous hydrolysis, indicating that the original particles had negligible effect. In the presence of modified particles, generation of hydrolyzed product was much faster, indicating that hydrolysis was clearly accelerated. As the particle concentration increased, the reaction rate also increased.

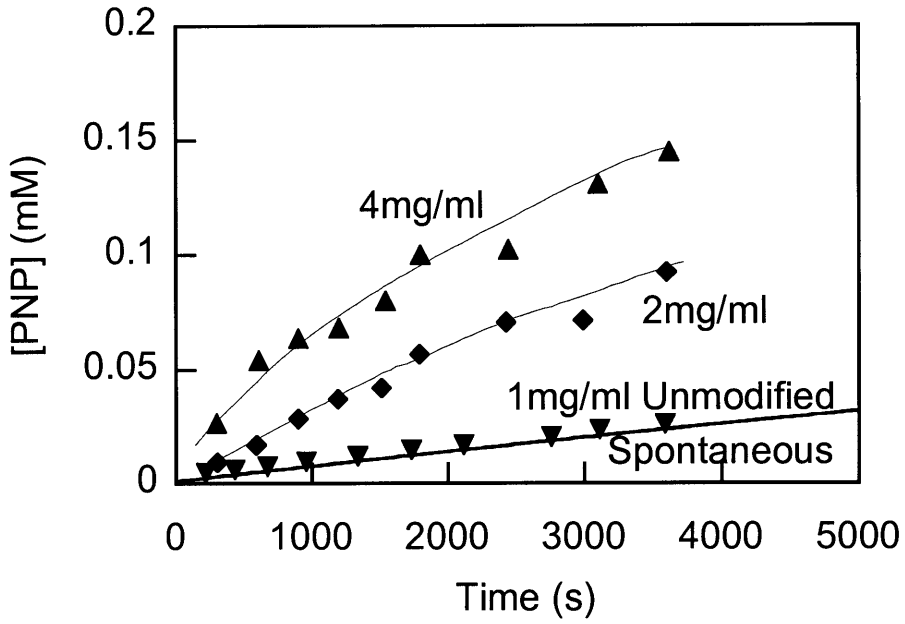

Figure 2-7. Concentration change of hydrolyzed product with addition of various particles. Spontaneous hydrolysis (black line), hydrolysis with 1mg/ml of unmodified particles, and with 2mg/ml and 4mg/ml of functionalized particles. Solution pH was kept at 8 with 50mM Tris buffer and 25°C. $[PNPA]_0 = 0.25mM$.

In the hydrolysis system, the hydrolysis product was generated by the spontaneous reaction, hydrolysis by hydroxyl ions and hydrolysis by the added nucleophiles. The reaction rate can be described by Equation 2-3. [20]

$$r = \frac{d[NP]}{dt} = \left(k_{spon} + k_{OH}\left[OH^-\right] + k_{cat}\left[NOH^-\right]\right)[PNPA] = r_{spon} + r_{cat} \qquad \textbf{Equation 2-3}$$

During the initial stage of the hydrolysis reaction, the majority of nucleophiles remained in the active form and the concentration of nucleophiles was roughly constant. Since system pH was kept constant, the first two terms in the parenthesis were also constant. Thus this equation is pseudo-first order and integrates to yield Equation 2-4.

$$-\ln\left(1-[PNP]_t/[PNPA]_0\right)=k_{obs}t \qquad \textbf{Equation 2-4}$$

in which

$$k_{obs}=k_{spon}+k_{OH}\left[OH^-\right]+k_{cat}\left[NOH^-\right] \qquad \textbf{Equation 2-5}$$

Raw kinetic data were transformed according to Equation 2-4 and plotted against time as shown in Figure 2-8, where the slope of the plot is k_{obs}. The observed kinetics constants were measured for a series of particle concentrations and the initial hydrolysis rates obtained from the above procedure were plotted with regard to particle concentrations, as shown in Figure 2-9. Spontaneous hydrolysis and hydrolysis by hydroxide ions were measured separately. The kinetic constant k_{cat} was then calculated by fitting the data points with a linear function from the plot of k_{obs} versus amidoxime concentration. The second order kinetic constant is $4.6\times10^{-5}(\text{mg/ml})^{-1}\text{s}^{-1}$ based on the particle weight concentration and $7.9\times10^{-5}(\text{mM})^{-1}\text{s}^{-1}$ based on the molar concentration of the amidoxime groups.

2.3.3 Particle Recycle

Because of the superparamagnetic property of the magnetic clusters, [34] particles were able to be recovered fully from the column after the first batch of reaction with the substrate. The PNPA hydrolysis kinetic constants with the recycled particles were obtained using the same experimental procedure as discussed above. As shown in Figure 2-10, the recycled particles had reactivity very similar to that of the original particles.

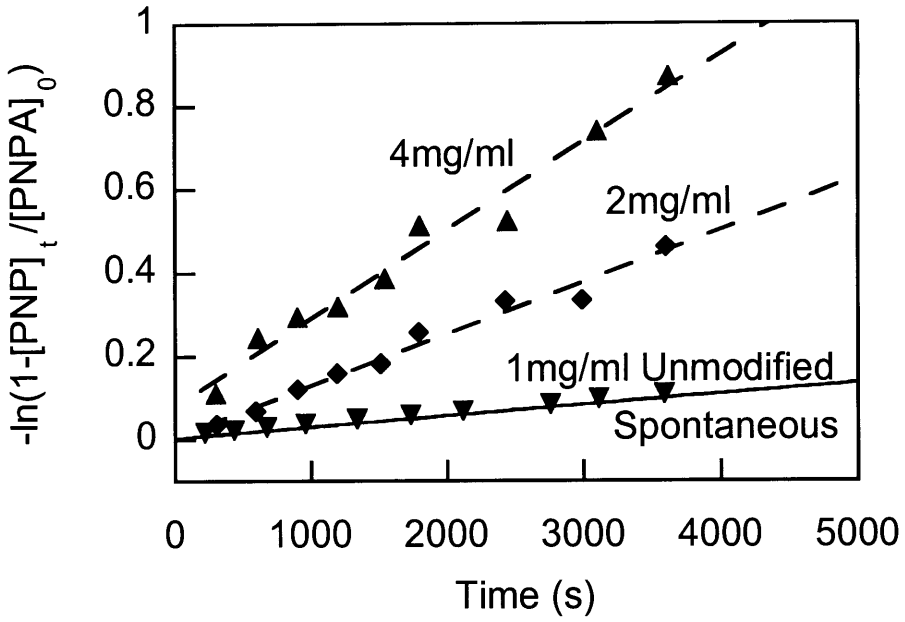

Figure 2-8. Pseudo-first order hydrolysis kinetics of PNPA with addition of various particle concentrations from spontaneous hydrolysis, hydrolysis with 1mg/ml unmodified particles, and that with 2mg/ml and 4mg/ml functionalized particles. Solution pH was kept at 8 with 50mM Tris buffer and 25°C. $[PNPA]_0 = 0.25mM$.

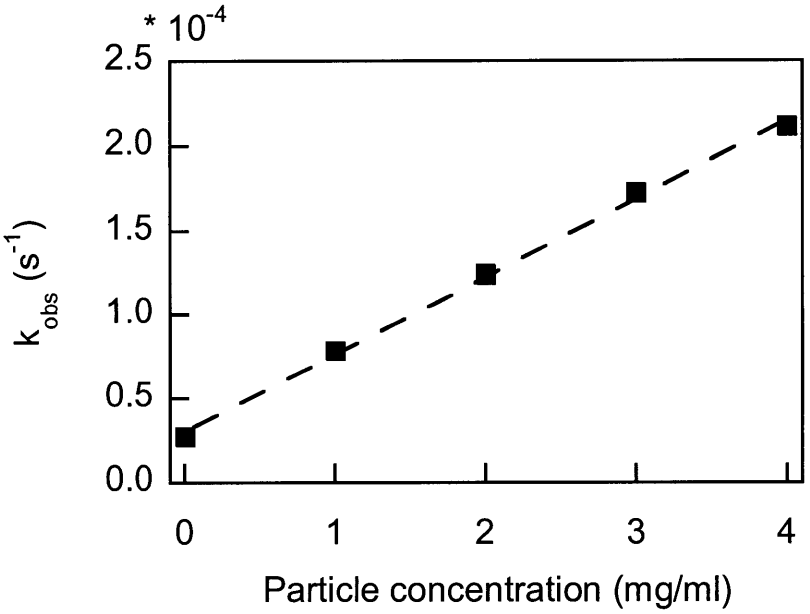

Figure 2-9. Dependence of the observed hydrolysis kinetics constants on particle concentration. The slope of the line provided the second order kinetic constant: k_{cat} = $4.6\times10^{-5}(mg/ml)^{-1}s^{-1}$ for particle dispersion.

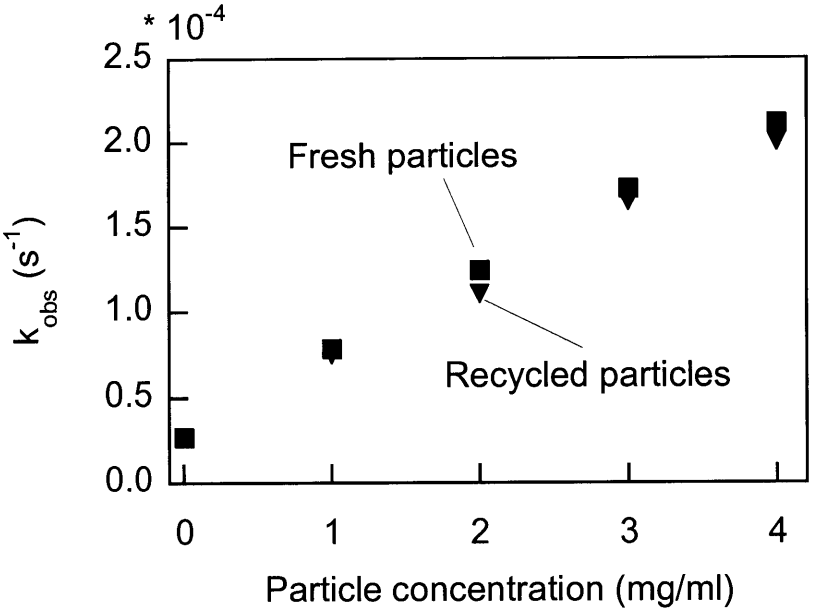

Figure 2-10. Observed hydrolysis kinetic constants of fresh particles (square) and recycled particles (triangle) at various particle concentrations. Solution was kept at pH 8 with 50mM Tris buffer and 25°C. $[PNPA]_0 = 0.25mM$.

2.3.4 Comparison with Homogenous Hydrolysis and Two-Phase Model

In order to determine whether the particles played a role other than that of simply providing functional groups, PNPA hydrolysis by functionalized particles was compared with that by a solution of the amidoxime compound, malonohydroxamamide, the structure of which is shown in Scheme 2-5.

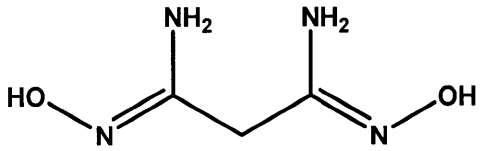

Scheme 2-5. Structure of malonohydroxamamide

Hydrolysis kinetics were measured under the same conditions as those for the particle system, including the addition of 50mM Tris buffer to keep system pH at 8, 0.2M of sodium chloride to maintain constant ionic strength, and various amounts of amidoxime. Because the amount of amidoxime added to the system was in the milli-molar range and much larger than the substrate concentration of 0.05mM, hydrolytic kinetics also showed pseudo-first order character. The kinetic constants, k_{obs}, for homogenous amidoxime

were obtained in the same way as those from the particle system. The comparison between particle and homogeneous systems is shown in Figure 2-11. Second-order kinetic constants were $4.6\times10^{-2}M^{-1}s^{-1}$ for malonohydroxamamide and $7.9\times10^{-2}M^{-1}s^{-1}$ for particle solution. The kinetic constants for the particle system were the same as those in Figure 2-9 with the particle weight concentration converted into amidoxime concentration according to the elemental analysis results.

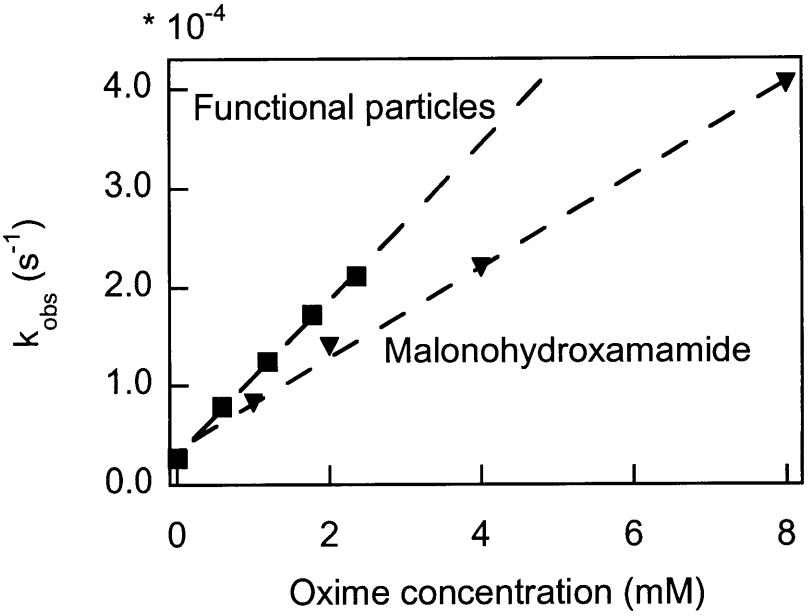

Figure 2-11. Comparison of observed hydrolytic kinetic constants catalyzed by malonohydroxamamide (triangle) and functionalized particles (square). Second-order kinetic constants were k_{cat} = $4.6\times10^{-2}M^{-1}s^{-1}$ for malonohydroxamamide and k_{cat} = 7.9 × $10^{-2}M^{-1}s^{-1}$ for particle solution. Solution pH was kept at 8 with 50mM Tris buffer and 25°C. $[PNPA]_0$ = 0.25mM for particle system and $[PNPA]_0$ = 0.05mM for malonohydroxamamide system.

A two-phase model, also called the pseudo-phase model, was invoked to explain why the particle system exhibits a larger second-order kinetic constant than does the homogenous amidoxime system, as represented in Scheme 2-6. The two phase model has been used extensively to describe the catalytic behavior of micellar systems [2, 5, 43-45]

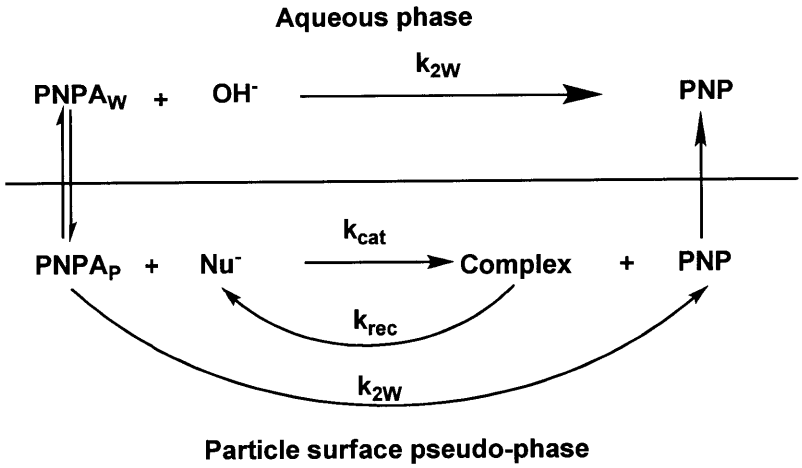

Scheme 2-6. Pseudo two-phase mechanism for the PNPA hydrolysis with the presence of amidoxime modified magnetic particles.

In the aqueous phase, PNPA undergoes spontaneous hydrolysis as described by Equation 2-6.

$$r_{bulk} = \left(k_{spon} + k_{OH}\left[OH^-\right]_{bulk}\right)\left[PNPA\right]_{bulk} \qquad \textbf{Equation 2-6}$$

Bulk concentrations refer to those in the aqueous phase. Given the certain degree of hydrophobic nature on the particle surface, the PNPA substrate could distribute favorably onto the particle surface, enabling a higher substrate concentration on the particle surface to be attained than that in the aqueous phase. Similar phenomena have been observed in absorption of hydrophobic proteins onto similar particles. [23] PNPA was also observed to be favorably distributed into an organic phase within water/organic solvent mixtures. [4] On the particle surface where the functional groups were located, the PNPA substrate underwent both the spontaneous hydrolysis and catalytic hydrolysis by amidoxime groups through the mechanism shown in Scheme 2-4. The decomposition reaction on the particle surface was therefore described by Equation 2-7.

$$r_{local} = \left(k_{spon} + k_{OH}\left[OH^-\right]_{local} + k_{cat}\left[NOH\right]_{local}\right)\left[PNPA\right]_{local} \qquad \textbf{Equation 2-7}$$

All concentrations in Equation 2-7 refer to those in the particle surface pseudo-phase. The overall concentration of hydrolyzed product, *p*-nitrophenol, was described by Equation 2-8.

$$\frac{d[PNP]_{overall}}{dt} = r_{bulk}\left(1-\frac{V_{local}}{V_{total}}\right)+r_{local}\frac{V_{local}}{V_{total}} \qquad \textbf{Equation 2-8}$$

in which V_{local} is the volume of the particle phase and V_{total} is the total volume, including both the aqueous phase and the particle phase. The following equations describe the relationship between concentrations in the bulk phase and those in the particle phase. The favorable localization of PNPA on the particle surface can be described by Equation 2-9.

$$[PNPA]_{local} = K_S[PNPA]_{bulk} \qquad \textbf{Equation 2-9}$$

in which K_s is the distribution coefficient of PNPA between the two phases.

The averaged concentration of PNPA based on the overall system is defined according to Equation 2-10.

$$(V_{total}-V_{local})[PNPA]_{bulk}+V_{local}[PNPA]_{local}=[PNPA]_{overall}V_{total} \qquad \textbf{Equation 2-10}$$

Because the particle volume fraction was small, estimated to be 0.3%vol for 1mg/ml particle dispersion, V_{local} was neglected from the first term and Equation 2-10 was simplified to Equation 2-11.

$$[PNPA]_{bulk} = \frac{[PNPA]_{overall}}{1+K_S\beta} \qquad \textbf{Equation 2-11}$$

in which $\beta = \frac{V_{local}}{V_{total}}$ is the volume fraction of the particle phase. The concentration of catalytic groups is given by Equation 2-12.

$$[NOH]_{local} = \frac{V_{total}}{V_{local}}[NOH]_{overall} = 1/\beta[NOH]_{overall}$$ **Equation 2-12**

These concentration relationships were substituted into Equation 2-8 and further simplified to Equation 2-13.

$$\frac{d[PNP]_{overall}}{dt} = \left(k_{spon} + k_{OH} \frac{[OH^-]_{bulk} + K_S\beta[OH^-]_{local}}{1+K_S\beta} + \frac{k_{cat}[NOH]_{local} K_S\beta}{1+K_S\beta} \right)[PNPA]_{overall}$$

Equation 2-13

For the particle concentration (less than 5mg/ml) studied previously, the particle volume fraction was less 1.5 percent. According to the literature, the distribution coefficient of PNPA between cumene and water is 100. [4] Because the hydrophobicity on the particles was much smaller than that of pure cumene, the K_S was much less than 100. As a result, $K_S\beta \ll 1$. This enables further simplification of Equation 2-13 to Equation 2-14.

$$\frac{d[PNP]_{overall}}{dt} = \left(k_{spon} + k_{OH}[OH^-] + K_S k_{cat}[NOH]_{average}\right)[PNPA]_{overall}$$ **Equation 2-14**

The term in the parenthesis represents the observed kinetic constant of the PNPA hydrolysis catalyzed by amidoxime modified particles, shown in Equation 2-15.

$$k_{obs} = k_{spon} + k_{OH}[OH^-] + K_S k_{cat}[NOH]_{average}$$ **Equation 2-15**

Comparison with the hydrolysis catalyzed by homogenous amidoxime molecules shown in Equation 2-5 indicated a clear difference between the two systems. The slope of the k_{obs} plot against amidoxime concentration is $K_S k_{cat}$ for the particle system and k_{cat} for the homogenous system. The slope difference in Figure 2-11 was attributed to the concentration effect of the substrate on the particle surface combined with the fact that

functional groups were only located on the particle surface. This combined concentration effect resulted in the enhancement of reactivity in the particle system versus that in the homogenous system. If the substrate was further assumed to undergo the same reaction mechanism with the same second order kinetic constants in both cases, it is concluded that the surface concentration of PNPA substrate was about twice that in the bulk solution. The absorption measurement has shown that presence of 5%wt particle reduced the final absorbance of *p*-nitrophenol ions from 0.574 to 0.517, about 10 percent concentration change. The volume fraction of the 5%wt particles in the dispersion was estimated to be 15%vol. These numbers were substituted into Equation 2-11 and K_s value was calculated to be 1.8. This supported the above model of preferred solubilization of PNPA on the particle surface.

2.4 Summary

In this chapter, amidoxime modified magnetic particles were prepared with hydrodynamic diameters of around 80nm. The particles were captured effectively by HGMS. Particles were stabilized by electrostatic interactions owing to the strong surface charge. Particle stability and morphology were not significantly altered after the chemical modifications to carry the functional amidoxime groups. Particles were tested against the hydrolysis of the model ester compound, *p*-nitrophenyl acetate, and were shown to accelerate the hydrolysis reaction significantly. The presence of hydrophobic domains on the particle surfaces concentrated the substrate and therefore caused enhancement of catalytic activity compared with homogenous amidoxime systems.

2.5 Bibliography

1. Zheng, Y.; Duanmu, C.; Gao, Y., A magnetic biomimetic nanocatalyst for cleaving phosphoester and carboxylic ester bonds under mild conditions. *Organic Letters* **2006,** 8, (15), 3215-3217.
2. Ghosh, K. K.; Kolay, S.; Satnami, M. L.; Moore, S.; Palepu, R. M.; Dafonte, P. R., Kinetics of reaction of oximate alpha-nucleophiles with p-nitrophenyl acetate in alkyltriphenyl phosphonium bromide micelles. *Journal Of Dispersion Science And Technology* **2007,** 28, (2), 213-218.

3. Chen, L.; Bromberg, L.; Hatton, T. A.; Rutledge, G. C., Catalytic hydrolysis of p-nitrophenyl acetate by electrospun polyacrylamidoxime nanofibers. *Polymer* **2007,** 48, (16), 4675-4682.
4. Abuin, E.; Lissi, E.; Biasutti, M. A.; Duarte, R., Kinetics of p-nitrophenyl acetate hydrolysis catalyzed by Mucor javanicus lipase in AOT reverse micellar solutions formulated in different organic solvents. *Protein Journal* **2007,** 26, (7), 475-479.
5. Ghosh, K. K.; Vaidya, J.; Satnami, M. L., The alpha-effect in micelles: Nucleophilic substitution reaction of p-nitrophenyl acetate with N-phenylbenzohydroxamate ion. *International Journal Of Chemical Kinetics* **2006,** 38, (1), 26-31.
6. Ghosh, K. K.; Satnami, M. L., Nucleophilic substitution reaction of carboxylate and phosphate esters with hydroxamate ions in microemulsions. *Colloids And Surfaces A-Physicochemical And Engineering Aspects* **2006,** 274, (1-3), 125-129.
7. Yatsimirsky, A. K., Metal ion catalysis in acyl and phosphoryl transfer: Transition states as ligands. *Coordination Chemistry Reviews* **2005,** 249, (17-18), 1997-2011.
8. Mancin, F.; Tecilla, P.; Tonellato, U., Metallomicelles made of Ni(II) and Zn(II) complexes of 2-pyridinealdoxime-based ligands as catalyst of the cleavage of carboxylic acid esters. *Langmuir* **2000,** 16, (1), 227-233.
9. Hampl, F.; Liska, F.; Mancin, F.; Tecilla, P.; Tonellato, U., Metallomicelles made of Ni(II) complexes of lipophilic 2-pyridineketoximes as powerful catalysts of the cleavage of carboxylic acid esters. *Langmuir* **1999,** 15, (2), 405-412.
10. Roa, A.; Goble, M. L.; Garcia, J. L.; Acebal, C.; Virden, R., Rapid burst kinetics in the hydrolysis of 4-nitrophenyl acetate by penicillin G acylase from Kluyvera citrophila. *Biochemical Journal* **1996,** 316, 409-412.
11. Martel, B.; Morcellet, M., Cyclodextrin-Poly(Vinylamine) Systems.2. Catalytic Hydrolysis Of P-Nitrophenyl Acetate. *European Polymer Journal* **1995,** 31, (11), 1089-1093.
12. Bender, M. L.; Marshall, T. H., Elastase-catalyzed hydrolysis of p-nitrophenyl trimethylacetate. *J. Am. Chem. Soc.* **1968,** 90, (1), 201-207.
13. Ge, Q. C.; Guo, Y. H.; Lin, H.; Gao, D. Z.; Lin, H. K.; Zhu, S. R., Role of trinuclear Zn(II) complexes in promoting the hydrolysis of 4-nitrophenyl acetate. *Canadian Journal Of Chemistry-Revue Canadienne De Chimie* **2004,** 82, (3), 409-417.
14. diTargiani, R. C.; Chang, S. C.; Salter, M. H.; Hancock, R. D.; Goldberg, D. P., Hydrolysis of 4-nitrophenyl acetate by a novel (N2S)zinc-hydroxide complex: A kinetic and thermodynamic study of a reactive peptide deformylase model. *Journal Of Inorganic Biochemistry* **2003,** 96, (1), 238-238.
15. Moss, R. A.; Kanamathareddy, S.; Vijayaraghavan, S., Kinetics of cleavage of paraoxon and parathion by cetyltrimethylammonium iodosobenzoate. *Langmuir* **2001,** 17, (20), 6108-6112.
16. Jiří Patočka, J. C., Kamil Kuča, Daniel Jun, Oxime reactivation of acetylcholinesterase inhibited by toxic phosphorus esters: in vitro kinetics and thermodynamics. *Journal of applied biomedicine* **2005**, (3), 91-99.
17. Ghosh, K. K.; Bal, S.; Satnami, M. L.; Rodriguez-Dafonte, P.; Palepu, R. M., Studies of nucleophilic substitution reactions of p-nitrophenyl acetate with some dihydroxamate ions in cationic micellar media. *Journal Of Dispersion Science And Technology* **2006,** 27, (3), 349-355.

18. Swidler, R.; Steinberg, G. M., The Kinetics of the Reaction of Isopropyl Methylphosphonofluoridate (Sarin) with Benzohydroxamic Acid. *J. Am. Chem. Soc.* **1956,** 78, (15), 3594-3598.
19. Moss, R. A.; Kim, K. Y.; Swarup, S., Efficient Catalytic Cleavage Of Reactive Phosphates By An Ortho-Iodosobenzoate Functionalized Surfactant. *Journal Of The American Chemical Society* **1986,** 108, (4), 788-793.
20. Moss, R. A.; Alwis, K. W.; Shin, J. S., Catalytic Cleavage Of Active Phosphate And Ester Substrates By Iodoso-Benzoates And Iodoxybenzoates. *Journal Of The American Chemical Society* **1984,** 106, (9), 2651-2655.
21. Chanda, A.; Khetan, S. K.; Banerjee, D.; Ghosh, A.; Collins, T. J., Total degradation of fenitrothion and other organophosphorus pesticides by catalytic oxidation employing Fe-TAML peroxide activators. *Journal Of The American Chemical Society* **2006,** 128, (37), 12058-12059.
22. Balakrishnan, V. K.; Buncel, E.; Vanloon, G. W., Micellar catalyzed degradation of fenitrothion, an organophosphorus pesticide, in solution and soils. *Environmental Science & Technology* **2005,** 39, (15), 5824-5830.
23. Ditsch, A.; Yin, J.; Laibinis, P. E.; Wang, D. I. C.; Hatton, T. A., Ion-exchange purification of proteins using magnetic nanoclusters. *Biotechnology Progress* **2006,** 22, (4), 1153-1162.
24. Moeser, G. D.; Roach, K. A.; Green, W. H.; Laibinis, P. E.; Hatton, T. A., Water-based magnetic fluids as extractants for synthetic organic compounds. *Industrial & Engineering Chemistry Research* **2002,** 41, (19), 4739-4749.
25. Moss, R. A.; Chung, Y. C., Immobilized Iodosobenzoate Catalysts For The Cleavage Of Reactive Phosphates. *Journal Of Organic Chemistry* **1990,** 55, (7), 2064-2069.
26. Lu, A. H.; Salabas, E. L.; Schuth, F., Magnetic nanoparticles: Synthesis, protection, functionalization, and application. *Angewandte Chemie-International Edition* **2007,** 46, (8), 1222-1244.
27. Bucak, S.; Jones, D. A.; Laibinis, P. E.; Hatton, T. A., Protein separations using colloidal magnetic nanoparticles. *Biotechnology Progress* **2003,** 19, (2), 477-484.
28. Wang, Y. H.; Lee, J. K., Recyclable nano-size Pd catalyst generated in the multilayer polyelectrolyte films on the magnetic nanoparticle core. *Journal Of Molecular Catalysis A-Chemical* **2007,** 263, (1-2), 163-168.
29. Wang, Z. F.; Shen, B.; Zou, A. H.; He, N. Y., Synthesis of Pd/Fe3O4 nanoparticle-based catalyst for the cross-coupling of acrylic acid with iodobenzene. *Chemical Engineering Journal* **2005,** 113, (1), 27-34.
30. Caruso, F.; Schuler, C., Enzyme multilayers on colloid particles: Assembly, stability, and enzymatic activity. *Langmuir* **2000,** 16, (24), 9595-9603.
31. Bromberg, L.; Hatton, T. A., Decomposition of toxic environmental contaminants by recyclable catalytic, superparamagnetic nanoparticles. *Industrial & Engineering Chemistry Research* **2007,** 46, (10), 3296-3303.
32. Bromberg, L.; Hatton, T. A., Nerve agent destruction by recyclable catalytic magnetic nanoparticles. *Industrial & Engineering Chemistry Research* **2005,** 44, (21), 7991-7998.

33. Takafuji, M.; Ide, S.; Ihara, H.; Xu, Z. H., Preparation of poly(1-vinylimidazole)-grafted magnetic nanoparticles and their application for removal of metal ions. *Chemistry Of Materials* **2004,** 16, (10), 1977-1983.
34. Ditsch, A.; Laibinis, P. E.; Wang, D. I. C.; Hatton, T. A., Controlled clustering and enhanced stability of polymer-coated magnetic nanoparticles. *Langmuir* **2005,** 21, (13), 6006-6018.
35. Moeser, G. D.; Roach, K. A.; Green, W. H.; Hatton, T. A.; Laibinis, P. E., High-gradient magnetic separation of coated magnetic nanoparticles. *Aiche Journal* **2004,** 50, (11), 2835-2848.
36. Ditsch, A.; Lindenmann, S.; Laibinis, P. E.; Wang, D. I. C.; Hatton, T. A., High-gradient magnetic separation of magnetic nanoclusters. *Industrial & Engineering Chemistry Research* **2005,** 44, (17), 6824-6836.
37. O'Shaughnessy, B.; Vavylonis, D., Irreversibility and polymer adsorption. *Physical Review Letters* **2003,** 90, (5).
38. Hudson, R. F.; Woodcock, R. C., Reaction Of Phosphylated Amide Oximes In Alkaline-Solution. *Justus Liebigs Annalen Der Chemie* **1971,** (1), 1050 - 1051.
39. Sun, Z. X.; Su, F. W.; Forsling, W.; Samskog, P. O., Surface characteristics of magnetite in aqueous suspension. *Journal Of Colloid And Interface Science* **1998,** 197, (1), 151-159.
40. Shen, X. C.; Fang, X. Z.; Zhou, Y. H.; Liang, H., Synthesis and characterization of 3-aminopropyltriethoxysilane-modified superparamagnetic magnetite nanoparticles. *Chemistry Letters* **2004,** 33, (11), 1468-1469.
41. Li, T. F.; Deng, Y. J.; Song, X. P.; Jin, Z. X.; Zhang, Y., The formation of magnetite nanoparticle in ordered system of the soybean lecithin. *Bulletin Of The Korean Chemical Society* **2003,** 24, (7), 957-960.
42. Michaelidou, A.; Hadjipavlou-Litina, D.; Matsini, I.; Tsitsogianni, E., Heterocyclic aryl(phenyl)acetic acid and aryl acetohydroxamic acids as antiinflammatory antioxidant agents and inhibitors of lipoxygenase and serine proteases. *Medicinal Chemistry* **2007,** 3, (5), 439-445.
43. Bunton, C. A.; Nome, F.; Quina, F. H.; Romsted, L. S., Ion Binding And Reactivity At Charged Aqueous Interfaces. *Accounts Of Chemical Research* **1991,** 24, (12), 357-364.
44. Biresaw, G.; Bunton, C. A., Size Vs Reactivity In Organized Assemblies - Deacylation And Dephosphorylation In Functionalized Assemblies. *Journal Of Physical Chemistry* **1986,** 90, (22), 5849-5853.
45. Couderc, S.; Toullec, J., Catalysis of phosphate triester hydrolysis by micelles of hexadecyltrimethylammonium anti-pyruvaldehyde 1-oximate. *Langmuir* **2001,** 17, (13), 3819-3828.

Chapter 3

Hydroxamic Acid Modified Magnetic Nanoparticles

3.1 Introduction

In the previous chapter, the amidoxime functional groups were attached to the magnetic nanoparticles through chemical attachment of a precursor group followed by chemical modification. The particles were active toward the hydrolysis of *p*-nitrophenyl acetate. In this chapter, another strategy was explored to attach more reactive nucleophiles as functional groups.

Hydroxamic acid and its derivatives have been studied extensively in the medicinal area for their potential use as inhibitors of hypertension, tumor growth, inflammation, infectious agents, asthma, arthritis, etc. [1-3] Furthermore, hydroxamic acid is able to chelate strongly with heavy metal ions. Polyhydroxamic acid gel, for example, removed uranium ions from environmental samples through selective adsorption to reduce the possibility of serious intoxication by excessive intake of heavy metal ions. [4] Hydrogels containing pendant hydroxamic acid groups as iron-specific chelating agents were studied for the potential treatment of iron overload, a severe clinical condition. [5]

The property of particular interest of hydroxamic acid is its strong nucleophilicity. Similar to oximes, iodosobenzoates, and hydroperoxides, hydroxamic acid is an α-effect nucleophile, meaning that it is a better nucleophile than predicted by Bronsted relations between nucleophilicity and basicity. [6] Hydroxamic acid, either in the monomeric form or in micelles/co-micelles formed with surfactants in solution, was effective in accelerating the hydrolysis of carboxyl and phosphate esters, which has been attracting considerable attention over the past decades because of its important implications in many chemical reactions. [7-12] However, most studies on catalysis by hydroxamic acid groups were concentrated on homogenous or micellar systems, which made it difficult to recycle and reuse the reactive reagents to reduce operational costs and environmental footprint. [13-15]

Hydroxamic acid groups have been immobilized on polymer particles for the recovery of uranium and iron ions and the acceleration of the nucleophilic substitution reactions in order to enable their recovery after usage. [4, 5] However, capture of polymer particles would be challenging if the particle size were very small and the surface area and hydroxamic acid group density would be reduced significantly if particle size were kept large. In order to solve the problems, we proposed to attach the hydroxamic acid groups onto the surfaces of magnetic nanoparticles. Magnetic nanoparticles have attracted extensive research for applications in biological and environmental separations because they enable fast and economical removal of target compounds from complex media by applying magnetic fields. [13, 14, 16] They can be prepared by co-precipitation of iron salts in water with a simple procedure on a large scale with off-the-shelf raw materials. The prepared particles are chemically stable and can be functionalized to carry reactive groups for various applications. [17-22] Surface modification enables all functional groups to be accessible and eliminates internal mass transfer resistances. Furthermore, small particles create large surface area and increase the amount of functional groups carried by the same weight of materials. [23]

In this chapter, colloidally stable magnetic nanoparticles with average diameter of around 100 nm were prepared through co-precipitation of iron (II) and iron (III) chlorides with 10-undecenoic acid as the second coating material. Hydroxamic acid groups were attached through the copolymerization of acrylamide monomer and the 10-undecenoic acid on the particle surface, followed by conversion of amide into hydroxamic acid groups. The prepared magnetite clusters were around 200nm due to crosslinking during the copolymerization. They were strongly negatively charged and colloidally stable over a wide range of solution pH and salt concentrations. These particles were tested against the hydrolysis of *p*-nitrophenyl acetate (PNPA), which acted as a model of organophosphate compounds. The particles accelerated the PNPA hydrolysis significantly. The particles were readily recovered from the aqueous milieu by high-gradient magnetic separation (HGMS). The recovered particles lost 80% reactivity due to Lossen rearrangement of acetyl hydroxamic acid, i.e., they were not catalytic. Strategies to prevent this loss and improve turnover rate of hydroxamic acid groups are discussed.

3.2 Experimental Section

3.2.1 Materials

Ferric chloride hexahydrate (97%), ferrous chloride tetrahydrate (99%), acrylic acid (99%), vinylsulfonic acid sodium salt (technical grade, 25% in water), 4-styrenesulfonic acid sodium salt hydrate, 10-undecenoic acid, sodium metabisulfite, potassium persulfate (99%), acrylamide (99%), hydroxylamine hydrochloride, and *p*-nitrophenyl acetate (PNPA), polyacrylamide solution (50%wt, MW = 10,000), were purchased from Sigma-Aldrich Chemical Company (Milwaukee, WI) and used as received. Ammonium hydroxide (30% in water), acetone, and sodium hydroxide were purchased from Mallinckrodt Baker Inc. (Phillipsburg, NJ) and used as received.

3.2.2 Particle Synthesis and Modification

As discussed in the previous chapter, the magnetic particles need to be in clusters in order to be captured efficiently by HGMS. Therefore, the two-step procedure was employed to prepare the original particles for further modifications. [24] The first polymer used for particle synthesis was a random copolymer of acrylic acid (AA), vinylsulfonic acid sodium salt (VSA), and 4-styrenesulfonic acid sodium salt hydrate (SSA) with the molar ratio of 2:1:1, respectively. The AA-VSA-SSA copolymer was prepared according to the published procedure described briefly as follows. [24] 1.05g of AA, 3.79g of VSA solution, and 1.5g of SSA were mixed with 0.1g of potassium persulfate as initiator and 0.4g of sodium metabisulfite as chain transfer agent. The solution volume was adjusted to 22mL by adding appropriate amount of water. The reaction was kept at 80°C for 3hr. The prepared copolymer solution was used directly for particle synthesis without purification.

The two-step procedure to prepare original magnetite nanoparticles was as follows. [24] 40mL of water was added to a three-neck flask and deaerated by nitrogen bubbling for 30min. Iron (II) chloride tetrahydrate (0.86g, 4.3mmol) and iron (III) chloride hexahydrate (2.36g, 8.6mmol) were dissolved into the deoxygenated water and the resulting solution was heated up to 80°C. While stirring, 2.5ml of the previously prepared AA-VSA-SSA terpolymer solution was mixed with 6mL of 30% aqueous ammonium

hydroxide and the mixture was added quickly to the iron salt solution, at which point the solution turned black immediately due to the formation of magnetite particles; the reaction was kept stirred for 15min. Then 0.5g of 10-undecenoic acid was added to the magnetite dispersion as the secondary coating material and the resulting dispersion was kept at 80°C for another 15min. After cooling down to room temperature, the particle dispersion was mixed with 50ml of acetone, decanted by using an electro-magnet, re-dispersed into 50ml of water and decanted after mixing with 50ml of acetone three more times. The clean particles were re-dispersed into 50mL of deionized water and sonicated for 1min using a Branson Sonifier Model 450 at an output of 40% to form uniform dispersion. The particle weight concentration was 20mg/ml. These particles were referred to as original particles.

The original particles were then copolymerized with acrylamide monomers to attach amide groups on the particles. [25, 26] 0.6g of acrylamide was added to 25ml of the previously-prepared particle dispersion and the solution pH was adjusted to 3.2 by gradually adding 1M hydrochloric acid. The solution was purged with nitrogen under vigorous stirring. Then 0.1g of potassium persulfate was added as the polymerization initiator and the reaction mixture was kept at 60°C for 2hr under continuous stirring. After the reaction was finished, 25ml of acetone was added to the reaction mixture to precipitate the magnetite particles coated with newly formed copolymer. The particles were re-dispersed into 25ml of water and decanted using an electro-magnet after mixing with 25ml of acetone for three times to remove the un-reacted monomers and other impurities. Finally, the purified particles were dispersed in 25ml water.

The attached amide groups were then converted into hydroxamic acid groups through the following procedure. [4, 27] 1.05g of hydroxylamine hydrochloride (15.1mmol) and 4ml of 5M sodium hydroxide solution were added to 25ml of acrylamide modified particle dispersion and the reaction mixture was kept at room temperature for 72hrs under stirring. The reaction mixture was then cleaned up with the HGMS separation to remove any un-reacted raw materials as well as other impurities. HGMS was performed with an L-1CN Frantz canister separator supplied by S. G. Frantz Co., Inc. (Trenton, NJ). The

HGMS system consisted of a cylindrical column with the diameter of 1cm packed with type 430 fine-grade stainless steel wool (40-66μm diameter) also supplied by S. G. Frantz Co., Inc.. The packing fraction was 12%vol. An electromagnet was used to generate a magnetic field with the intensity of 1.3 Tesla between the two plates. The particle solution was passed through the column at a flow rate of 4ml/min with the magnet on to capture the particles. The liquid flow was controlled by a peristaltic pump. Then 20ml of water were passed through the column to wash out any material absorbed by the particles and the column wires. The electromagnet was turned off and particles were fully washed out of the column with 20ml of deionized water. They were collected through magnetic decantation with addition of 20ml of acetone and dried under vacuum until constant weight.

Polyhydroxamic acid (PHA) was also prepared using the same procedure as used in the particle conversion step. Polyacrylamide with a molecular weight of 10,000 was utilized. After the conversion procedure, the reaction solution was dialyzed exhaustively (membrane MW cutoff (MWCO), 3500) against DI water. The purified solution was lyophilized and the dry polymer sample was stored dry at 2-8 °C until further use.

3.2.3 Particle Characterization

Chemical bond changes were characterized with a Nexus-870 FT-IR spectrometer (Thermo Nicolet Corp., Madison, WI). All particle samples were ground, mixed with KBr, and then pressed to form pellets. The sample was measured in absorbance mode by collecting 256 scans with a resolution of $4cm^{-1}$ after subtracting KBr background.

Dynamic light scattering (DLS) was used to measure the hydrodynamic diameter of the particles before and after modification. DLS experiments were performed with the Brookhaven BI-200SM light scattering system at a measurement angle of 90°. The samples were diluted to 0.005%wt Fe_3O_4 with 10mM buffer. The utilized buffers were citrate buffer with pH 3 to 6, phosphate buffer with pH 7 to 8, borate buffer with pH 9, and carbonate buffer with pH 10 and 11. Sample temperature was kept at 25°C during the measurement. Particle diameter was extracted by fitting the measured autocorrelation

function with an exponential model in the provided software. Quoted particles sizes were based on an intensity-averaged size distribution and the averages of four independent measurements.

The Zeta potentials of particle suspensions were measured on a Brookhaven ZetaPals Zeta Potential Analyzer. Particles were diluted to 0.005%wt Fe_3O_4 with 10mM buffer. The buffers used were the same as those in DLS measurement. Zeta potential was converted from the electrophoretic mobility measured over 25 cycles by fitting to the Smoluchowski equation, as shown in Equation 3-1, where μ_e is the measured electrophoretic mobility and η and ε are the viscosity and dielectric constant of the dispersion medium respectively. The quoted Zeta potentials are number averages of five measurements.

$$\zeta = \frac{\eta}{\varepsilon}\mu_e \qquad \textbf{Equation 3-1}$$

Thermo gravimetric analysis (TGA) was conducted on a TGA Q50 instrument (TA Instruments) to analyze the particle weight change with increasing temperature. Approximately 15mg of dried magnetic particles was loaded each time and the furnace was purged with nitrogen to prevent oxidation. The heating profile was as follows: heat to 150°C at 5°C/min; hold at 150°C for 30min; heat to 900°C at 5°C/min. The sample weight was then recorded as a function of temperature.

Nitrogen elemental analysis was carried out by Atlantic Microlab, Inc. (Norcross, GA) to quantify the nitrogen content needed to calculate density of the functional groups after particle modification.

X-ray photoelectron spectroscopy (XPS) measurements were carried out on vacuum-dried particle to analyze the surface elemental composition with a Kratos Axis Ultra Imaging XPS (Kratos Analytical Ltd., Manchester, UK) equipped with a monochromatized Al Kα X-ray source operated at 150W with a spot of 300μm ×700μm.

The base pressure was better than 1×10^{-9}Torr and the analysis pressure better than 2×10^{-8} Torr. Survey spectra (0-1100eV binding energy range) were collected at a 90^{o} angle (with respect to the sample surface) and a pass energy of 160eV. High resolution analysis was done with a pass energy of 20eV and a step energy of 0.1eV.

The particle stability in salt solution was also measured. Magnetic fluids were diluted to 0.01%wt in solutions of various sodium chloride concentrations, from 0.1 to 2.0M with 0.1M increment, mixed well, and left at room temperature for 24 hours. The highest concentration at which no particle coagulation occurred was recorded.

3.2.4 Kinetics Measurement

Reactivity of the modified particles was tested against the hydrolysis of *p*-nitrophenyl acetate. The hydrolysis kinetics was followed by measuring the change of the hydrolysis product, *p*-nitrophenyl ion, at 404nm absorbance using a Hewlett-Packard 8453 UV/Vis spectrophotometer. All samples were measured at 25^{o}C and solution pH was kept constant at 8 with 50mM Tris buffer to prevent any pH change during the hydrolysis. Typical measurements were taken on samples comprising magnetic particles, 0.25mM *p*-nitrophenyl acetate substrate, 0.2M NaCl, and 50mM Tris buffer. The sample had an ethanol/water volume ratio of 1:4. The presence of ethanol ensured PNPA solubility in the solution. 0.5ml of reaction mixture was withdrawn at certain time intervals and particles were removed by HGMS. 2ml of 50mM Tris buffer at pH 8 was used to wash the column to recover any trapped hydrolysis product.

The particle recovery was carried out as follows. The particles first reacted with 5mM PNPA under the same conditions as above. After 24hrs, the magnetic particles were recycled by HGMS and then washed out of the column with pure water. The dispersion was then placed within 50mM CAPS buffer at pH 10.6 for 48hrs to allow the acetylated hydroxamic acid to react fully. Finally the particles were collected through magnetic decantation with the addition of 20ml of acetone and dried in a vacuum oven. The recycled particles were then subjected to the same reaction procedure as discussed above.

PNPA hydrolysis accelerated by polyhydroxamic acid was also performed under the same conditions as those used for the particle hydrolysis reaction. The kinetic parameters from this homogenous system were compared with those from the particle system.

3.3 Results and Discussion

3.3.1 Particle Preparation and Characterization

As discussed in the previous chapter, particle size and colloidal stability are the two most important characteristics of magnetic particles. In this work, original magnetic clusters were synthesized through a two-step procedure to ensure formation of magnetic clusters of multiple individual magnetite particles with hydrodynamic diameters larger than 50nm rather than individual particles less than 10nm in diameters to ensure effective capture by HGMS. [24, 28] In the first step, the magnetite cores formed and then aggregated to form the magnetic clusters because of the instability generated by insufficient availability of the first coating material. In the first coating terpolymer, carboxyl groups chelated with magnetite surface, vinyl sulfonic acid and styrenesulfonic acid provided pH-independent negative charges to stabilize the particles over a broad pH range, and SSA increased coating thickness and enhanced particle stability. [24, 29] The second coating material was 10-undecenoic acid, which provided the carboxyl groups to complex the particle surface and the carbon-carbon double bond to polymerize with monomer precursors.

Attachment of the precursor amide groups was accomplished through free radical copolymerization between the double bond of 10-undecenoic acid and that of acrylamide molecules. The reaction is depicted in Scheme 3-1.

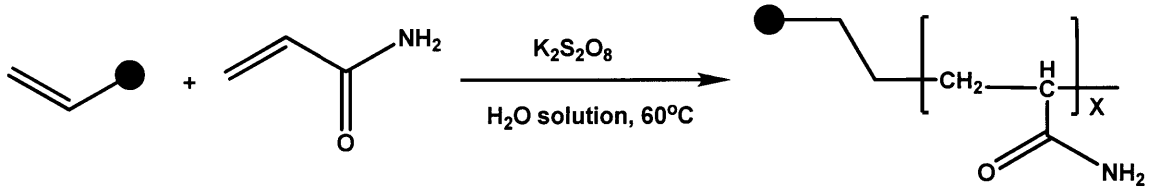

Scheme 3-1. Attachment of amide groups through copolymerization

Acrylamide was employed because it provided the carbon-carbon double bond for the copolymerization and amide groups that would be converted into target hydroxamic acid

groups. The solution pH was controlled at 3.2 so that the reactivity of acrylamide would be lowered from the protonation of amide groups to be more comparable with the reactivity of 10-undecenoic acid. [25] As a result, the acrylamide monomers formed a copolymer with the 10-undecenoic acid on the particle surface instead of forming a polyacrylamide homopolymer in the solution. Furthermore, the particles were still dispersed uniformly at this solution pH so that crosslinking between magnetic clusters would be reduced.

During the conversion reaction step, the amide groups reacted with hydroxylamine to form the intermediates through nucleophilic substitution on the nitrogen atom of the amide groups and then yielded the hydroxamic acid groups through the release of ammonia. As a result, the reaction mixture released gas bubbles continuously and the solution pH decreased from 12 at the start of the reaction to 9.8 at the end. The reaction is depicted in Scheme 3-2.

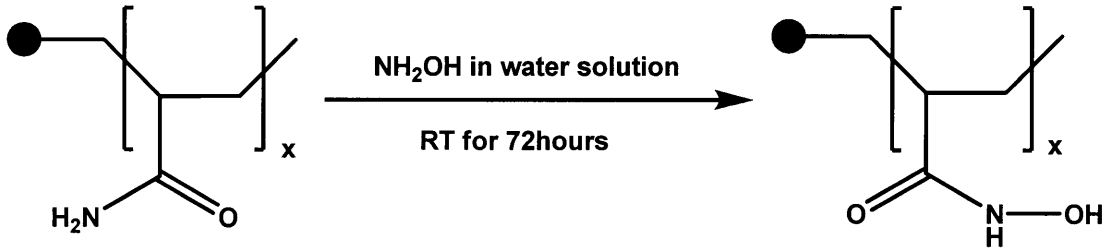

Scheme 3-2. Conversion of amide groups into hydroxamic acid groups through the reaction with hydroxylamine at room temperature

The modified particles were tested by FT-IR and compared with the original particles as well as the pure polyhydroxamic acid. The results are shown in Figure 3-1. The original particles had absorbance bands at 625, 1556, 1630, and 2932cm^{-1}, corresponding to vibrational frequencies of magnetite, carboxylate groups, carbon double bond stretching from 10-undecenoic acid, and CH stretching from 10-undecenoic acid respectively. After the modification, two major absorbance bands appeared at 1658 and 3192 cm^{-1}, corresponding to the amide bond stretching and OH stretching respectively. The peak at 1658cm^{-1} was very sharp with high intensity, indicating the large amount of amide bonds present on the particle surface and therefore the successful acrylamide attachment. The

pure polyhydroxamic acid showed two major peaks at the same positions. This indicates that the conversion yielded hydroxamic acid groups successfully.

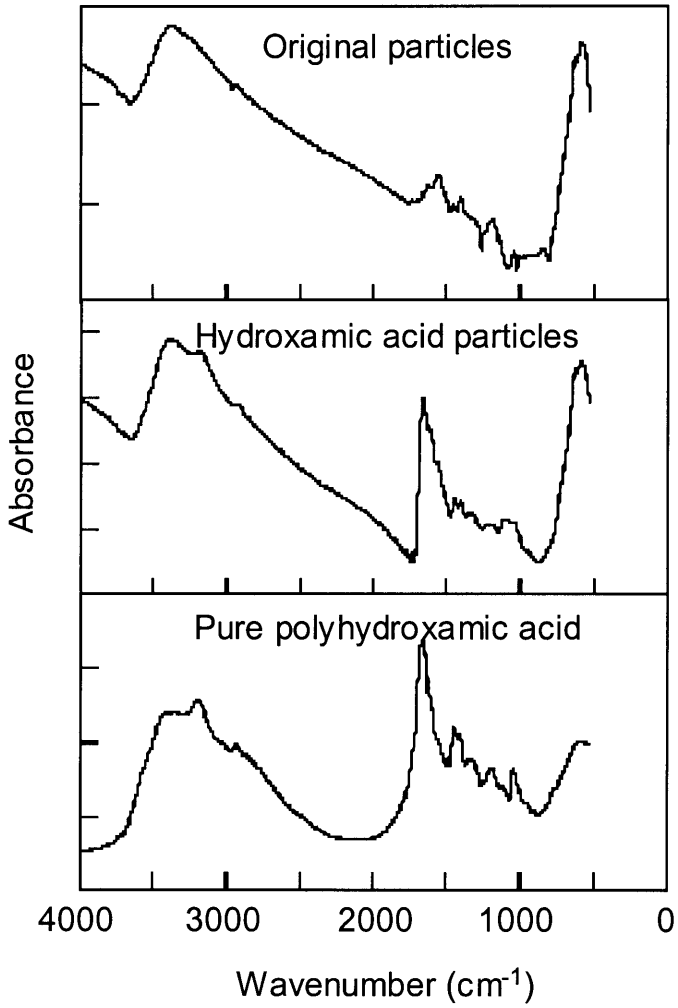

Figure 3-1. FT-IR spectra of particles before and after hydroxamic acid modification and of the pure polyhydroxamic acid. The hydroxamic acid modified particles clearly showed absorbance at 1658 and 3192cm^{-1}, corresponding well with the pure polyhydroxamic acid, indicating the successful modification.

Hydrodynamic diameters of the particles before and after the modification procedure were measured with dynamic light scattering. As shown in Figure 3-2, the average hydrodynamic diameter of the particles was increased significantly from around 100nm to around 210nm by the modification procedure. Hydrodynamic diameters of the modified particles at lower solution pH 3 and 4 were much lower probably due to the intra-molecular aggregation between hydroxamic acid groups on particle surface. The copolymerization procedure resulted in crosslinking between the original magnetic

clusters because of the multiple copolymerization centers attached on the particle surface. The particles functioned similarly to crosslink agents and this resulted in the dramatic particle size increase. Furthermore, this significant particle size increase also suggested that the particles would be captured by HGMS even more efficiently than the original magnetic clusters.

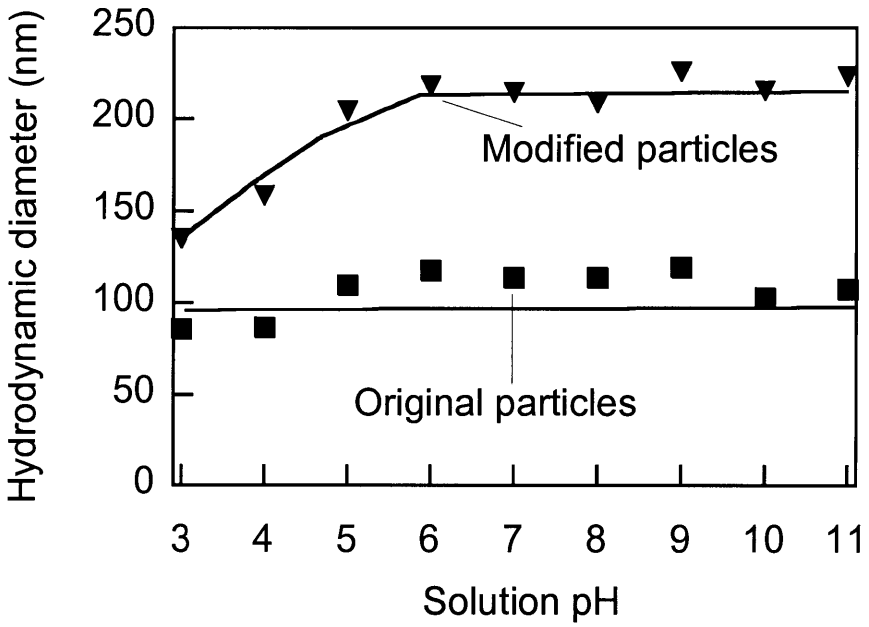

Figure 3-2. Hydrodynamic diameters of particles before and after the modification reaction at various solution pH. Original particles were from the two-step preparation procedure and modified particles were those after the hydroxamic acid modification procedure. Particle concentration was kept at 0.005%wt for measurement. All samples were measured in 0.01M buffer, citrate buffer for pH 3 to 6, phosphate buffer for pH 7 to 8, borate buffer for pH 9, and carbonate buffer for pH 10 and 11.

The magnetic clusters were stabilized in water through electrostatic interactions and the surface charges were characterized with Zeta potential. Zeta potentials of particles at various pH values are shown in Figure 3-3. The original particles were strongly negatively charged over the whole pH range studied because of the presence of sulfonic groups from the first coating polymer even though the second coating material, 10-undecenoic acid, did not carry any charge. The small decrease of surface charge at low solution pH was because the small amount of acrylate groups from the first coating polymer started to protonate. After the modification procedure, particles remained negatively charged over the whole pH range. The sharp decrease in surface charge

starting around pH 9 was due to the protonation of hydroxamic acid groups, which have a pKa of 8.5. [10] At low solution pH, the surface charge continued decreasing probably because the hydroxamic acid groups started intra-molecular aggregation and therefore shielded some sulfonic groups. The clustered particles were stabilized colloidally in water by electrostatic repulsion from the strong surface charge and able to maintain excellent colloidal stability after modification to withstand months without measurable sedimentation.

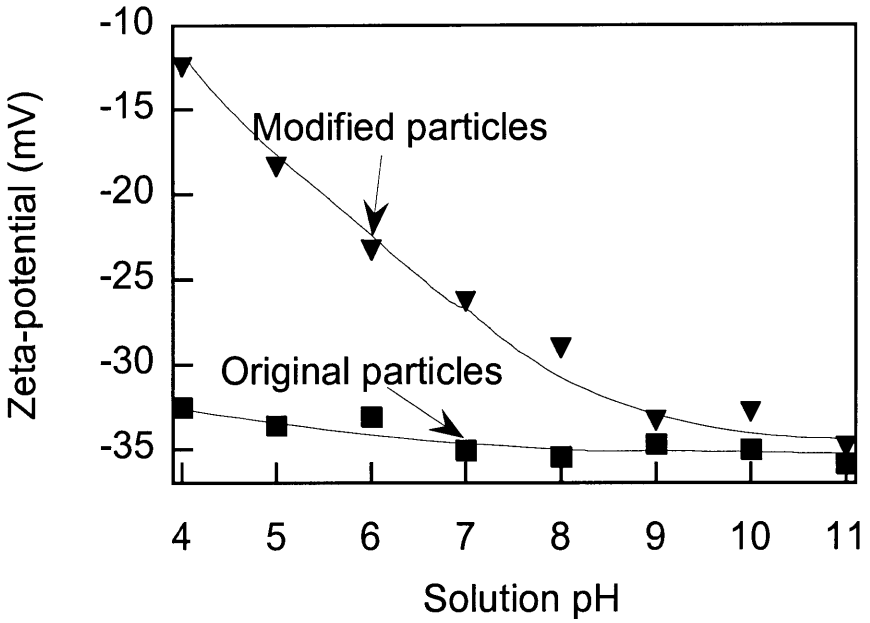

Figure 3-3. Zeta potential of particles before (square) and after (triangle) the modification procedure at various solution pH. Particle concentration was kept at 0.005%wt for measurement. All samples were measured in 0.01M buffer, citrate buffer for pH 4 to 6, phosphate buffer for pH 7 to 8, borate buffer for pH 9, and carbonate buffer for pH 10 and 11.

Thermo gravimetric analysis (TGA) was employed to determine the amount of chemically bound material on the particles. The TGA results are shown in Figure 3-4, in which the residual mass percentage is plotted as a function of temperature. During the first phase of the decomposition, the side chains of the attached polymer were gradually decomposed. During the second phase starting around 550°C, the groups chemically bound to the magnetite surface were decomposed. The residual magnetite weight percentage was used to compute the bound-polymer/magnetite mass ratio, which was 1.2

after the chemical modification. This is consistent with the result obtained through iron titration test.

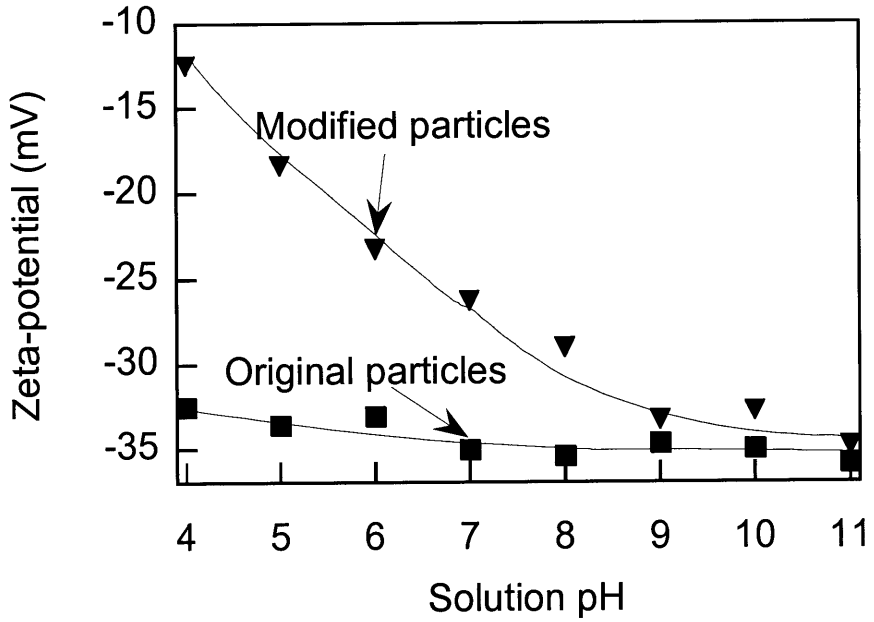

Figure 3-4. TGA analysis of hydroxamic acid modified magnetic particles after the chemical modification.

Elemental analysis showed that the nitrogen content of the particles was 3.8%wt. In the particles only the acrylamide and hydroxamic acid groups contained nitrogen. 3.8%wt of nitrogen corresponded with 24%wt of polyacrylamide and polyhydroxamic acid combined, assuming 50% conversion efficiency due to the different molecular weights of the monomers. Based on the TGA analysis, the total coating on the modified particles was 55%wt of the dry particles. Therefore, the originally coated polymer and 10-undecenoic acid during the initial particle preparation comprised 30%wt of the final particles. The added coating from the copolymerization and conversion procedure was almost identical to the total coating during the initial particle preparation. The nitrogen content was further converted into the molar concentration of nitrogen and 1mg/mL particle solution corresponded to 2.7mM of amide groups and hydroxamic acid groups combined. This translated into the group surface density of 24 amide and hydroxamic acid groups on $1nm^2$ of particle surface, indicating that the copolymerization procedure was highly efficient for attachment of a large amount of amide groups.

Pure polyhydroxamic acid was tested by XPS and the spectrum with the high resolution results is shown in Figure 3-5. As shown in the insert, XPS provided clear distinction between these amide groups and hydroxamic acid groups, with a molar ratio of 1:1. XPS was also utilized to analyze the modified particles and the result is shown in Figure 3-6 including the high resolution measurement. However, attempt to differentiate between these two groups failed probably because the possible interaction with particle surface iron element rendered the two groups indistinguishable by XPS.

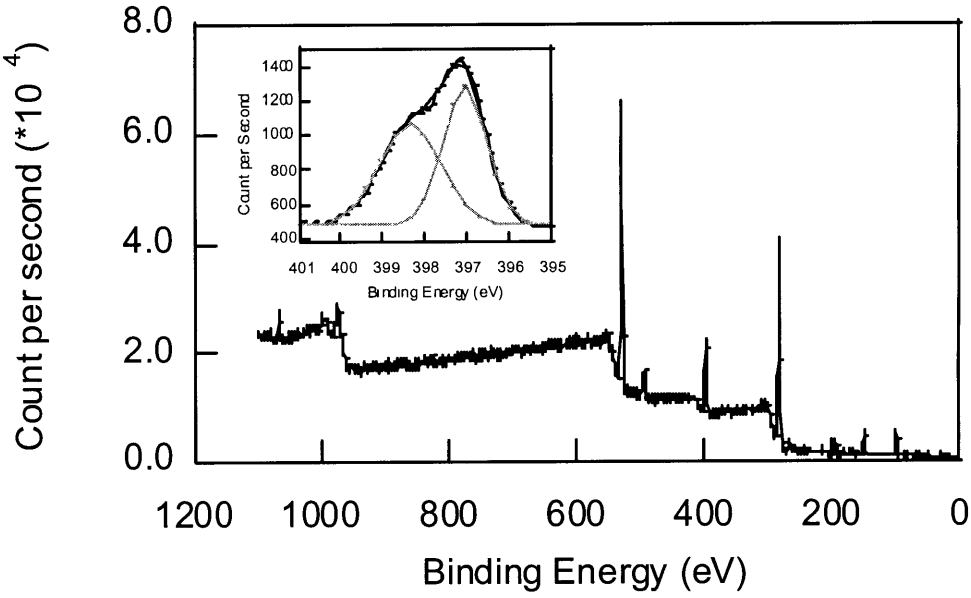

Figure 3-5. XPS spectrum of pure polyhydroxamic acid. The insert was from high resolution measurement. In the insert, black line was XPS data and red line the fitting results. Two green lines were two individual fitting peaks at 397.03eV and 398.33eV, which are from amide groups and hydroxamic acid groups respectively.

The stability test showed that the original particles were stable in 0.2M sodium chloride solution and started to aggregate in 0.3M salt solution at neutral pH. In comparison, the hydroxamic acid modified particles were stable even in 2M salt solution. Since the Zeta potentials of the original particles were more negative than the modified particles and the salt presence dampened the electric double layer, this vast stability difference can be only attributed to the increased coating thickness through the modification process. This increased coating thickness would increase the distance between magnetite cores when the clusters approached each other and reduce the van der Walls interactions significantly. The process also eliminated the hydrophobic effects of carbon chain of 10-undecenoic

acid because these groups were buried in the formed copolymer layer. Both effects worked together to enhance particle stability.

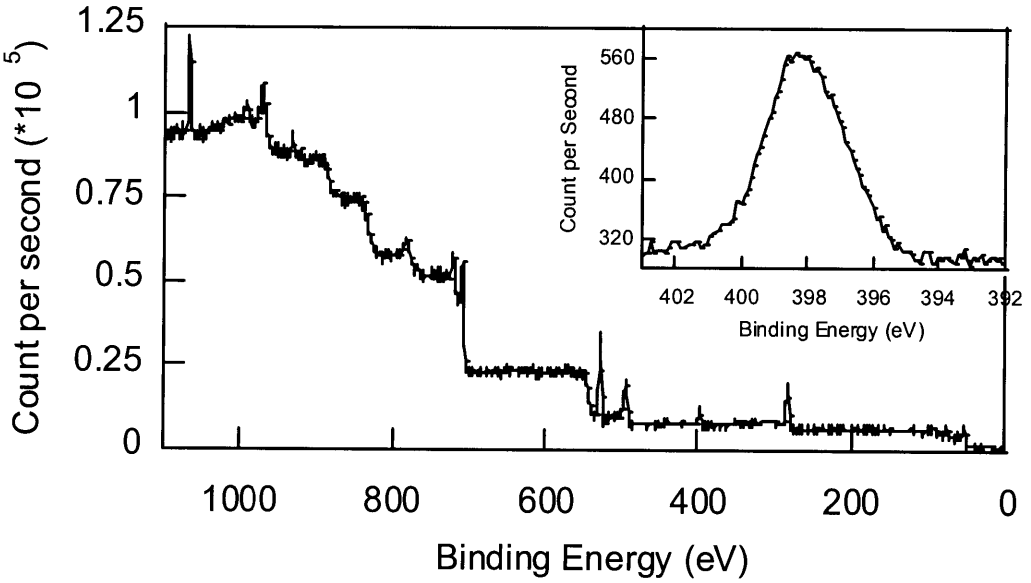

Figure 3-6. XPS spectrum of hydroxamic acid modified particles. The insert was from the high resolution measurement. Nitrogen peak was at 398eV.

Results from elemental analysis, TGA, Zeta potential, and particle stability tests indicated that the particle surface was overwhelmingly covered by the polyacrylamide and polyhydroxamic acid coating after the modification process.

3.3.2 Hydrolysis Kinetics of *p*-Nitrophenyl Acetate

As discussed above, a significant number of hydroxamic acid groups were attached to the surface of magnetic particles. Due to their superparamagnetic properties, the particles could be easily captured by HGMS and re-dispersed into water. The functional groups could be reused for the targeted applications if regenerated.

Nucleophilic properties of the functional particles were studied with regard to the hydrolysis of a model carboxyl ester, *p*-nitrophenyl acetate (PNPA). PNPA hydrolysis accelerated by hydroxamic acid groups was shown to proceed mainly via the formation and the subsequent decomposition of the acetylated hydroxamic acid intermediate. [30, 31] The reaction mechanism is shown in Scheme 3-3. This reaction releases protons and

therefore changes the solution pH. Since solution pH also affects the reaction rate, the solution was kept at pH 8 with 50mM Tris buffer. The released *p*-nitrophenol was in equilibrium with the *p*-nitrophenol ions and the overall concentration of the hydrolyzed product was calculated with the same procedure as shown in chapter 2.

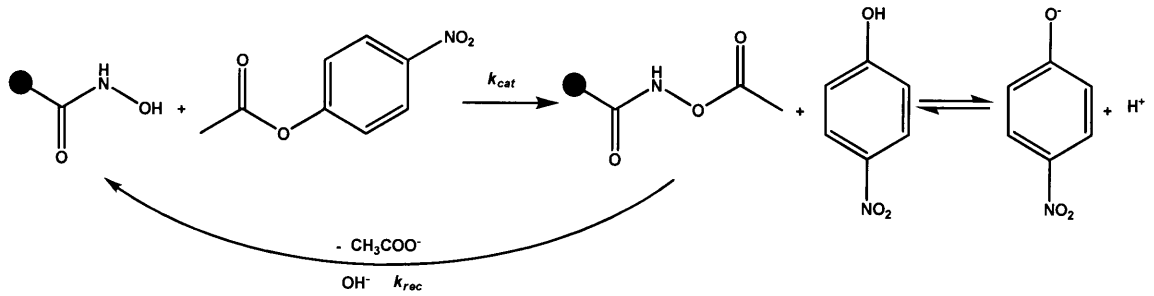

Scheme 3-3. Acetylation reaction of hydroxamic acid groups on the particle surface by PNPA and deacetylation by hydroxide ions

The concentration changes of hydrolyzed product with time under various solution conditions are shown in Figure 3-7.

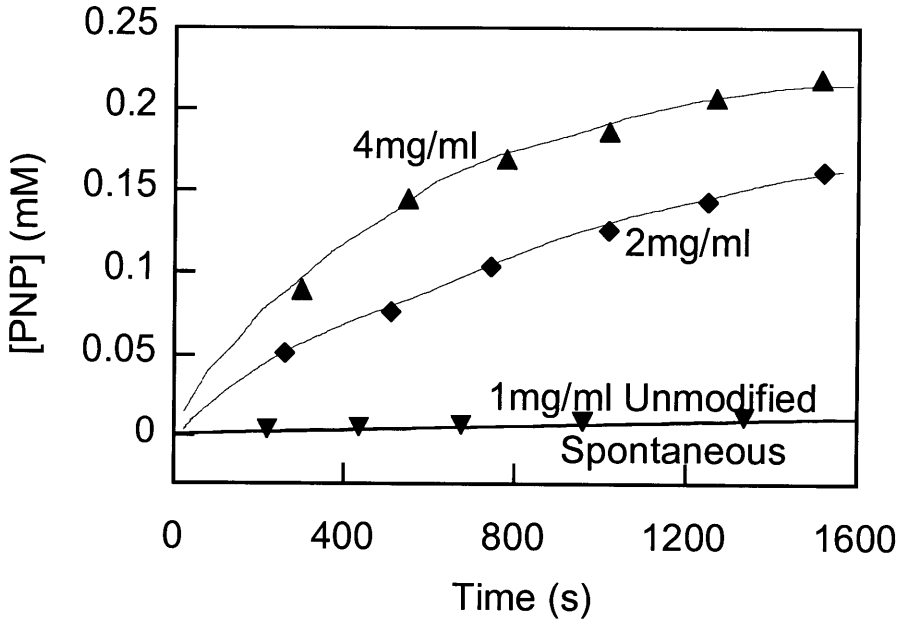

Figure 3-7. Concentration change of hydrolysis product with addition of various particles, from spontaneous hydrolysis (black line), hydrolysis with 1mg/ml unmodified particles, and with 2mg/ml and 4mg/ml functionalized particles. Solution pH was kept at 8 with 50mM Tris buffer and 25°C. $[PNPA]_0 = 0.25mM$.

The hydrolysis with the addition of the original particles produced almost the same concentration change with time as the spontaneous hydrolysis. This suggests that the original particles did not affect the PNPA hydrolysis. However, the product concentration increased much more quickly with the addition of hydroxamic acid modified particles, indicating that hydroxamic acid groups accelerated the PNPA hydrolysis significantly.

As shown in the literature, the PNPA hydrolysis accelerated by hydroxamic acid groups is first order with respect to the PNPA substrate and the hydroxamic acid groups respectively in addition to the spontaneous hydrolysis. [10, 30] The overall rate of production of *p*-nitrophenolate is described by Equation 3-2. [32]

$$r = \frac{d[NP]}{dt} = \left(k_{spon} + k_{OH}\left[OH^-\right] + k_{cat}\left[NOH^-\right]\right)[PNPA] = r_{spon} + r_{cat} \qquad \textbf{Equation 3-2}$$

Since solution pH was kept constant at 8 with Tris buffer, the first two terms in the parenthesis are constant. The majority of hydroxamic acid groups remained active and its concentration was almost constant during the initial reaction stage. Thus the initial reaction followed pseudo-first order kinetics. The equation is then integrated to give Equation 3-3.

$$-\ln\left(1-[PNP]_t/[PNPA]_0\right) = k_{obs}t \qquad \textbf{Equation 3-3}$$

in which

$$k_{obs} = k_{spon} + k_{OH}\left[OH^-\right] + k_{cat}\left[NOH^-\right] \qquad \textbf{Equation 3-4}$$

The data acquired through the previously described experimental procedure were the *p*-nitrophenolate concentration at various points of time. These data were plotted in Figure 3-8 according to Equation 3-3, slope of the plot equals to k_{obs}.

The observed kinetic constants were measured on a series of particle concentrations and spontaneous hydrolysis was measured separately. These kinetic constants were plotted

with regard to particle concentrations, shown in Figure 3-9. Data points were fitted with a linear function, the slope of which was k_{cat}.

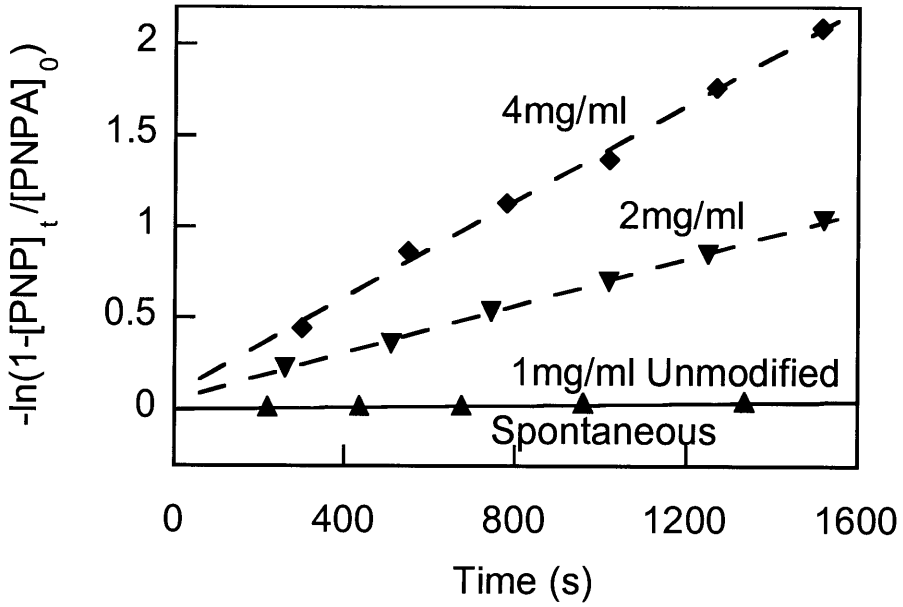

Figure 3-8. Pseudo-first order kinetics from spontaneous hydrolysis, hydrolysis with 1mg/ml unmodified particles, and with 2mg/ml and 4mg/ml hydroxamic acid modified particles of PNPA. Solution pH was kept at 8 with 50mM Tris buffer and 25°C. $[PNPA]_0$ = 0.25mM.

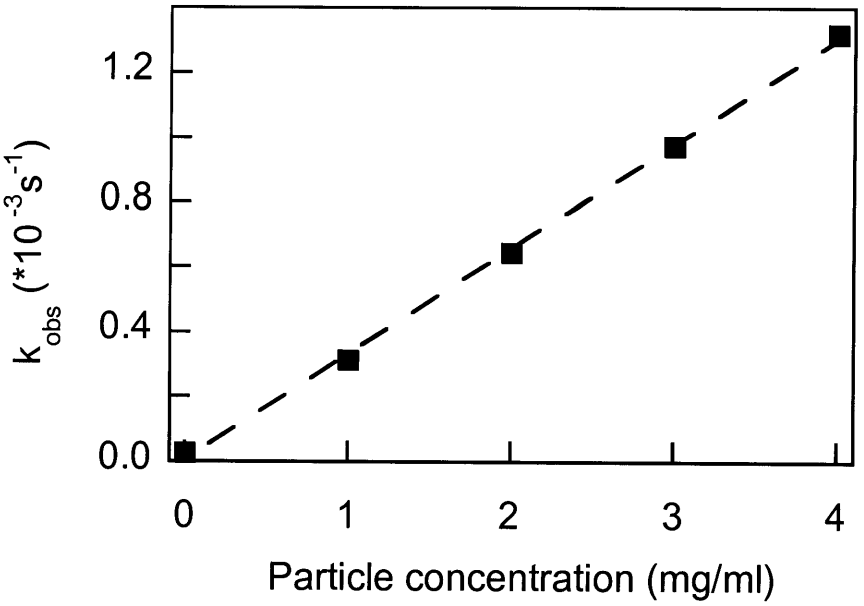

Figure 3-9. Dependence of observed kinetic constants on the added particle concentrations. The second order kinetic constant based on particle weight concentration was $k_{cat} = 3.2\times10^{-4}(mg/ml)^{-1}s^{-1}$

The kinetic constant of spontaneous hydrolysis was $2.7\times10^{-5}s^{-1}$ and that of the hydrolysis reaction with addition of 4mg/ml of hydroxamic acid modified particles was $1.3\times10^{-3}s^{-1}$. This corresponded with the second order kinetic constant based on particle weight concentration of $k_{cat} = 3.2\times10^{-4}(mg/ml)^{-1}s^{-1}$. This was attributed to the strong nucleophilic properties of the hydroxamic acid groups and the significant number of hydroxamic acid groups present on the particle surfaces. The linear relationship between the pseudo-first order kinetic constants and particle concentration suggests that particles functioned as individual reactive centers and there was no significant inter-particle interaction to affect the hydroxamic acid reactivity in the particle concentration range that we studied.

The PNPA hydrolysis accelerated by polyhydroxamic acid was studied under the same solution conditions. The kinetic constant under the pseudo-first order conditions with addition of 1mM PHA (on a monomer basis) was $6.0\times10^{-4}s^{-1}$ obtained through the same procedure, whereas the kinetic constant with addition of 1mM acetohydroxamic acid was $2.0\times10^{-3}s^{-1}$. Both monomeric and polymeric hydroxamic acid hydrolyzed PNPA much faster than spontaneous hydrolysis, reflecting the strong reactivity. The hydroxamic acid groups in the polymeric form were less reactive than the corresponding monomeric compounds for the acetylation reaction by PNPA due to the steric hindrance by the polymer chains, consistent with literature reports. [10] Furthermore, 2mg/ml of particles afforded a pseudo-first order kinetic constant similar to that of 1mM of polyhydroxamic acid. However, 2mg/ml of particle solution corresponded to 5.4mM nitrogen. The large difference could be attributed to the following possible factors. First, the presence of the negative surface charge decreased the ability of the hydroxylamine to approach the amide groups and reduced the conversion efficiency from amide groups to hydroxamic acid groups during the conversion step. Secondly, amide groups buried inside the clusters were unavailable for the conversion reaction and the conversion reaction was not as effective as in the homogenous polymer system. Thirdly, hydroxamic acid groups on the particle surface were most easily approachable by the PNPA substrate and those inside the clusters were not very accessible. If we assume the particle with the diameter of 200 nm are fully packed with amide groups on the surface, then the overall concentration of amide groups on the particle surface will be around 0.5mM with 1mg/ml particle

dispersion. Therefore, 2mg/ml particle solution has 1mM amide groups and the subsequent conversion will generate similar concentration of hydroxamic acid groups for the particles as that of the homogeneous polymer solution. This explains why 2mg/ml particle solution has similar pseudo-first kinetic constant as 1mM polyhydroxamic acid.

3.3.3 Particle Recycle and Reuse

Recovery and reuse of these functional particles are critical to reduce the environmental footprint of the chemical treatment and the quantity of particles used. After the first reaction with excess substrate, the magnetic clusters were recovered fully from the column after removal of the magnetic field. The recycled particles were then reused with a fresh batch of PNPA solution under the same experimental conditions as the original batch. Kinetic constants for the PNPA hydrolysis were obtained with the same experimental procedure, and compared with those from the freshly modified particles, as shown in Figure 3-10. The recycled particles retained around 20% of the reactivity of the freshly prepared particles.

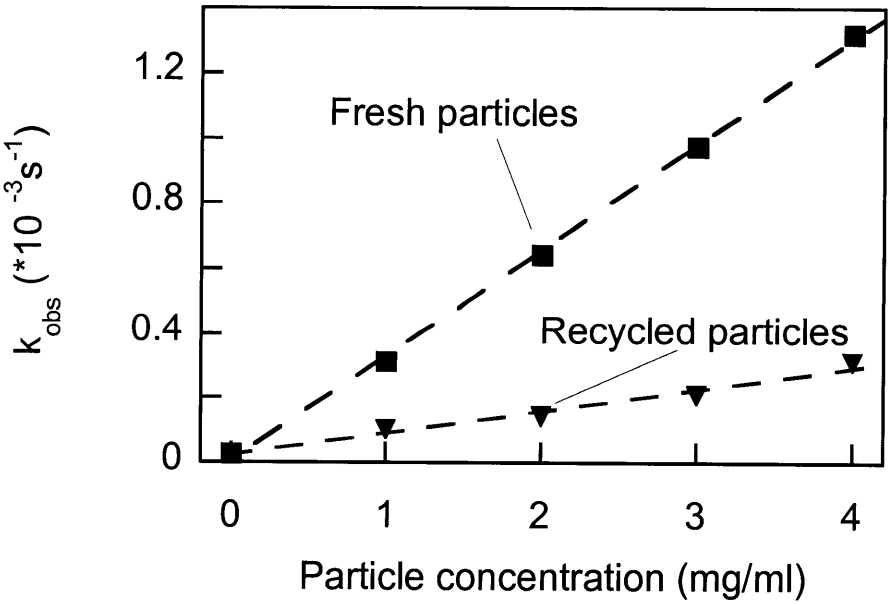

Figure 3-10. Observed hydrolysis kinetic constants of fresh particles (square) and recycled particles (triangle) at various particle concentrations. Solution pH was kept at 8 with 50mM Tris buffer and 25°C. $[PNPA]_0 = 0.25mM$.

This loss in reactivity is because the acetylated hydroxamic acid groups also underwent Lossen rearrangement in addition to the deacetylation reaction as shown in the PNPA hydrolysis mechanism. [33] The Lossen rearrangement mechanism is shown in Scheme 3-4. The deacetylation step was very slow. For example, the acetylated N-phenylisobutyrohydroxamic acid underwent deacetylation with a kinetic constant of around $2.8\times10^{-5}s^{-1}$ at pH 9. [10] There was no difference between the deacetylation rate of acetylated polymeric hydroxamic acid unit and that of the monomeric acids. [10] Therefore, the acetylated hydroxamic acid groups on the particle surface underwent deacetylation with similar reaction rate. For the Lossen rearrangement, the acetylated hydroxamic acid with similar structure as that on the particle surface underwent the rearrangement with a rate of $2.2\times10^{-4}s^{-1}$ in 0.1M ammonia. Therefore the rearrangement rate would be much slower under the conditions that we studied. As a result, the rearrangement competed with the regeneration of the hydroxamic acid groups.

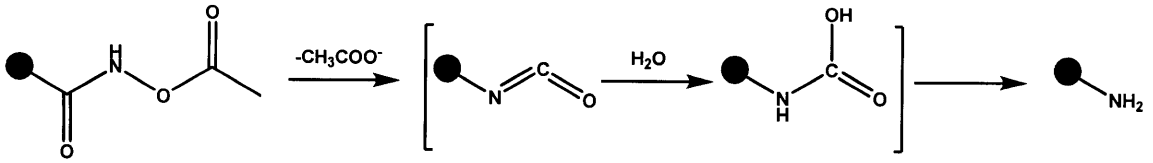

Scheme 3-4. Lossen rearrangement mechanism of acetylated hydroxamic acid groups

The above Lossen rearrangement could be suppressed by alkyl substitution on the hydroxamic acid nitrogen. As a result, the deacetylation reaction would be the primary reaction pathway for the acetylated hydroxamic acid groups. [34] However, this substitution would introduce steric hindrance into the nucleophilic groups and reduce their activity significantly. The reactivity against PNPA hydrolysis was reduced by almost seven fold when a methyl group was introduced to the hydroxamic group. [30]

Furthermore, several strategies have been proposed in the literature to enhance the deacetylation process and turn the hydroxamic acid over faster. The deacetylation rate of acetylated hydroxamic acids with the presence of imidazole groups in the molecules, such as imidazole-4-carbohydroxamic acids and N-(4-imidazolylmethyl) benzo-hydroxamic acid, was 100 times faster than those without imidazole groups. [30, 31] The deacetylation of acetyl intermediate of bi-functional polymers with imidazole and

hydroxamic acid groups was also remarkably accelerated because of the intramolecular catalysis by imidazole groups and fast deacetylation reaction of the formed acetylated imidazole, leading to much enhanced turnover rates of catalytic sites and improved overall catalytic efficiency. [35-37] Therefore, it is possible to incorporate the imidazole groups in the polymer chains to improve the turnover rate of the acetylated hydroxamic acid and the overall efficiency of the functionalized magnetic particles.

3.4 Summary

In this chapter, a new strategy was employed to attach strong nucleophilic groups, hydroxamic acid, on the surfaces of magnetic particles. The modified magnetic particles had average diameter of 200 nm for effective capture by HGMS. Particles were colloidally stabilized by strong surface charge and resulting electrostatic interactions. After the modification procedure, the particles contained significant amount of amide and hydroxamic acid groups. The modified particles were tested against a model carboxyl ester, *p*-nitrophenyl acetate. These particles significantly accelerated the hydrolysis reaction. The acetylated particles were partially regenerated in basic solution and 80% of its reactivity was lost due to the Lossen rearrangement of the acetylated hydroxamic acid groups. Suggestions are given on how this degeneration of reactivity may be reduced.

3.5 Bibliography

1. Boularot, A.; Giglione, C.; Petit, S.; Duroc, Y.; AlvesdeSousa, R.; Larue, V.; Cresteil, T.; Dardel, F.; Artaud, I.; Meinnel, T., Discovery and Refinement of a New Structural Class of Potent Peptide Deformylase Inhibitors. *J. Med. Chem.* **2007,** 50, (1), 10-20.

2. Jain, R.; Chen, D.; White, R. J.; Patel, D. V.; Yuan, Z., Bacterial peptide deformylase inhibitors: A new class of antibacterial agents. *Current Medicinal Chemistry* **2005,** 12, (14), 1607-1621.

3. Muri, E. M. F.; Nieto, M. J.; Sindelar, R. D.; Williamson, J. S., Hydroxamic acids as pharmacological agents. *Current Medicinal Chemistry* **2002,** 9, (17), 1631-1653.

4. Pal, S.; Ramachandhran, V.; Prabhakar, S.; Tewari, P. K.; Sudersanan, M., Polyhydroxamic acid sorbents for uranium recovery. *Journal Of Macromolecular Science Part A-Pure And Applied Chemistry* **2006,** 43, (4-5), 735-747.

5. Polomoscanik, S. C.; Cannon, C. P.; Neenan, T. X.; Holmes-Farley, S. R.; Mandeville, W. H.; Dhal, P. K., Hydroxamic acid-containing hydrogels for nonabsorbed

iron chelation therapy: Synthesis, characterization, and biological evaluation. *Biomacromolecules* **2005,** 6, (6), 2946-2953.
6. Morales-Rojas, H.; Moss, R. A., Phosphorolytic reactivity of o-iodosylcarboxylates and related nucleophiles. *Chemical Reviews* **2002,** 102, (7), 2497-2521.
7. Ghosh, K. K.; Kolay, S.; Bal, S.; Satnami, M. L.; Quagliotto, P.; Dafonte, P. R., Effect of cationic gemini surfactants on the hydrolysis of carboxylate and phosphate esters using hydroxamate ions. *Colloid And Polymer Science* **2008,** 286, (3), 293-303.
8. Ghosh, K. K.; Bal, S.; Satnami, M. L.; Rodriguez-Dafonte, P.; Palepu, R. M., Studies of nucleophilic substitution reactions of p-nitrophenyl acetate with some dihydroxamate ions in cationic micellar media. *Journal Of Dispersion Science And Technology* **2006,** 27, (3), 349-355.
9. Bunton, C. A.; Gillitt, N. D.; Foroudian, H. J., A quantitative treatment of dephosphorylation by an amphiphilic hydroxamate ion. The role of micellar charge. *Langmuir* **1998,** 14, (16), 4415-4421.
10. Kunitake, T.; Okahata, Y.; Ando, R., Reaction Of Hydroxamic Acid Group In Polymer With Para-Nitrophenyl Acetate. *Bulletin Of The Chemical Society Of Japan* **1974,** 47, (6), 1509-1515.
11. Ghosh, K. K.; Satnami, M. L., Nucleophilic substitution reaction of carboxylate and phosphate esters with hydroxamate ions in microemulsions. *Colloids And Surfaces A-Physicochemical And Engineering Aspects* **2006,** 274, (1-3), 125-129.
12. Zheng, Y.; Duanmu, C.; Gao, Y., A magnetic biomimetic nanocatalyst for cleaving phosphoester and carboxylic ester bonds under mild conditions. *Organic Letters* **2006,** 8, (15), 3215-3217.
13. Ditsch, A.; Yin, J.; Laibinis, P. E.; Wang, D. I. C.; Hatton, T. A., Ion-exchange purification of proteins using magnetic nanoclusters. *Biotechnology Progress* **2006,** 22, (4), 1153-1162.
14. Moeser, G. D.; Roach, K. A.; Green, W. H.; Laibinis, P. E.; Hatton, T. A., Water-based magnetic fluids as extractants for synthetic organic compounds. *Industrial & Engineering Chemistry Research* **2002,** 41, (19), 4739-4749.
15. Moss, R. A.; Chung, Y. C., Immobilized Iodosobenzoate Catalysts For The Cleavage Of Reactive Phosphates. *Journal Of Organic Chemistry* **1990,** 55, (7), 2064-2069.
16. Bucak, S.; Jones, D. A.; Laibinis, P. E.; Hatton, T. A., Protein separations using colloidal magnetic nanoparticles. *Biotechnology Progress* **2003,** 19, (2), 477-484.
17. Lu, A. H.; Salabas, E. L.; Schuth, F., Magnetic nanoparticles: Synthesis, protection, functionalization, and application. *Angewandte Chemie-International Edition* **2007,** 46, (8), 1222-1244.
18. Wang, Y. H.; Lee, J. K., Recyclable nano-size Pd catalyst generated in the multilayer polyelectrolyte films on the magnetic nanoparticle core. *Journal Of Molecular Catalysis A-Chemical* **2007,** 263, (1-2), 163-168.
19. Wang, Z. F.; Shen, B.; Zou, A. H.; He, N. Y., Synthesis of Pd/Fe3O4 nanoparticle-based catalyst for the cross-coupling of acrylic acid with iodobenzene. *Chemical Engineering Journal* **2005,** 113, (1), 27-34.
20. Caruso, F.; Schuler, C., Enzyme multilayers on colloid particles: Assembly, stability, and enzymatic activity. *Langmuir* **2000,** 16, (24), 9595-9603.

21. Bromberg, L.; Hatton, T. A., Decomposition of toxic environmental contaminants by recyclable catalytic, superparamagnetic nanoparticles. *Industrial & Engineering Chemistry Research* **2007,** 46, (10), 3296-3303.
22. Bromberg, L.; Hatton, T. A., Nerve agent destruction by recyclable catalytic magnetic nanoparticles. *Industrial & Engineering Chemistry Research* **2005,** 44, (21), 7991-7998.
23. Takafuji, M.; Ide, S.; Ihara, H.; Xu, Z. H., Preparation of poly(1-vinylimidazole)-grafted magnetic nanoparticles and their application for removal of metal ions. *Chemistry Of Materials* **2004,** 16, (10), 1977-1983.
24. Ditsch, A.; Laibinis, P. E.; Wang, D. I. C.; Hatton, T. A., Controlled clustering and enhanced stability of polymer-coated magnetic nanoparticles. *Langmuir* **2005,** 21, (13), 6006-6018.
25. Lu, H.; Li, G. F.; Fang, S. B.; Jiang, Y. Y., Fluorescent Properties Of Polymer Rare-Earth Ion Complexes.2. Poly(Acrylic Acid-Co-Acrylamide) Rare-Earth Ion Complexes. *Journal Of Applied Polymer Science* **1990,** 39, (6), 1389-1398.
26. Olle, B.; Bucak, S.; Holmes, T. C.; Bromberg, L.; Hatton, T. A.; Wang, D. I. C., Enhancement of oxygen mass transfer using functionalized magnetic nanoparticles. *Industrial & Engineering Chemistry Research* **2006,** 45, (12), 4355-4363.
27. Isikver, Y.; Saraydin, D.; Sahiner, N., Poly(hydroxamic acid) hydrogels from poly(acrylamide): preparation and characterization. *Polymer Bulletin* **2001,** 47, (1), 71-79.
28. Ditsch, A.; Lindenmann, S.; Laibinis, P. E.; Wang, D. I. C.; Hatton, T. A., High-gradient magnetic separation of magnetic nanoclusters. *Industrial & Engineering Chemistry Research* **2005,** 44, (17), 6824-6836.
29. O'Shaughnessy, B.; Vavylonis, D., Irreversibility and polymer adsorption. *Physical Review Letters* **2003,** 90, (5).
30. Kunitake, T.; Horie, S., Multifunctional Hydrolytic Catalyzes.3. Catalytic Hydrolysis Of P-Nitrophenyl Acetate By Imidazole-4-Carbohydroxamic Acids. *Bulletin Of The Chemical Society Of Japan* **1975,** 48, (4), 1304-1309.
31. Kunitake, T.; Okahata, Y.; Tahara, T., Multifunctional Hydrolytic Catalysis.6. Catalytic Hydrolysis Of P-Nitrophenyl Acetate By N-(4-Imidazolylmethyl)Benzohydroxamic Acid. *Bioorganic Chemistry* **1976,** 5, (2), 155-167.
32. Moss, R. A.; Alwis, K. W.; Shin, J. S., Catalytic Cleavage Of Active Phosphate And Ester Substrates By Iodoso-Benzoates And Iodoxybenzoates. *Journal Of The American Chemical Society* **1984,** 106, (9), 2651-2655.
33. Bright, R. D.; Hauser, C. R., The Influence of Substituents on the Rates of Decomposition of the Potassium Salts of Dihydroxamic Acids. The Lossen Rearrangement. *J. Am. Chem. Soc.* **1939,** 61, (3), 618-629.
34. Gruhn, W. B.; Bender, M. L., N-methylacetohydroxamic acid catalyzed ester hydrolysis. *J. Am. Chem. Soc.* **1969,** 91, (21), 5883-5885.
35. Kunitake, T.; Okahata, Y., Multifunctional Hydrolytic Catalyzes.4. Catalytic Hydrolysis Of Para-Nitrophenyl Acetate By Copolymers Containing Complementary Functional Groups (Hydroxamate And Imidazole). *Macromolecules* **1976,** 9, (1), 15-22.
36. Kunitake, T.; Okahata, Y., Multifunctional Hydrolytic Catalysis.2. Hydrolysis Of Para-Nitrophenyl Acetate By A Polymer Catalyst Which Contains Hydroxamate And Imidazole Functions. *Bioorganic Chemistry* **1975,** 4, (2), 136-148.

37. Bender, M. L.; Turnquest, B. W., General Basic Catalysis of Ester Hydrolysis and Its Relationship to Enzymatic Hydrolysis. *J. Am. Chem. Soc.* **1957,** 79, (7), 1656-1662.

Chapter 4

Organophosphate Decomposition

4.1 Introduction

Organophosphate compounds (OP) represent major classes of chemical warfare agents as well as pesticides. [1] They are neurotoxins that inhibit the acetylcholinesterase, an essential enzyme to break down acetylcholine and maintain normal nerve function, of many different animal species. [2] Release of chemical warfare agents in case of warfare or terrorist attack poses serious threats toward both military and civilian targets. It is critical to clean up and decompose the OP compounds from those targets quickly if contaminated. The extensive use of organophosphate pesticides in agriculture has also resulted in the risk of environmental contamination through air drift, surface runoff, and leaching from the field. [2] OP compounds can have the capacity for environmental persistence and post cumulative problem without proper treatment. [3, 4] Therefore, an economical strategy is necessary to deal with possible OP contamination.

Among various approaches to accelerate the OP decomposition process and lead the reaction into desired products, catalytic decomposition has been widely tested because of enhanced reaction rates and high specificity. [5-9] Three types of catalysts have been focused upon for OP decomposition. The first is highly reactive α-nucleophiles, such as oximates, [10, 11] hydroxamates, [12] hydrogen peroxide anions, [13, 14] iodosobenzoate and its derivatives, [15-17] etc. In these groups, the electron lone pair from the catalytic atom collaborates with another lone pair of electrons on the α-atom and therefore increases the nucleophilicity dramatically. The second group is metal complexes and metallomicelles. [6, 18] However, the introduction of heavy metals into the system can potentially cause further problems without a clear strategy to remove them after use. The third group includes biological catalysts, such as organophosphorus hydrolase (OPH) enzymes. However, lack of sufficient quantities of enzymes, weak enzyme stability, and substrate specificity has limited their large-scale applications.

Therefore, the α-nucleophiles are the focus of this research because of the strong hydrolytic reactivity, excellent chemical stability in the targeted complex systems, and relatively straightforward preparation. In the previous two chapters, we have demonstrated two strategies to attach such groups on the surface of magnetic particles. In both cases, the prepared magnetic particles were colloidally stable in water dispersions and were captured effectively by high gradient magnetic separation (HGMS). In the two strategies, the hydroxamic acid modified particles were more effective with regard to the quantity of functional groups attached and the efficacy of functional groups with regard to the hydrolysis of model carboxyl ester, *p*-nitrophenyl acetate (PNPA). This is indicative of the reactivity towards the hydrolysis of organophosphate esters. Therefore, the hydroxamic acid modified particles were investigated for the hydrolysis of organophosphate esters.

In this chapter, the hydrolysis reaction of organophosphate compounds, such as diisopropyl fluorophosphate (DFP) and methyl- and ethyl- paraoxon, accelerated by α-nucleophiles, such as hydroxamic acid and pyridine-2-aldoxime methochloride (2-PAM), was measured in homogenous systems to understand the reaction mechanism. Effects on the reaction mechanism and reaction rates of the solution conditions, substrate properties, and the properties of nucleophiles are discussed. Secondly, the OP hydrolysis reaction by hydroxamic acid modified particles was investigated for their reactivity and recovery properties and potential applications of such systems are discussed.

4.2 Experimental Section

4.2.1 Chemical Reagents

Diisopropyl fluorophosphates (DFP), methyl-paraoxon, ethyl-paraoxon, 3-(cyclohexylamino)-1-propanesulfonic acid (CAPS), tris(hydroxymethyl) aminomethane (Trizma base), pyridine-2-aldoxime methochloride (2-PAM) and acetohydroxamic acid (AHA) (98%), and polyacrylamide (50%wt in water, Mw=10,000) were purchased from Sigma-Aldrich Chemical Company (Milwaukee, WI) and used as received. Dimethyl phosphate and diethyl phosphate (75%wt, balanced with phosphoric acid) were

purchased from Acros Organics (Geel, Belgium) and used as received. Sodium hydroxide was purchased from Mallinckrodt Baker Inc. (Phillipsburg, NJ) and used as received. Water was obtained from the Milli-Q water system.

All organophosphate compounds are extremely toxic. Particular care was taken when handling these chemicals. Buffers at pH 8 and 9 were prepared with Trizma base. Buffer at pH 9.5 and 10.6 were prepared with CAPS. Polyhydroxamic acid (PHA) was prepared from polyacrylamide through the procedure described in chapter 3.

4.2.2 NMR Measurement of Organophosphate Decomposition

The hydrolysis of the organophosphate compounds over time was analyzed by phosphorus 31 nuclear magnetic resonance spectroscopy (^{31}P NMR). This technique can differentiate various phosphorus-containing species in the system and detect their concentration changes to enable measurement of the hydrolysis kinetics. Solution mixtures consisted of nucleophilic compounds, 50mM of buffer to keep solution pH constant, 5mM of organophosphate compounds, and 20%vol of deuterium oxide serving as signal lock. The ^{31}P NMR test was performed on a Varian 501 spectrometer (202MHz for phosphorus). Longitudinal relaxation times, T1, of all organophosphate compounds were first determined to be less than 4 seconds under the same conditions as those in kinetic measurements. The delay time, d1, was therefore set to be 20 seconds to allow full relaxation of the phosphorus nuclei after the magnetic pulse for quantitative measurement of phosphorus-containing species. Sixteen scans were collected to produce high-quality signal. The middle point of the collection time period was considered as the time point when the measurement was conducted. The acquired data then underwent Fourier transformation, phase correction, and baseline correction to obtain the final NMR spectra. Individual peaks in the spectra were integrated to calculate the relative concentrations of each phosphorus-containing component in the system and then analyze the hydrolysis mechanism and hydrolytic kinetics.

4.2.3 Turnover Test of 2-PAM

Catalyst turnover is critical for the hydrolysis of organophosphate compounds when adding α-nucleophiles to the hydrolysis system. The turnover of 2-PAM was investigated for DFP hydrolysis with ^{31}P NMR. The solution mixture consisted of 5mM of DFP, 1mM of 2-PAM, and 50mM Tris buffer at pH 8. The solution mixture has 20%vol of deuterium oxide as signal lock. A varian-501 spectrometer was utilized to follow the hydrolytic kinetics. After the initial 20-30% decomposition, the original DFP was allowed to be fully decomposed and the solution was kept at room temperature for another ten days to ensure any intermediates were fully decomposed. Then another batch of pure DFP was added to the solution mixture to give a DFP concentration of 5mM. The hydrolytic kinetics of DFP was measured again by NMR spectrometry under the same conditions. The kinetic constants acquired from the second NMR measurement were compared with those from the first to study the 2-PAM turnover.

4.2.4 Kinetics Measurement of Hydroxamic Acid Modified Particles

Hydrolytic kinetics of methyl-paraoxon and ethyl-paraoxon by the hydroxamic acid modified particles were determined by following the concentration change of hydrolyzed product, *p*-nitrophenol ion. The reaction mixture consisted of magnetic particles, 50mM Tris buffer to keep the solution pH at 9, 0.2M sodium chloride to keep the ionic strength constant, and 0.5mM of paraoxon compounds. At certain time intervals, 0.5ml of the reaction mixture was drawn out and passed through the HGMS column to remove the particles and 2ml of Tris buffer at pH 9 were used to wash out any material trapped by the column wires. The HGMS procedure was the same as that described in chapter 3. A Hewlett-Packard 8453 UV/Vis spectrophotometer was utilized to measure the absorbance of the collected solution. Absorbance at 404nm by the *p*-nitrophenol ion was used to calculate the concentration of hydrolyzed product and thus the hydrolysis rate. Spontaneous hydrolysis was also measured with UV/Vis for methyl-paraoxon and ethyl-paraoxon under the same solution conditions with 0.05mM substrate. Homogenous paraoxon hydrolysis by acetohydroxamic acid and polyhydroxamic acid was also performed in a similar fashion.

4.3 Results and Discussion

4.3.1 Spontaneous Hydrolysis

Spontaneous hydrolysis of methyl-paraoxon and ethyl-paraoxon was followed by both UV/Vis and ^{31}P NMR. The UV/Vis technique measured only the reaction pathway in which *p*-nitrophenol was released, whereas ^{31}P NMR analyzed all hydrolysis products.

Methyl-paraoxon and ethyl-paraoxon underwent similar spontaneous hydrolysis. There were two types of hydrolysis products shown in the NMR spectrum for each substrate. The NMR spectrum of the methyl-paraoxon system in 50mM Tris buffer at pH 8 after 8670min is shown in Figure 4-1, in which the chemical shift at -18.205ppm was from methyl-paraoxon. Peak areas at the chemical shifts of -17.756ppm and -11.040ppm increased over time while the substrate peak gradually shrank, indicating the presence of two hydrolytic products. NMR comparison with commercially available dimethyl phosphate under the same solution conditions suggested that the chemical shift at -11.040ppm was from the product when hydroxyl groups substituted the *p*-nitrophenyl groups. It was then reasonably postulated that the chemical shift at -17.756ppm was from the product when the methyl group was removed.

Ethyl-paraoxon behaved similarly to methyl-paraoxon. In Figure 4-2, the chemical shift at -20.534ppm was from the original substrate whereas chemical shifts at -13.299ppm and -18.985ppm were from the two hydrolytic products when hydroxyl groups substituted the *p*-nitrophenol groups and when one ethyl group was removed, respectively, in 50mM Tris buffer at pH 8 after 23 days. Even after this long time, the majority of ethyl-paraoxon substrate still remained intact, indicating the environmental persistence of such substrates.

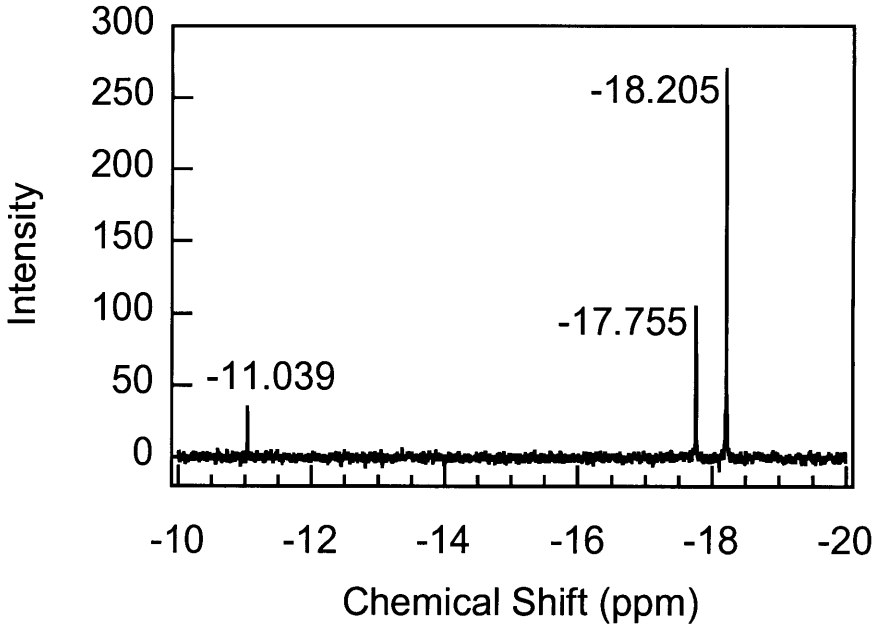

Figure 4-1. NMR spectrum of hydrolytic system of 5mM of methyl-paraoxon in 50mM Tris buffer at pH 8 after 8670 min with 20% deuterium oxide as signal lock.

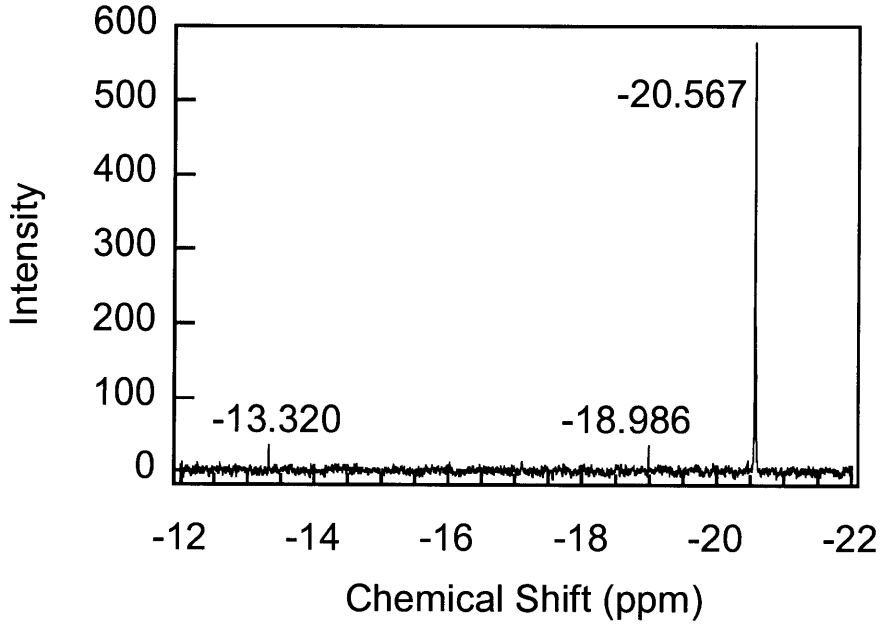

Figure 4-2. NMR spectrum of hydrolytic system of ethyl-paraoxon in 50mM Tris buffer at pH 8 with 20% deuterium oxide as signal lock after 23 days.

It has been shown in the literature that nucleophiles attack both the phosphorus and alkyl carbon atom of the organophosphate esters during the hydrolysis or ethanolysis reactions. [19, 20] The importance of these pathways depends on the properties of the substrates,

nucleophiles and the solution conditions. For example, the cleavage of the P-O bond of a chiral thiophosphonate substrate by phosphotriesterase (PTE) was shown to proceed through an SN_2-like single displacement reaction with a net inversion of the configuration at the phosphorus center. [21-23] Fenitrothion was mainly subjected to SN_2 attack on phosphorus in alkaline systems. [24]

Similar to the literature reports, hydroxyl ions attacked both the methyl or ethyl groups and the *p*-nitrophenol groups during the spontaneous hydrolysis of methyl-paraoxon and ethyl-paraoxon. In 50mM Tris buffer solution at pH 8, the reaction on the methyl groups was almost three times faster than that on the *p*-nitrophenol groups for methyl-paraoxon, while the reaction on the ethyl groups proceeded at the same rate as that on the *p*-nitrophenol groups. The spontaneous hydrolysis of OP compounds within the buffer solution is described by Equation 4-1, in which the total reaction rate included the substitution reaction on both phosphorus and carbon atoms.

$$r_{total} = \frac{d[OP]}{dt} = -\left(k_{spon} + k_{OH}\left[OH^-\right]\right)[OP] = r_P + r_C = -\left(k_C + k_{PNP}\right)[OP] \qquad \textbf{Equation 4-1}$$

Since the solution pH was kept constant, the hydroxyl concentration was constant and the hydrolysis followed pseudo first order kinetics. Measurement by UV/Vis followed only the reaction mechanism in which *p*-nitrophenol was released. This part of the hydrolysis kinetics was shown in Equation 4-2.

$$r_P = \frac{d[PNP]}{dt} = k_{PNP}[OP] \qquad \textbf{Equation 4-2}$$

Divided by Equation 4-1, Equation 4-2 was then transformed into Equation 4-3

$$\frac{d[PNP]}{d[OP]} = -\frac{k_{PNP}}{k_C + k_{PNP}} \qquad \textbf{Equation 4-3}$$

The overall concentration change of organophosphate was described by Equation 4-4.

$$[OP] = [OP]_0 \exp\left(-\left(k_C + k_{PNP}\right)t\right) \qquad \textbf{Equation 4-4}$$

This was substituted into Equation 4-3, integrated, and simplified into Equation 4-5.

$$\frac{[PNP]_t}{[OP]_0} = \left(1 - \exp\left(-\left(k_C + k_{PNP}\right)t\right)\right)\frac{k_{PNP}}{k_C + k_{PNP}} \qquad \textbf{Equation 4-5}$$

This could be further manipulated into Equation 4-6.

$$-\ln\left(1 - \frac{[PNP]_t}{[OP]_0}\right) = -\ln\left(1 - \left(1 - \exp\left(-\left(k_C + k_{PNP}\right)t\right)\right)\frac{k_{PNP}}{k_C + k_{PNP}}\right) \qquad \textbf{Equation 4-6}$$

Since the reaction rate was very slow and the $-\left(k_C + k_{PNP}\right)t$ term was small during the initial stage of the decomposition reaction and the two reaction rates were comparable, it was then simplified by using Tyler expansion twice to obtain Equation 4-7.

$$-\ln\left(1 - \frac{[PNP]_t}{[OP]_0}\right) = k_{PNP}t \qquad \textbf{Equation 4-7}$$

The measured concentration change was then simplified based on this equation and the observed kinetic constants were obtained through linear fitting of the logarithmic term versus time plot.

The results for the hydrolysis of methyl-paraoxon are shown in Figure 4-3. The fitting results are not shown since they overlap with the measurement results and are not differentiable. The results of ethyl-paraoxon hydrolysis showed similar trends. The nearly linear behavior of the results indicates that the *p*-nitrophenol ion products were from the hydrolysis of methyl- and ethyl- paraoxon products only. The products when methyl- or ethyl- groups were substituted would not undergo substitution reaction to release *p*-nitrophenol ions.

The hydrolysis kinetic constants of methyl- and ethyl- paraoxon releasing *p*-nitrophenol are plotted against solution pH in Figure 4-4. The kinetic constants were linearly dependent on solution pH with a slope of 0.8 on a logarithmic scale, suggesting that the

reaction is first order with respect to hydroxyl ions and OP substrate respectively. Hydrolysis of methyl-paraoxon was two to three times faster than that of ethyl-paraoxon at each solution pH, reflecting that the steric hindrance from the two ethoxide groups was much larger than that of the two methoxide groups in the second order nucleophilic substitution of hydroxyl ions on phosphorus. This is consistent with the claims in the literature that organophosphate triesters were hydrolyzed through the associative mechanism, in which the nucleophiles approached the neutral OP substrates and formed a pentacoordinated transition state or transient intermediate prior to expelling the leaving group when the pKa values of the leaving groups were very small. [25-29] During the measurement, the presence of either the pentacoordinate intermediate or the transition state was not detected in the NMR spectrum, indicating that the formation of an intermediate or transition state was the rate-limiting step and the intermediate was readily decomposed if it formed.

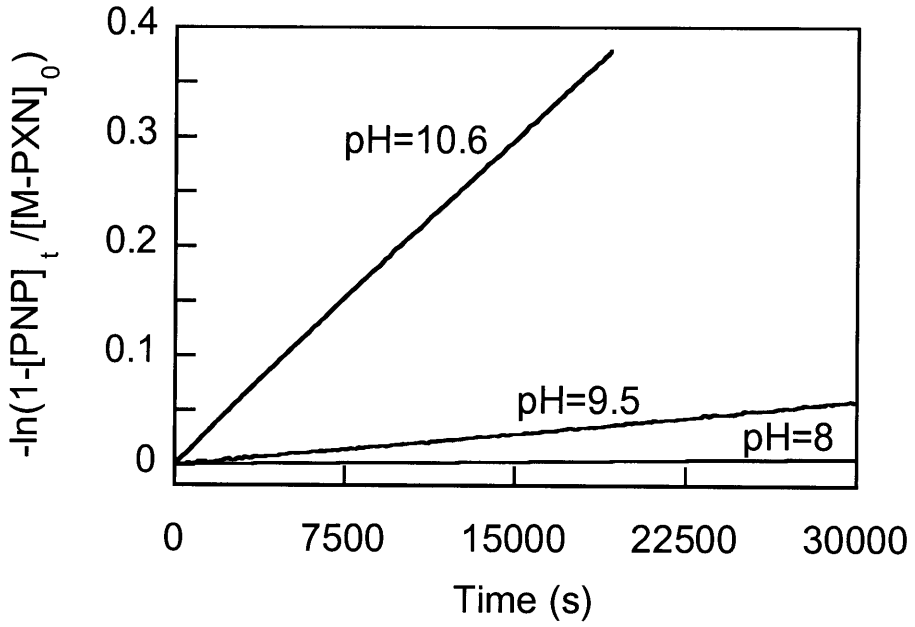

Figure 4-3. Pseudo-first order kinetics of spontaneous hydrolysis of methyl-paraoxon at different solution pH. Measurements were taken at 25°C.

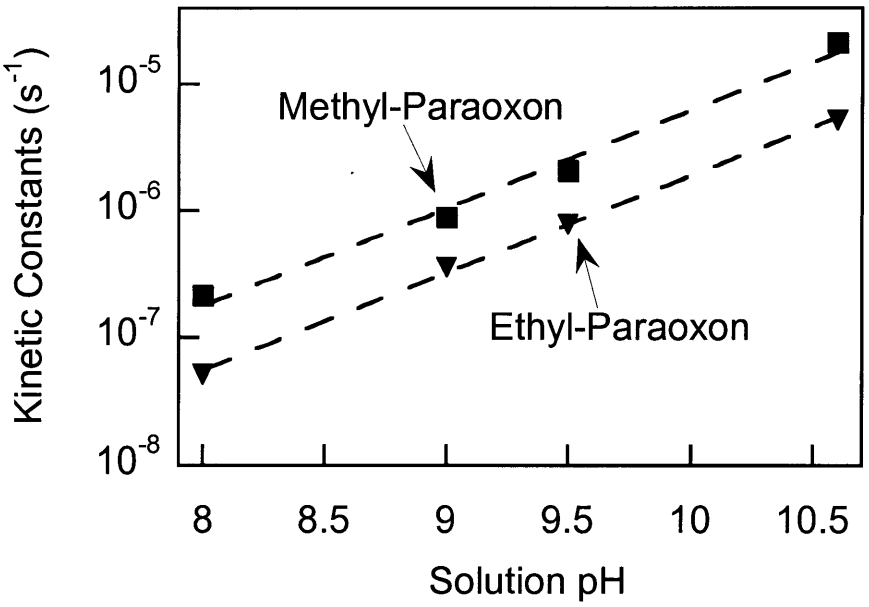

Figure 4-4. Dependence of kinetic constants from spontaneous hydrolysis of methyl- and ethyl- paraoxon on solution pH. 50mM Tris buffer was used to keep solution pH at 8 and 9 and 50mM CAPS buffer to keep solution pH at 9.5 and 10.6 respectively.

The NMR data were also used to calculate the kinetic constants. The peaks in the acquired NMR spectra were integrated and the relative percentage of each peak was calculated. The kinetic constants for the mechanism of removing methyl and releasing *p*-nitrophenol groups were obtained through the same procedure as that used in the UV/Vis measurement. In Table 4-1 are shown the kinetic constants of the two mechanisms at different solution pH when methyl-paraoxon is hydrolyzed by hydroxyl ions. The kinetic constant of reaction on the *p*-nitrophenol groups increases almost 85 times with the increase of solution pH from 8 to 10.6. However, the kinetic constant of reaction on the methyl groups only increases slightly at the same time. This indicates the reaction on the methyl groups is first order overall and independent of hydroxyl ions. It therefore follows a dissociative mechanism, whereas the reaction on the *p*-nitrophenol groups is second order and follows an associative mechanism. The slight difference between kinetics constants obtained with UV/Vis method and those by NMR method was probably due to the presence of 20% D_2O in the NMR measurement.

	Reaction on p-nitrophenol	Reaction on methyl
pH=8	$1.1\times10^{-7}s^{-1}$	$4.2\times10^{-7}s^{-1}$
pH=10.6	$9.3\times10^{-6}s^{-1}$	$1.4\times10^{-6}s^{-1}$

Table 4-1. Kinetic constants of methyl-paraoxon hydrolysis on the *p*-nitrophenol and alkyl groups respectively. 50mM Tris buffer was used to keep solution pH at 8 and 50mM CAPS buffer to keep solution pH at 10.6.

The NMR spectrum of the diisopropyl fluorophosphate (DFP) hydrolysis mixture after 292min is shown in Figure 4-5. The doublet occurring at -22.172ppm and -26.981ppm was from DFP substrate. There was only one product peak at -14.834ppm. It was proposed in the literature that DFP forms a pentacoordinate intermediate with the attacking nucleophiles and that the intermediate decomposes through the departure of fluoride ion. The formation step was always rate-determining during hydrolysis in aqueous solution based on experimental results as well as ab initio molecular orbital calculations. [29] The fact that there was only one product peak throughout the process indicated that the pentacoordinate intermediate decomposed very fast and as a result the concentration of the intermediate was too low to be detected by ^{31}P NMR. Kinetic constants at different solution pH are listed in Table 4-2. The strong dependence of hydrolysis rate on solution pH and pseudo-first order reaction kinetics at each pH suggested that the reaction is first order with regard to the substrate and hydroxyl ions respectively. This is consistent with the pentacoordinate intermediate formation mechanism.

The hydrolysis rate of DFP was much faster than that of paraoxon triesters under the same solution conditions. This is because the presence of the fluoride pulls the electronic density away from the phosphorus atom and enables the phosphorus center to have a more positive charge characteristic and therefore to be more electrophilic. As a result, the substrate is more susceptible to the nucleophilic attack. Furthermore, the fluoride ion is a much stronger leaving group than *p*-nitrophenol because of a much smaller pKa. Therefore, the fluoride carrying substrates are more easily decomposed by attacking nucleophiles.

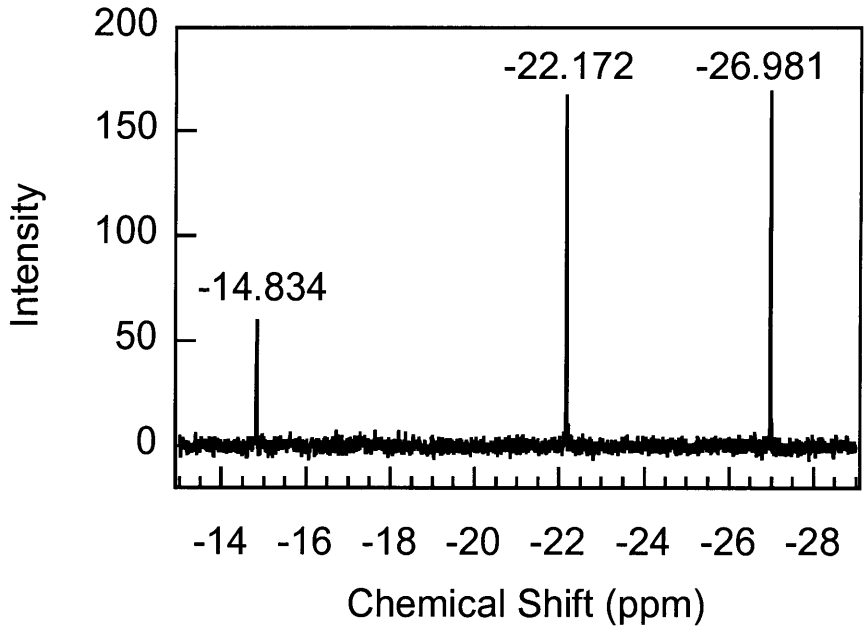

Figure 4-5. Spontaneous hydrolysis of DFP in 50mM Tris buffer at pH 8 after 292min. 20%vol of deuterium oxide was added to lock the NMR signal.

	TES buffer at pH 7	Tris buffer at pH 8
Kinetic constants	$1.9\times10^{-6}s^{-1}$	$9.6\times10^{-6}s^{-1}$

Table 4-2. Kinetic constants of DFP hydrolysis at different solution pH

4.3.2 Reaction of Paraoxon and DFP with Oxime

Hydrolysis of the previous substrates by α-nucleophiles was also studied with ^{31}P NMR and UV/Vis. The reaction acceleration by 2-PAM is discussed first and the reaction with hydroxamic acid groups will be discussed in the next section.

The NMR spectrum of the reaction mixture consisting of 5mM of DFP and 3mM of 2-PAM is shown in Figure 4-6. There was only one product peak in addition to the doublet from the DFP substrate. It was located at -14.823ppm, the same position as that from the spontaneous hydrolysis.

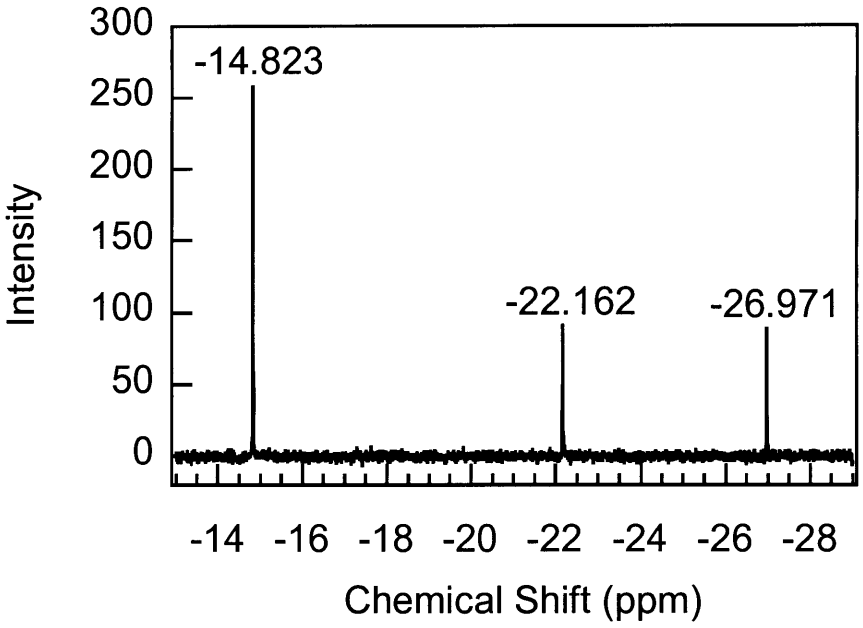

Figure 4-6. NMR spectrum of DFP hydrolysis by 3mM of 2-Pyridinealdoxime methyl chloride at 79min in 50mM Tris buffer at pH 8.

The turnover of added nucleophiles after the first batch of reaction was studied in the case of DFP hydrolysis by 2-PAM. As described in the experimental procedures, the recovered 2-PAM was challenged with another batch of DFP substrate and the concentration change was again measured by ^{31}P NMR. The DFP hydrolysis by 2-PAM is described by Equation 4-8.

$$r = \frac{d[DFP]}{dt} = -\left(k_{spon} + k_{OH}[OH^-] + k_{cat}[NOH^-]\right)[DFP] \qquad \textbf{Equation 4-8}$$

in which DFP is hydrolyzed through spontaneous hydrolysis as well as hydrolysis by 2-PAM. The change in concentration of the added 2-PAM is described by Equation 4-9.

$$\frac{d[NOH^-]}{dt} = -k_{cat}[NOH^-][DFP] + k_{rec}[OH^-][Complex] \qquad \textbf{Equation 4-9}$$

in which the added 2-PAM was consumed by the reaction with DFP and assumed to be recovered from the presumably formed complex. The above equation may not reflect the true reaction mechanism; rather it was used to test if 2-PAM can be regenerated from the complex formed in the reaction mixture.

The spontaneous hydrolysis was measured separately under the same experimental conditions without the addition of 2-PAM to provide $k_{spon} + k_{OH}\left[OH^-\right] = 9.8\times10^{-6}s^{-1}$. The turnover rate was further assumed to be slow and the turnover term in Equation 4-9 was neglected. The second order kinetic constant k_{cat} was then obtained by non-linear least square fitting through MATLAB calculation with the concentration change of DFP measured by ^{31}P NMR. The experimental data and the fitting results are shown in Figure 4-7.

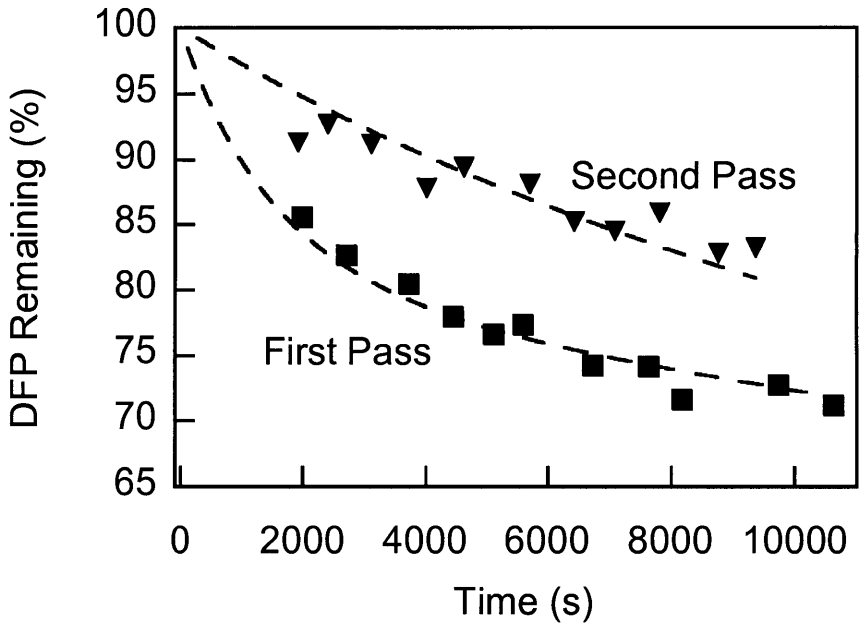

Figure 4-7. 2-PAM turnover test with DFP as substrate. The first pass refers to the DFP hydrolysis with fresh 2-PAM and the second pass refers to another 5mM of DFP added after the system has been fully hydrolyzed in 10 days. The lines were from the non-linear least square fitting with the kinetic equations.

The k_{cat} obtained in the first pass was $0.13M^{-1}s^{-1}$, reflecting the strong reactivity of 2-PAM toward the DFP hydrolysis. However, the k_{cat} obtained through the same procedure was only $0.018\ M^{-1}s^{-1}$ when DFP was again hydrolyzed in the system after the hydrolysis of excessive amount of DFP in the first pass. This indicates that either only a small amount of 2-PAM was recovered after reaction with an excess of DFP or the system accelerated DFP hydrolysis a little bit without any 2-PAM recovered. Either of these two scenarios suggests that 2-PAM functioned more as a reactant than as a catalyst for the DFP hydrolysis system.

Methyl-paraoxon and ethyl-paraoxon hydrolyzed by 2-PAM generated the products with the same chemical shifts as those from the spontaneous hydrolysis under the same solution conditions, as shown in Figure 4-8 and Figure 4-9 respectively.

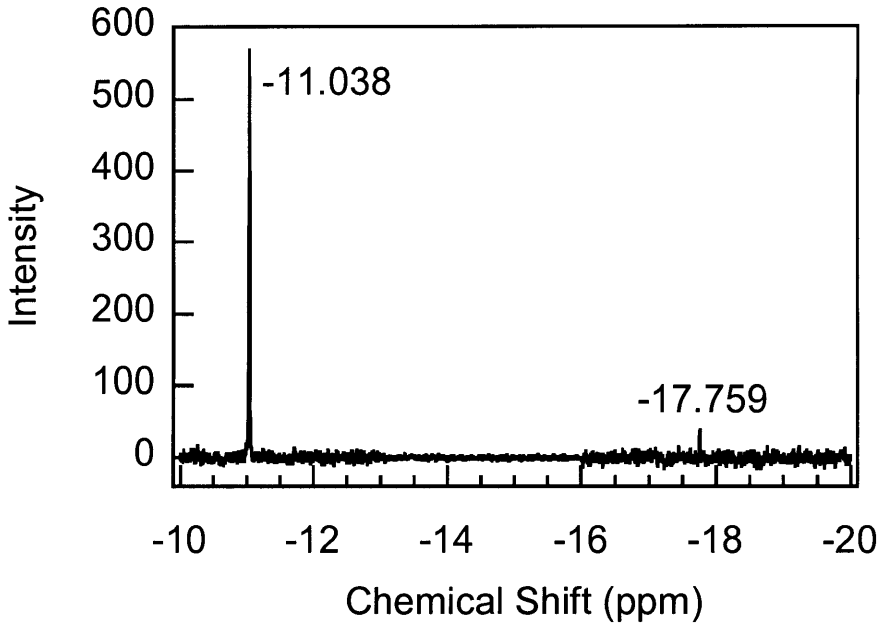

Figure 4-8. Methyl-paraoxon hydrolysis with 10mM PAM-Cl in 50mM Tris buffer at pH 8 after 3240min

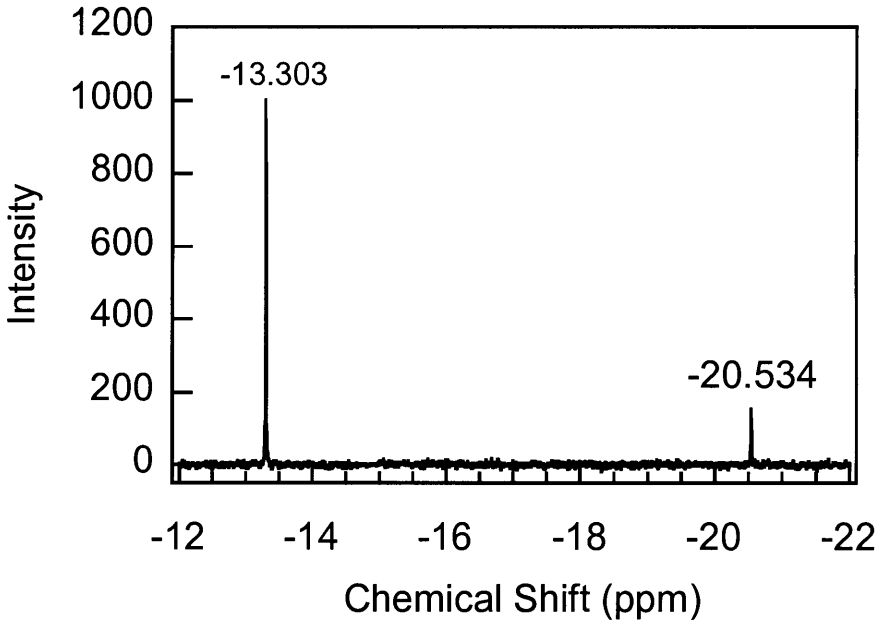

Figure 4-9. Ethyl-paraoxon hydrolysis in 10mM PAM-Cl in 50mM Tris buffer at pH 8 after 3840min

During DFP hydrolysis, 2-PAM substituted the fluoride ions. For hydrolysis of methyl-paraoxon and ethyl-paraoxon, 2-PAM substituted the *p*-nitrophenol groups. It has been determined in the literature that oximes and OP compounds form phosphoryl oxime intermediates, also strong inhibitors of AChEs. [30] Therefore, dimethyl-, diethyl-, and diisopropyl- phosphoryl oxime were formed between OP substrates and 2-PAM as a result. The reaction is first order with regard to the substrate and 2-PAM respectively.

The compound diethyl-phosphoryl 2-PAM (DEP-2PAM) was prepared in organic solvent and tested to have a half-life of only 10 seconds in 10mM Tris buffer (pH 7.8) at 29°C. [31] The instability of phosphoryl 2-PAM was echoed in other literature findings.[32, 33] Therefore, the dimethyl-, diethyl-, and diisopropyl-phosphoryl oximes formed with 2-PAM and methyl-paraoxon, ethyl-paraoxon, and DFP would also be very unstable because of the structural similarity with those in the literatures.

Furthermore, it was shown that the phosphonyl oxime intermediates formed between pyridinium oximes, obidoxime chloride (LuH6) and trimedoxime bromide (TMB4), had significantly different chemical shifts from the final organophosphoric acid measured by ^{31}P NMR. [32] The product formed during hydrolysis of the three organophosphates, however, had the same chemical shifts as the products from the spontaneous hydrolysis, indicating that the generated products from the 2-PAM reactions were the same organophosphoric acids as those from the spontaneous hydrolysis. The phosphoryl oximes, if formed, were not detected by ^{31}P NMR during the hydrolysis reaction due to their instability.

It has been shown that the phosphoryl oxime intermediates undergo two parallel decomposition pathways: Beckmann elimination pathway to yield organophosphoric acid and transform the oxime groups into nitrile groups, and SN_2P substitution by hydroxide ions to yield organophosphoric acid and recovered oximes. The stability and decomposition pathway of the phosphoryl oximes are determined by the characteristics of the substitute groups on the phosphorus center, the structure of the oxime groups, and the solution conditions. [30, 32, 34] When the other two substitute groups on the phosphorus

center were alkoxide groups in the phosphoryl pyridinealdoximes, the elimination mechanism was dominant. When the two substitute groups were alkyl groups, the substitution mechanism was dominant and oxime groups were almost fully regenerated. When the two substitute groups consisted of one alkyl group and one alkoxide group, both mechanisms were functioning and the parent oxime was partially regenerated. [34-36] O-isopropyl methylfluorophosphonyl 2-PAM formed by sarin and 2-PAM in water underwent the elimination reaction catalyzed by hydroxide ions and oximate ions, producing as end product 2-cyano-1-methylpyridinium cation. [37] Dimethylphosphoryl-, diethylphosphoryl-, and diisopropylphosphoryl-obidoxime conjugates were decomposed by hydroxyl ions to yield obidoxime mononitrile confirmed by mass spectrometry. [38, 39]

The reaction mechanism of the organophosphate decomposition by 2-PAM is summarized in Scheme 4-1.

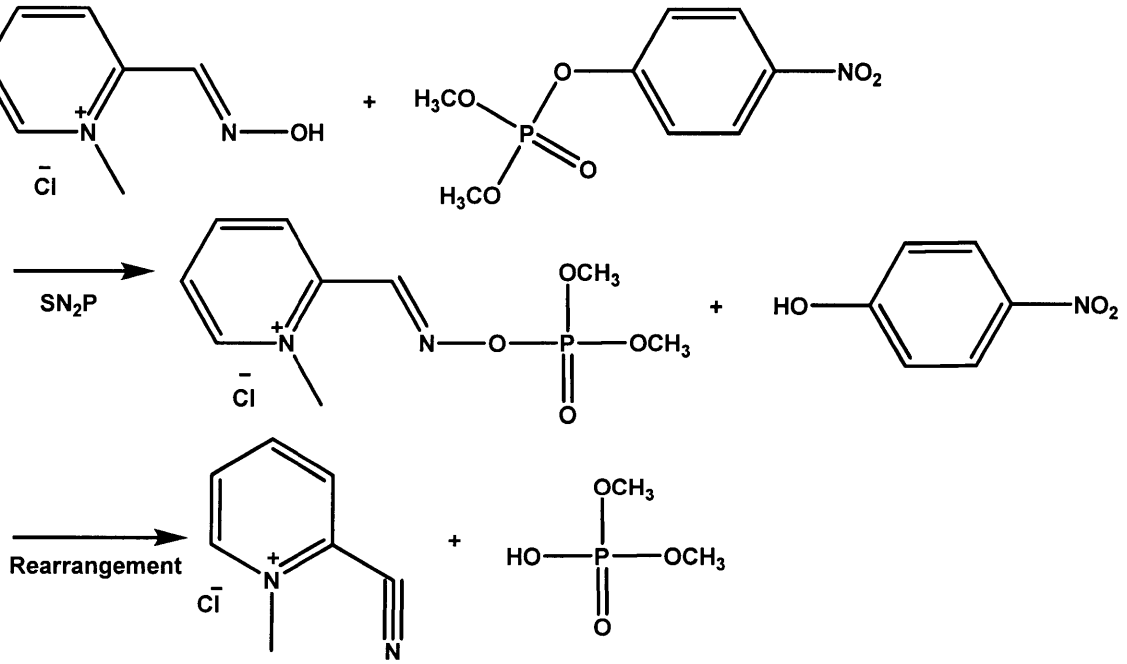

Scheme 4-1. Organophosphate decomposition of methyl-paraoxon by 2-PAM to form unstable intermediate, dimethyl phosphoryl oxime, and then the fast rearrangement to yield the final products. Ethyl-paraoxon and DFP would follow similar mechanism.

As the reaction mechanism and the recovery experiment suggested, 2-PAM added to the system did not function as a real catalyst. It was consumed stoichiometrically during the hydrolysis reaction to yield the nitrile product irreversibly. Therefore, it was not the

regenerated 2-PAM that caused the faster DFP hydrolysis relative to the spontaneous hydrolysis in the second pass of the turnover experiment.

4.3.3 Organophosphate Hydrolysis by Hydroxamic Acid

Decomposition of methyl-paraoxon and ethyl-paraoxon by acetohydroxamic acid yielded products with the same chemical shifts as those from spontaneous hydrolysis under the same solution conditions, as shown in Figure 4-10 and Figure 4-11 respectively. Similar to 2-PAM, peaks at -11.040ppm and -13.321ppm grew much faster than those in spontaneous hydrolysis for methyl-paraoxon and ethyl-paraoxon respectively. These products were formed when the hydroxamic acid groups attacked the *p*-nitrophenol groups through nucleophilic substitution.

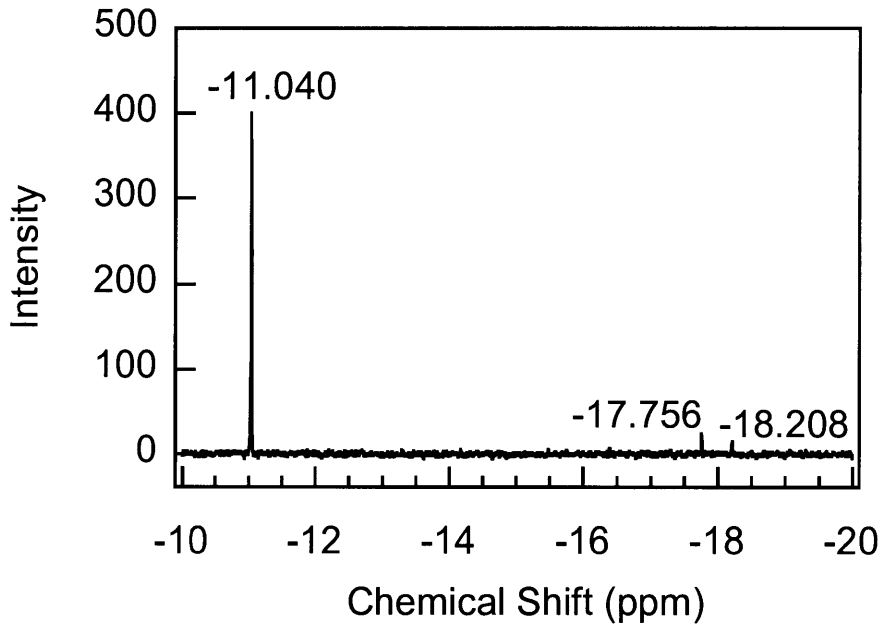

Figure 4-10. Methyl-paraoxon hydrolysis in 20mM acetohydroxamic acid in 50mM Tris buffer at pH 8 after 4115min

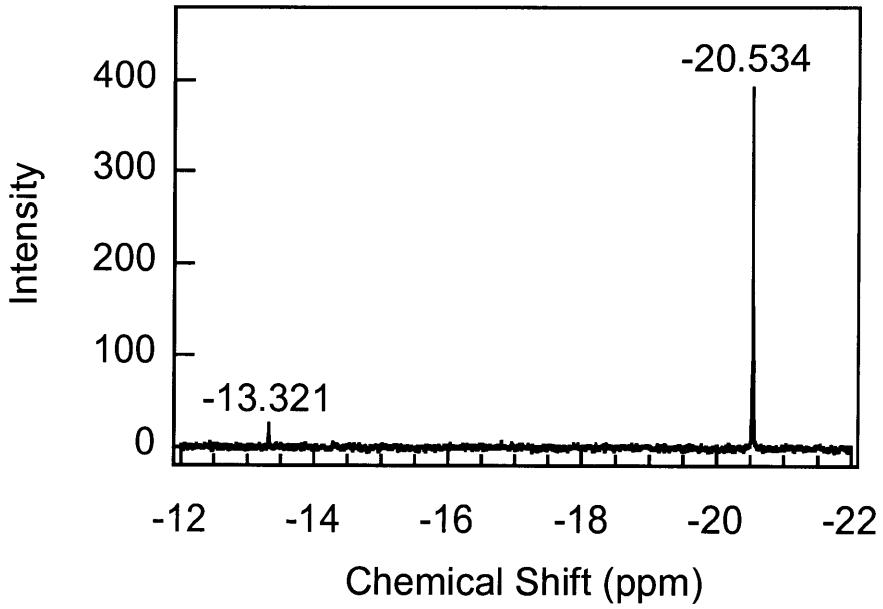

Figure 4-11. Ethyl-paraoxon hydrolysis with 1mM acetohydroxamic acid in 50mM CAPS buffer at pH 9.5 after 182 min

The NMR spectrum of the reaction mixtures consisting of 5mM of DFP and 20mM acetohydroxamic acid in 50mM Tris buffer at pH 8 is shown in Figure 4-12. The only product also has the same chemical shift as that from spontaneous hydrolysis.

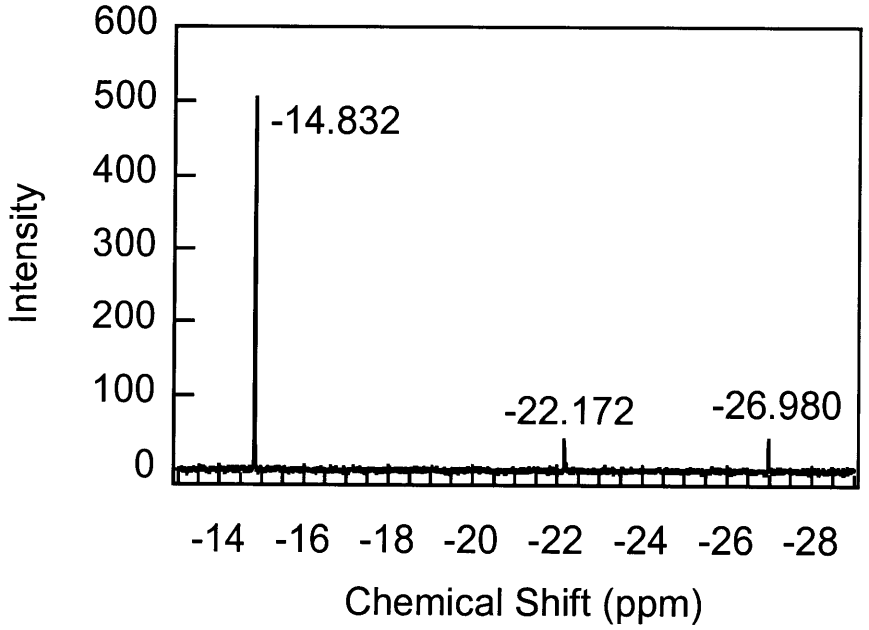

Figure 4-12. NMR spectrum of 5mM of DFP hydrolyzed by 20mM acetohydroxamic acid at 140 min in 50mM Tris buffer at pH 8

Methyl-paraoxon and ethyl-paraoxon hydrolyzed by hydroxamic acid nucleophiles were proposed to form phosphoryl hydroxamic acid intermediates through substitution of the *p*-nitrophenol groups, as shown in Scheme 4-2.

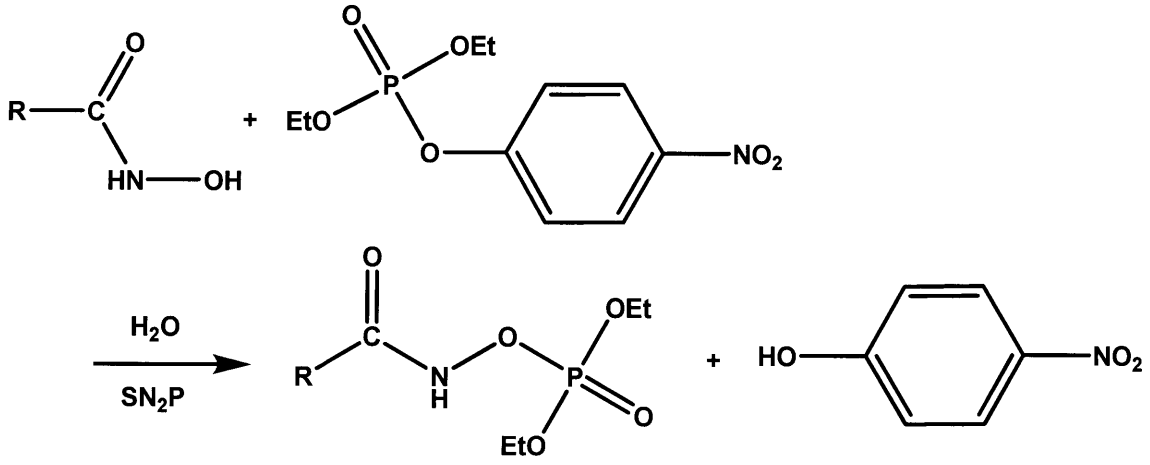

Scheme 4-2. Proposed mechanism of ethyl-paraoxon hydrolysis by hydroxamic acid groups to yield the phosphoryl hydroxamic acid and *p*-nitrophenol

DFP hydrolyzed by hydroxamic acid nucleophiles was proposed to form the phosphoryl hydroxamic acid through nucleophilic substitution, as shown in Scheme 4-3. [40]

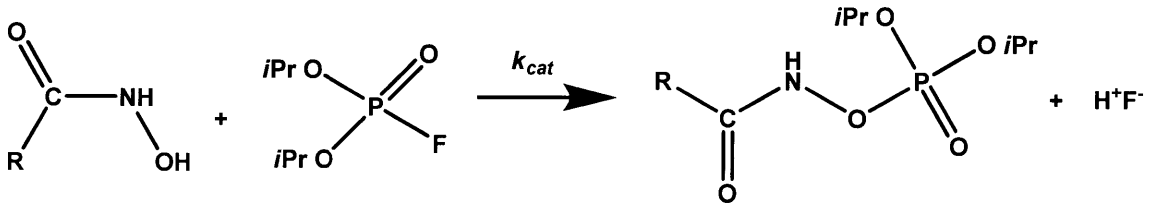

Scheme 4-3. Proposed mechanism of DFP hydrolysis by hydroxamic acid groups to yield the hydrolyzed product and the phosphoryl hydroxamic acid intermediate

However, the presence of these intermediates was not detected with ^{31}P NMR during the hydrolysis of methyl-paraoxon, ethyl-paraoxon, and DFP with both acetohydroxamic acid and polyhydroxamic acid. The only products generated from the hydrolysis systems were dimethyl, diethyl, and diisopropyl phosphoric acid, the same products of spontaneous hydrolysis. This indicates that the phosphoryl hydroxamic acid intermediates were very unstable and that they degenerated into the organophosphoric acid.

It has been shown that when hydroxamic acids were mixed under neutral solution conditions with organophosphates, such as diisopropyl fluorophosphate (DFP) and O-

isopropyl methylfluorophosphonate (sarin), hydroxamic acids were quickly phosphorylated to form highly unstable phosphoryl hydroxamic acid intermediate. [41] Addition of more than thirty types of hydroxamic acid significantly accelerated sarin and DFP hydrolysis. [40] The strong electron-withdrawing capability of the phosphoryl groups from the P-O double bond increased the tendency for a positive charge on nitrogen and therefore facilitated the migration of the alkyl group to undergo Lossen rearrangement. [42] Therefore, phosphoryl hydroxamic acids rearranged extremely rapidly in a basic milieu and could not be isolated. The rearrangement was also facilitated as the electron-releasing power of the substitute group on hydroxamic acid increased. [43] This intermediate underwent Lossen rearrangement to give the organophosphoric acid and isocynate. The isocynate group then reacted with the hydroxamic acid to yield the stable final product, O-alkylcarbamyl alkylhydroxamate.[40-42, 44, 45]

The rearrangement mechanism of diisopropylphosphoryl hydroxamic acid intermediate is summarized in Scheme 4-4. This mechanism also applies to the hydrolysis of methyl-paraoxon and ethyl-paraoxon by hydroxamic acid due to the similar chemical structures.

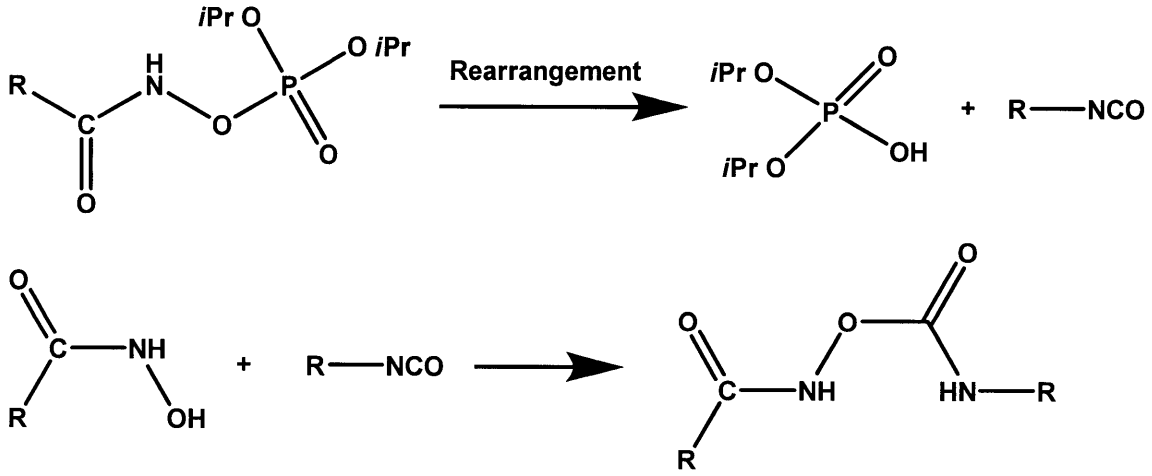

Scheme 4-4. Rearrangement mechanism of the phosphoryl hydroxamic acid

4.3.4 Organophosphate Decomposition by Hydroxamic Acid Modified Magnetic Nanoparticles

Hydroxamic acid modified magnetic particles were prepared through the procedure described in chapter 3 and they were much more effective against the hydrolysis of *p*-nitrophenyl acetate than amidoxime modified particles based on the same particle weight.

The particles were tested with regard to the hydrolysis of methyl-paraoxon and ethyl-paraoxon. As previously discussed, nucleophilic groups attack the *p*-nitrophenol groups and yield dimethyl- and diethyl phosphate. The reaction kinetics was followed by UV/Vis to measure the hydrolysis product, the *p*-nitrophenol ion, at the absorbance of 404nm. The nucleophilic substitution reaction is first order with respect to the organophosphate substrate and the nucleophiles. The overall hydrolysis reaction including the spontaneous hydrolysis and hydrolysis by hydroxyl ions is described in Equation 4-10.

$$r_{PNP} = \frac{d[PNP]}{dt} = k_{PNP}\left[NOH^-\right][OP] = \left(k_{spon} + k_{OH}\left[OH^-\right] + k_{cat}\left[NOH^-\right]\right)[OP] \qquad \textbf{Equation 4-10}$$

Since the substrates added into the system were at a concentration of 0.5mM and the effective concentration of hydroxamic acid groups added was 1mM, the concentration of nucleophiles remained roughly constant during the initial stage of the hydrolysis reaction. The solution pH was kept constant at 9 with 50mM Tris buffer and the first two terms remained constant over the whole hydrolysis process. Therefore, this equation was simplified into Equation 4-11 through the same procedure as that for the homogenous system.

$$-\ln\left(1 - \frac{[PNP]_t}{[OP]_0}\right) = k_{PNP}t \qquad \textbf{Equation 4-11}$$

in which the observed kinetic constant included both spontaneous hydrolysis and hydrolysis by added nucleophiles, as shown in Equation 4-12.

$$k_{PNP} = k_{spon} + k_{OH}\left[OH^-\right] + k_{cat}\left[NOH^-\right] \qquad \textbf{Equation 4-12}$$

The obtained concentration change of *p*-nitrophenol was then transformed according to Equation 4-11. The data points at various times were fitted with a linear function and the fitted slope was the observed kinetic constant for the nucleophilic hydrolysis. The hydrolysis reactions of methyl-paraoxon and ethyl-paraoxon by hydroxamic acid modified particles are shown in Figure 4-13 and Figure 4-14 respectively. The addition of hydroxamic acid modified particles increased the hydrolysis rate of both paraoxon.

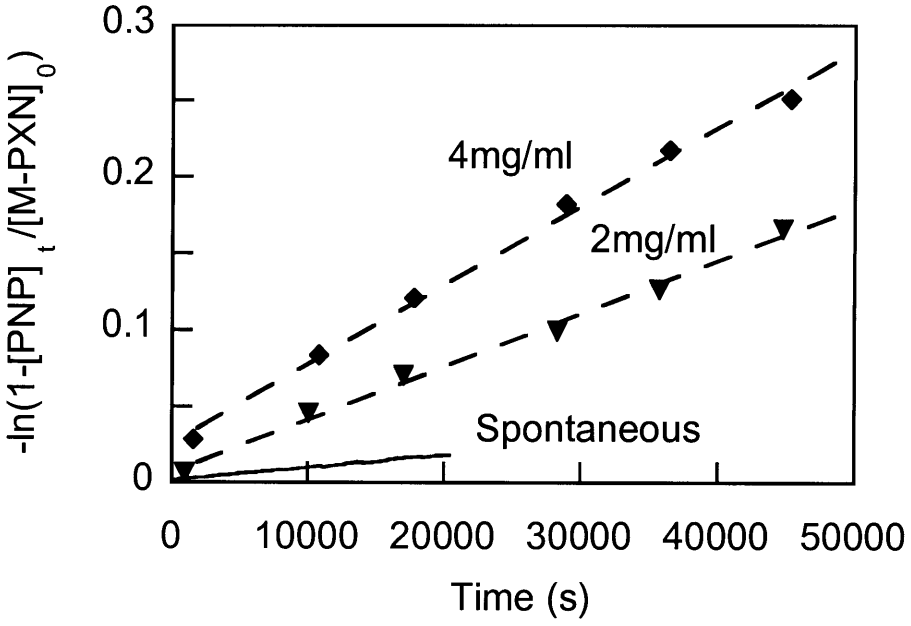

Figure 4-13. Pseudo-first order hydrolytic kinetics from spontaneous hydrolysis, and hydrolysis with 2mg/ml and 4mg/ml hydroxamic acid functionalized particles of methyl-paraoxon. Solution pH was kept at 9 with 50mM Tris buffer and 25°C. [Methyl-Paraoxon]$_0$ = 0.5mM.

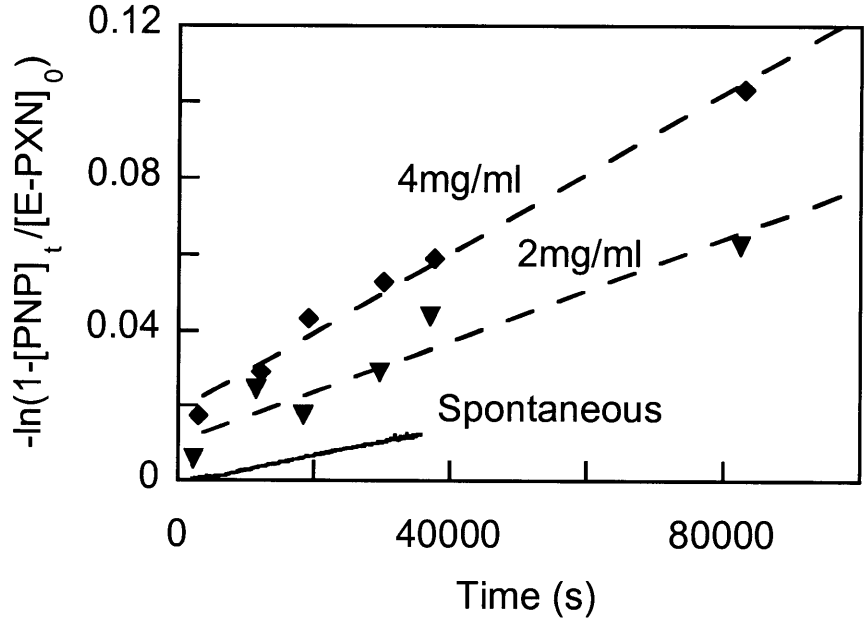

Figure 4-14. Pseudo-first order hydrolysis kinetics from spontaneous hydrolysis, and hydrolysis with 2mg/ml and 4mg/ml hydroxamic acid functionalized particles of ethyl-paraoxon. Solution pH was kept at 9 with 50mM Tris buffer and 25°C. [Ethyl-Paraoxon]$_0$ = 0.5mM.

The obtained kinetic constants were then plotted against the particle concentration. The results for the hydrolysis of methyl-paraoxon and ethyl-paraoxon are shown in Figure 4-15 and Figure 4-16 respectively.

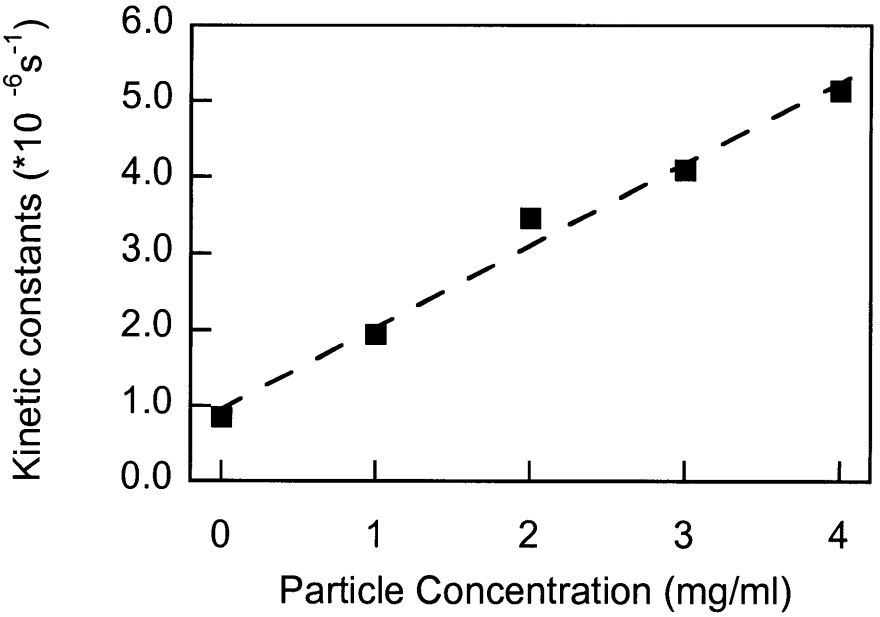

Figure 4-15. Dependence of observed hydrolytic kinetic constants of methyl-paraoxon on particle concentration. Slope of the linear fitting was second order kinetic constant: $k_{cat} = 1.1\times10^{-6}(mg/ml)^{-1}s^{-1}$

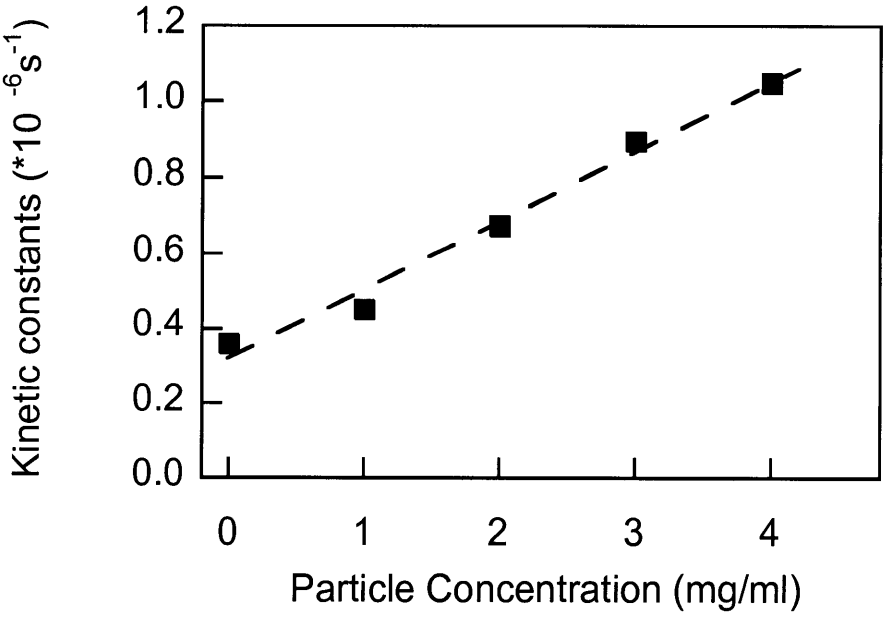

Figure 4-16. Dependence of observed hydrolytic kinetic constants of ethyl-paraoxon on particle concentration. Slope of the linear fitting was second order kinetic constant: $k_{cat} = 1.8\times10^{-7}(mg/ml)^{-1}s^{-1}$

The kinetic constants increased linearly with the increase in particle concentration, indicating that there were no inter-particle interactions to affect the hydrolytic capability of the hydroxamic groups on the particle surface.

The homogenous hydrolysis of methyl-paraoxon and ethyl-paraoxon accelerated by acetohydroxamic acid and polyhydroxamic acid was also measured with the UV/Vis technique. The kinetic constants for the OP hydrolysis were obtained through the same procedure as done previously with the modified particles. The second order kinetic constants of these nucleophiles are listed in Table 4-3 and Table 4-4 for methyl-paraoxon and ethyl-paraoxon respectively. These results showed that the monomeric acetohydroxamic acid was much more reactive toward OP hydrolysis than both the polyhydroxamic acid and the modified particles due to the steric hindrance from the polymer chains. 2mg/ml particle dispersion had similar kinetic constants as 1mM PHA against both substrates, consistent with the result from PNPA hydrolysis as well.

Nucleophiles	Second order kinetic constant
Acetohydroxamic acid (AHA)	$2.5\times10^{-5}mM^{-1}s^{-1}$
Polyhydroxamic acid (PHA)	$1.8\times10^{-6}mM^{-1}s^{-1}$
Hydroxamic acid modified particles	$1.1\times10^{-6}(mg/ml)^{-1}s^{-1}$

Table 4-3. Second order kinetic constants of hydrolysis of methyl-paraoxon by hydroxamic acid nucleophiles at pH 9

Nucleophiles	Second order kinetic constant
Acetohydroxamic acid (AHA)	$7.5\times10^{-6}mM^{-1}s^{-1}$
Polyhydroxamic acid (PHA)	$4.4\times10^{-7}mM^{-1}s^{-1}$
Hydroxamic acid modified particles	$1.8\times10^{-7}(mg/ml)^{-1}s^{-1}$

Table 4-4. Second order kinetic constants of hydrolysis of ethyl-paraoxon by hydroxamic acid nucleophiles at pH 9

The substrate structures also affect the hydrolysis enhancement significantly. Since the two ethyl groups provide greater steric hindrance toward the incoming nucleophiles than

do the methyl groups, paraoxon hydrolysis by nucleophiles was much slower than was methyl-paraoxon hydrolysis. The comparison between AHA and PHA has shown that the reactivity differences between these two nucleophiles are 3.5, 14, and 17 in the hydrolysis of *p*-nitrophenyl acetate, methyl-paraoxon, and ethyl-paraoxon respectively. This suggests that the steric hindrance from the substrate decreases the accessibility of the phosphorus center for the polymeric form more than that for the monomeric form.

4.3.5 Catalyst Recovery and Stability of Magnetic Nanoparticles

After the magnetic particles reacted with the first batch of OP substrates and were recovered by HGMS, they were readily washed out of the column with water. They were then used for the hydrolysis reaction of another batch of OP substrates. Unfortunately, no reaction acceleration was observed for the hydrolysis of either methyl-paraoxon or ethyl-paraoxon from the hydroxamic acid modified particles. This is due to the fact that the phosphoryl hydroxamic acid groups underwent Lossen rearrangement to form the stable alkylcarbamyl hydroxamate, and were not converted back to the original hydroxamic acid groups under the solution conditions. However, due to the presence of strong surface changes from sulfonic acid groups during the particle synthesis, the particles maintained the excellent colloidal stability even after the hydroxamic acid groups were consumed as a result of the decomposition.

It has been shown that the Lossen rearrangement would be reduced if the proton attached with the nitrogen atom in the hydroxamic acid groups was substituted with alkyl groups because of the lone electron pair of nitrogen would not be available for Lossen rearrangement. [46] However, this substitution would significantly reduce the nucleophilicity of the hydroxamic acid group and therefore its reactivity toward the hydrolysis of carboxyl and phosphorus esters due to the added steric hindrance. [47]

4.4 Conclusions

In this chapter, the spontaneous hydrolysis of OP substrates was studied first, including diisopropyl fluorophosphate, methyl-paraoxon and ethyl-paraoxon. It was found that the

substrates were attacked on the alkyl groups and the phosphorus atom to substitute the *p*-nitrophenol groups in the case of methyl- and ethyl-paraoxon. The attack on the phosphorus followed an associative mechanism and therefore a second order nucleophilic substitution, whereas the attack on the alkyl groups followed a dissociative mechanism and therefore a first order nucleophilic substitution. The DFP substrate was attacked only on the phosphorus through the second order nucleophilic substitution mechanism.

The OP hydrolysis was then investigated with the addition of α-nucleophiles in homogenous solutions, including 2-PAM and acetohydroxamic acid. The added nucleophiles only attacked the phosphorus atom to substitute the *p*-nitrophenol groups in methyl- and ethyl- paraoxon and the fluoride ions in DFP through second order nucleophilic substitution. In all three substrates, the hydrolysis products were the same as those from the spontaneous hydrolysis without detecting the presence of any intermediates, indicating unstable nature of the intermediates. The unstable phosphoryl 2-PAM underwent Beckman elimination to yield corresponding nitrile compound and therefore 2-PAM was consumed stoichiometrically during the OP hydrolysis. The turnover experiment also corresponded well with such a reaction mechanism. Phosphoryl hydroxamic acid underwent Lossen rearrangement and as a result the original hydroxamic acid groups lost their reactivity toward OP hydrolysis.

The hydroxamic acid modified particles prepared in chapter 3 were tested against the hydrolysis of methyl- and ethyl- paraoxon and have been shown to accelerate the hydrolysis. Similar to the PNPA hydrolysis, 2mg/ml particle dispersion had comparable observed kinetic constants with 1mM polyhydroxamic acid. The reactivity was much lower than monomer hydroxamic acid due to the steric hindrance from the polymer chains. The particles lost their reactivity after the reaction due to Lossen rearrangement of the phosphoryl hydroxamic acid, though the particles were still colloidally stable after the reaction due to the strong surface charge and resulted electrostatic interactions.

4.5 Bibliography

1. Chambers, J. E.; Levi, P. E., *Organophosphates: chemistry, fate, and effects*. Academic Press: San Diego, 1992; p xviii, 443 p.
2. Bajgar, J., Organophosphates/nerve agent poisoning: Mechanism of action, diagnosis, prophylaxis, and treatment. In *Advances In Clinical Chemistry, Vol. 38*, Elsevier Academic Press Inc: San Diego, 2004; Vol. 38, pp 151-216.
3. Ray, D. E., Chronic effects of low level exposure to anticholinesterases - a mechanistic review. *Toxicology Letters* **1998,** 103, 527-533.
4. Somani, S. M.; Romano, J. A., *Chemical Warfare Agents: Toxicity at Low Levels*. CRC Press: 2000; p 447.
5. Chen, L.; Bromberg, L.; Hatton, T. A.; Rutledge, G. C., Catalytic hydrolysis of p-nitrophenyl acetate by electrospun polyacrylamidoxime nanofibers. *Polymer* **2007,** 48, (16), 4675-4682.
6. Yatsimirsky, A. K., Metal ion catalysis in acyl and phosphoryl transfer: Transition states as ligands. *Coordination Chemistry Reviews* **2005,** 249, (17-18), 1997-2011.
7. Mancin, F.; Tecilla, P.; Tonellato, U., Metallomicelles made of Ni(II) and Zn(II) complexes of 2-pyridinealdoxime-based ligands as catalyst of the cleavage of carboxylic acid esters. *Langmuir* **2000,** 16, (1), 227-233.
8. Roa, A.; Goble, M. L.; Garcia, J. L.; Acebal, C.; Virden, R., Rapid burst kinetics in the hydrolysis of 4-nitrophenyl acetate by penicillin G acylase from Kluyvera citrophila. *Biochemical Journal* **1996,** 316, 409-412.
9. Bender, M. L.; Marshall, T. H., Elastase-catalyzed hydrolysis of p-nitrophenyl trimethylacetate. *J. Am. Chem. Soc.* **1968,** 90, (1), 201-207.
10. Ghosh, K. K.; Kolay, S.; Satnami, M. L.; Moore, S.; Palepu, R. M.; Dafonte, P. R., Kinetics of reaction of oximate alpha-nucleophiles with p-nitrophenyl acetate in alkyltriphenyl phosphonium bromide micelles. *Journal Of Dispersion Science And Technology* **2007,** 28, (2), 213-218.
11. Couderc, S.; Toullec, J., Catalysis of phosphate triester hydrolysis by micelles of hexadecyltrimethylammonium anti-pyruvaldehyde 1-oximate. *Langmuir* **2001,** 17, (13), 3819-3828.
12. Ghosh, K. K.; Sinha, D.; Satnami, M. L.; Dubey, D. K.; Shrivastava, A.; Palepu, R. M.; Dafonte, P. R., Enhanced nucleophilic reactivity of hydroxamate ions in some novel micellar systems for the cleavage of Parathion. *Journal Of Colloid And Interface Science* **2006,** 301, (2), 564-568.
13. Chanda, A.; Khetan, S. K.; Banerjee, D.; Ghosh, A.; Collins, T. J., Total degradation of fenitrothion and other organophosphorus pesticides by catalytic oxidation employing Fe-TAML peroxide activators. *Journal Of The American Chemical Society* **2006,** 128, (37), 12058-12059.
14. Balakrishnan, V. K.; Buncel, E.; Vanloon, G. W., Micellar catalyzed degradation of fenitrothion, an organophosphorus pesticide, in solution and soils. *Environmental Science & Technology* **2005,** 39, (15), 5824-5830.
15. Moss, R. A.; Kanamathareddy, S.; Vijayaraghavan, S., Kinetics of cleavage of paraoxon and parathion by cetyltrimethylammonium iodosobenzoate. *Langmuir* **2001,** 17, (20), 6108-6112.

16. Moss, R. A.; Kim, K. Y.; Swarup, S., Efficient Catalytic Cleavage Of Reactive Phosphates By An Ortho-Iodosobenzoate Functionalized Surfactant. *Journal Of The American Chemical Society* **1986,** 108, (4), 788-793.
17. Moss, R. A.; Alwis, K. W.; Shin, J. S., Catalytic Cleavage Of Active Phosphate And Ester Substrates By Iodoso-Benzoates And Iodoxybenzoates. *Journal Of The American Chemical Society* **1984,** 106, (9), 2651-2655.
18. Ge, Q. C.; Guo, Y. H.; Lin, H.; Gao, D. Z.; Lin, H. K.; Zhu, S. R., Role of trinuclear Zn(II) complexes in promoting the hydrolysis of 4-nitrophenyl acetate. *Canadian Journal Of Chemistry-Revue Canadienne De Chimie* **2004,** 82, (3), 409-417.
19. Balakrishnan, V. K.; Dust, J. M.; vanLoon, G. W.; Buncel, E., Mechanisms of abiotic degradation and soil-water interactions of pesticides and other hydrophobic organic compounds part 4 - Catalytic pathways in the ethanolysis of fenitrothion, an organophosphorothioate pesticide. A dichotomy in the behaviour of crown/cryptand cation complexing agents. *Canadian Journal Of Chemistry-Revue Canadienne De Chimie* **2001,** 79, (2), 157-173.
20. Balakrishnan, V. K.; Han, X. M.; Vanloon, G. W.; Dust, J. M.; Toullec, J.; Buncel, E., Acceleration of nucleophilic attack on an organophosphorothioate neurotoxin, fenitrothion, by reactive counterion cationic micelles. Regioselectivity as a probe of substrate orientation within the micelle. *Langmuir* **2004,** 20, (16), 6586-6593.
21. Lewis, V. E.; Donarski, W. J.; Wild, J. R.; Raushel, F. M., Mechanism And Stereochemical Course At Phosphorus Of The Reaction Catalyzed By A Bacterial Phosphotriesterase. *Biochemistry* **1988,** 27, (5), 1591-1597.
22. Aubert, S. D.; Li, Y. C.; Raushel, F. M., Mechanism for the hydrolysis of organophosphates by the bacterial phosphotriesterase. *Biochemistry* **2004,** 43, (19), 5707-5715.
23. Lai, K.; Stolowich, N. J.; Wild, J. R., Characterization Of P-S Bond Hydrolysis In Organophosphorothioate Pesticides By Organophosphorus Hydrolase. *Archives Of Biochemistry And Biophysics* **1995,** 318, (1), 59-64.
24. Greenhalgh, R.; Dhawan, K. L.; Weinberger, P., Hydrolysis Of Fenitrothion In Model And Natural Aquatic Systems. *Journal Of Agricultural And Food Chemistry* **1980,** 28, (1), 102-105.
25. Aqvist, J.; Kolmodin, K.; Florian, J.; Warshel, A., Mechanistic alternatives phosphate monoester hydrolysis: what conclusions can be drawn from available experimental data? *Chemistry & Biology* **1999,** 6, (3), R71-R80.
26. Maegley, K. A.; Admiraal, S. J.; Herschlag, D., Ras-catalyzed hydrolysis of GTP: A new perspective from model studies. *Proceedings Of The National Academy Of Sciences Of The United States Of America* **1996,** 93, (16), 8160-8166.
27. Admiraal, S. J.; Herschlag, D., Mapping The Transition-State For Atp Hydrolysis - Implications For Enzymatic Catalysis. *Chemistry & Biology* **1995,** 2, (11), 729-739.
28. Hengge, A. C.; Cleland, W. W., Direct Measurement Of Transition-State Bond-Cleavage In Hydrolysis Of Phosphate-Esters Of P-Nitrophenol. *Journal Of The American Chemical Society* **1990,** 112, (20), 7421-7422.
29. Zheng, F.; Zhan, C. G.; Ornstein, R. L., Theoretical studies of reaction pathways and energy barriers for alkaline hydrolysis of phosphotriesterase substrates paraoxon and related toxic phosphofluoridate nerve agents. *Journal Of The Chemical Society-Perkin Transactions 2* **2001**, (12), 2355-2363.

30. Lamb, J. C.; Steinberg, G. M.; Solomon, S.; Hackley, B. E., Reaction of 4-Formyl-1-methylpyridinium Iodide Oxime with Isopropyl Methylphosphonofluoridate. *Biochemistry* **1965,** 4, (11), 2475-2484.
31. Leader, H.; Vincze, A.; Manisterski, B.; Rothschild, N.; Dosoretz, C.; Ashani, Y., Characterization of O,O-diethylphosphoryl oximes as inhibitors of cholinesterases and substrates of phosphotriesterases. *Biochemical Pharmacology* **1999,** 58, (3), 503-515.
32. Luo, C. Y.; Saxena, A.; Smith, M.; Garcia, G.; Radic, Z.; Taylor, P.; Doctor, B. P., Phosphoryl oxime inhibition of acetylcholinesterase during grime reactivation is prevented by edrophonium. *Biochemistry* **1999,** 38, (31), 9937-9947.
33. Ashani, Y.; Bhattacharjee, A. K.; Leader, H.; Saxena, A.; Doctor, B. P., Inhibition of cholinesterases with cationic phosphonyl oximes highlights distinctive properties of the charged pyridine groups of quaternary oxime reactivators. *Biochemical Pharmacology* **2003,** 66, (2), 191-202.
34. VAN HOOIDONK, C.; Kraaij, G. W.; Ginjaar, L., ON REACTIVITY OF ORGANOPHOSPHORUS COMPOUNDS.4. ALKALINE HYDROLYSIS OF SOME O-PHOSPHYLATED 2-PYRIDINE OXIMES. *RECUEIL DES TRAVAUX CHIMIQUES DES PAYS-BAS* **1968,** 87, 673-686.
35. Fukuto, T. R.; Metcalf, R. L.; Jones, R. L.; Myers, R. O., Structure, reactivity, and biological activity of O-(diethyl phosphoryl)oximes and O-(methylcarbamoyl)oximes of substituted acetophenones and.alpha.-substituted benzaldehydes. *J. Agric. Food Chem.* **1969,** 17, (5), 923-930.
36. Blanch, J. H.; Andersen, J., Stability of N-heterocyclic oxime derivatives. Part IV. The kinetics of the sodium hydroxide-catalysed hydrolysis of phosphonylated ketoximes in water at 15, 20, 25, and 30°. *Journal Of The Chemical Society (B) - Physical Chemistry* **1968**, 169-173.
37. Blanch, J. H., Stability of N-heterocyclic oxime derivatives. Part V. Kinetics of the reaction of 2-hydroxyiminomethyl-1-methylpyridinium iodide and isopropyl methylphosphonofluoridate in water at 15, 25, and 35°C and at pH 5.7–7.7. *Journal Of The Chemical Society (B) - Physical Chemistry* **1969**, 1172-1178.
38. Kiderlen, D.; Eyer, P.; Worek, F., Formation and disposition of diethylphosphoryl-obidoxime, a potent anticholinesterase that is hydrolyzed by human paraoxonase (PON1). *Biochemical Pharmacology* **2005,** 69, (12), 1853-1867.
39. Stenzel, J.; Worek, F.; Eyer, P., Preparation and characterization of dialkylphosphoryl-obidoxime conjugates, potent anticholinesterase derivatives that are quickly hydrolyzed by human paraoxonase (PON1(192Q)). *Biochemical Pharmacology* **2007,** 74, (9), 1390-1400.
40. Hackley, B. E.; Plapinger, R.; Stolberg, M.; Wagner-Jauregg, T., Acceleration of the Hydrolysis of Organic Fluorophosphates and Fluorophosphonates with Hydroxamic Acids. *J. Am. Chem. Soc.* **1955,** 77, (13), 3651-3653.
41. Hurd, C. D.; Bauer, L., A Novel Rearrangement of Hydroxamic Acids Using Sulfonyl Chlorides. *J. Am. Chem. Soc.* **1954,** 76, (10), 2791-2792.
42. Samuel, D.; Silver, B. L., The Elucidation of the Reaction of Benzohydroxamic Acid with Benzenesulfonyl Chloride and with Diisopropyl Phosphofluoridate Using Oxygen-18 as Tracer. *J. Am. Chem. Soc.* **1963,** 85, (8), 1197-1198.
43. Bauer, L.; Exner, O., Chemistry Of Hydroxamic Acids And N-Hydroxyimides. *Angewandte Chemie-International Edition In English* **1974,** 13, (6), 376-384.

44. Swidler, R.; Steinberg, G. M., The Kinetics of the Reaction of Isopropyl Methylphosphonofluoridate (Sarin) with Benzohydroxamic Acid. *J. Am. Chem. Soc.* **1956,** 78, (15), 3594-3598.
45. Cadogan, J. I. G.; Eastlick, D. T.; Challis, J. A.; Cooper, A., Reactivity Of Organophosphorus Compounds.28. Fast, Neighboring Group-Induced Rearrangement During Alkaline-Hydrolysis Of "Alpha-Hydroxyimino-Para-Nitrobenzyl Phosphates, Phosphonates, And Phosphinates. *Journal Of The Chemical Society-Perkin Transactions 2* **1973**, (13), 1798-1804.
46. Salomon, C. J.; Breuer, E., Spontaneous lossen rearrangement of (phosphonoformyl)hydroxamates. The migratory aptitude of the phosphonyl group. *Journal Of Organic Chemistry* **1997,** 62, (12), 3858-3861.
47. Kunitake, T.; Horie, S., Multifunctional Hydrolytic Catalyzes.3. Catalytic Hydrolysis Of P-Nitrophenyl Acetate By Imidazole-4-Carbohydroxamic Acids. *Bulletin Of The Chemical Society Of Japan* **1975,** 48, (4), 1304-1309.

Chapter 5

Conclusions and Future Work

5.1 Research Summary

An economic strategy is required to decontaminate organophosphate compounds in large scale, including OP pesticides in groundwater system and chemical nerve agents on the battle field. Previous research in this area was focused mainly on homogeneous or micellar decomposition with addition of various kinds of nucleophiles to improve the reaction rate. However, these systems did not afford the recovery and reuse of the nucleophiles and therefore reduce the usage of active reactants and environmental footprint. To solve these problems, we proposed to use magnetic particles to carry nucleophiles and use the functional particles for such applications. Therefore, this research aims at developing functional magnetic particles, which are able to catalyze the decomposition reaction and which can be recycled and reused. In this research, strong α–nucleophilic groups are the focus since they are highly reactive toward the target substrates, relatively straightforward to prepare with simple off-the-shelf chemicals, and stable under a variety of environmental conditions, such as solution pH and presence of a large amount of organic compounds, etc.

Amidoxime modified magnetic particles were initially prepared by separating the particle synthesis and modification procedures. The original particles were synthesized by following the two-step procedure to obtain particles with average hydrodynamic diameter of around 80nm for effective capture by high gradient magnetic separation (HGMS). The precursor cyanoacetohydrazide was reacted with the free carboxyl groups on the particle surfaces through carbodiimide chemistry. The nitrile groups were then converted into target amidoxime groups. The attachment and conversion were confirmed by various analytical techniques. The modified particles had similar average hydrodynamic diameter as the original ones and were captured effectively by HGMS. They were stabilized by electrostatic interactions resulted from the strong surface charges. Particle stability and

morphology were not altered after the chemical modifications. Particles were tested against the hydrolysis of the model ester compound, *p*-nitrophenyl acetate. These amidoxime-modified particles accelerated the hydrolysis reaction and were easily recycled by HGMS without loss of reactivity. The particle system has shown higher reactivity compared with homogenous amidoxime systems based on the same concentration of functional groups, which was rationalized using pseudo-phase exchange model based on the similarity with micellar systems. This enhancement was attributed to the increased concentration of the substrate on the particle surface due to the presence of hydrophobic centers.

In order to improve the reactivity of the modified magnetic particles, stronger nucleophilic groups, hydroxamic acid, were attached on the surface. Unsaturated carboxylic acid was used as the second coating in the two-step procedure. The acrylamide monomers were copolymerized with the double bond from the second coating and these amide groups were then converted into the targeted hydroxamic acid groups. The modified magnetic particles had average diameter of 200nm due to the crosslinking during the copolymerization process. They were effectively captured by HGMS. Particles were colloidally stabilized by strong surface charge and resulting electrostatic interactions. After the modification procedure, the particle surface coverage with amide and hydroxamic acid groups was high. The modified particles were tested against PNPA hydrolysis. These particles significantly accelerated the hydrolysis reaction. They were five times more reactive than the amidoxime modified particles based on the same weight of materials. The acetylated particles were partially regenerated in basic solution, although 80% of their reactivity was lost due to the Lossen rearrangement of the acetylated hydroxamic acid groups.

Spontaneous hydrolysis of OP substrates, including diisopropyl fluorophosphate, methyl-paraoxon and ethyl-paraoxon, was found to mainly follow the second order nucleophilic substitution by hydroxyl ions. However, the paraoxon substrates could be also attacked on the alkyl groups through a first order dissociative mechanism. The added α-nucleophiles, such as 2-PAM and acetohydroxamic acid, only attacked the phosphorus

atom to substitute the *p*-nitrophenol groups in methyl- and ethyl- paraoxon and the fluoride ions in DFP through second order nucleophilic substitution. For reactions between all three substrates and both nucleophiles, the hydrolysis products were the same as those from the spontaneous hydrolysis with no detected intermediates, indicating the unstable nature of any intermediates that may be formed. The unstable phosphoryl 2-PAM underwent Beckman elimination to yield the corresponding nitrile compound, which has been corroborated by turnover experiments and FT-IR measurements. Phosphoryl hydroxamic acid underwent the Lossen rearrangement and the original hydroxamic acid groups lost their reactivity against OP hydrolysis. The hydroxamic acid modified particles were also tested against the hydrolysis of methyl- and ethyl- paraoxon and shown to accelerate the hydrolysis, though the acceleration was relatively modest. Similar to polyhydroxamic acid, the reactivity was much lower than that of monomeric hydroxamic acid due to the steric hindrance from the polymer chains. The particles lost their reactivity after the reaction due to Lossen rearrangement of the phosphoryl hydroxamic acid.

5.2 Experience Reflection

A variety of chemical pathways have been tested to attach iodosobenzoate groups on the particle surface in organic solvents. The groups were tested because they were reactive, really catalytic, and turned over against the hydrolysis of carboxyl and phosphate esters. However, these efforts all failed for the following reasons. First, the reaction scheme required multiples steps, including the attachment and following modification, and this resulted in very low yield and thus no noticeable catalytic capability. Secondly, some of the attempts required very harsh experimental conditions and the magnetite particles were not able to survive those conditions. Thirdly, since the reactions were carried out in the organic solvents and the particles need to be distributed into organic solvents first, particles formed large aggregates with the small surface areas and resulting low concentration of functional groups available for the modification. This probably contributed the most to the low modification efficiency.

Because of the intrinsic charged properties from the coating polymer to achieve the desired colloidal stability, the prepared particles were essentially not appropriate for the transformation reactions in organic solvents. However, many of the conversion reactions can only be carried out in organic solvents. This will pose serious challenges to attach those groups on the type of particles that we prepared.

5.3 Future Work

In this research, particular focus was on the attachment of functional groups on the surfaces of magnetic nanoparticles and two general strategies have been tested successfully. These strategies could be applied to attach other kinds of functional groups with similar chemical properties as these used in the tests. Future work could focus on two separate areas. One is the continuous improvement of the hydrolytic reactivity and turnover rate of the nucleophiles attached on the particle surfaces. The other is to use the above strategies to attach other functional groups or particles for high-value added applications.

5.3.1 Attachment of More Reactive Nucleophiles with High Turnover

The hydroxamic acid modified particles were fairly reactive against the hydrolysis of carboxyl and phosphate esters. However, particle reuse was problematic due to Lossen rearrangement. This reaction pathway could be suppressed by alkyl substitution on the hydroxamic acid nitrogen by using the methyl hydroxylamine hydrochloride as the reagent during the conversion step from amide groups to hydroxamic acid groups and ensure the acetylated and phosphorylated hydroxamic acid groups only follow the hydrolysis pathway for full recovery and reuse. The imidazole groups could also be incorporated into the copolymer chains on the particle surface to form a charge relay system with the hydroxamic acid groups and therefore increase overall catalytic efficiency. [1, 2] Because of crosslinking caused during the copolymerization step in preparing hydroxamic acid groups, the original particles could be smaller in size to reduce the final particle size and therefore increase the functional group density on the surface to increase accessibility.

Another major group of important candidates for the OP decomposition are organophosphate hydrolysis enzymes. They have shown very active hydrolytic reactivity and great turnover rate. [3-5] Due to the limited amount produced and intrinsic instability of the enzyme, they were not widely used for such applications. Even though there have been attempts to immobilize enzymes on solid surfaces through chemical attachment and layer-by-layer techniques, the enzymes were confined to be inside the solid support and there were significant mass transfer resistances. These enzymes could be attached to the surfaces of the magnetic particles through the same chemistry as that used in the amidoxime modification. As a result, the enzymes will be located on the particle surfaces and mass transfer resistances eliminated. The immobilization also increases enzyme stability and makes it more suitable for the applications even though there will be a certain degree of activity loss.

Mimic hydrolases are not only important to reveal hydrolytic reaction mechanisms of enzymes, but they are also potentially applicable for highly efficient and selective hydrolysis of carboxyl esters and phosphoric esters. [6, 7] Hydroxamic acid derivatives containing benzo-15-crown-5 and their copper(II), zinc(II), cobalt(II) and manganese(II) complexes have been prepared and tested against the hydrolysis of bis(4-nitrophenyl)phosphate (BNPP). A more than 200,000-fold improvement in hydrolysis rate relative to that observed for against spontaneous reaction has been shown. [8] The metal ion is proposed to activate the phosphate group and a nucleophilic H_2O molecule and stabilize the pentacoordinate phosphorus transition state by cooperative action in metalloenzymes. Such nucleophiles have similar structures as the simpler groups and very much higher reactivity. These mimic enzymes combine the stability of small nucleophilic molecules and strong reactivity of enzymes and they will be ideal candidates for such applications. However, the complex structures of these functional groups make their attachment to particle surfaces challenging, especially with the need to maintain colloidal stability in the presence of the positive charge from the metalloenzymes.

5.3.2 Attachment of Functional Groups or Nanoparticles for High Value-Added Applications

In addition to the application in decomposing OP substrates, the proved strategies could also be used to attach other functional groups for high value added applications. For example, targeting ligands attached to the particles can bind specifically with receptors on targeted cell surfaces and therefore be used to aid in the separation of these cells. The same strategy can be used to attach specific antigens to separate target antibodies based on affinity interactions. These functional magnetic particles can be recycled and reused. Highly expensive and important biological growth factors can also be attached to the particle surfaces to promote target reactions and then easily separated out from the reaction medium for reuse. [9, 10] This can significantly reduce the factor usage and operational cost.

5.4 Bibliography

1. Kunitake, T.; Okahata, Y., Multifunctional Hydrolytic Catalyzes.4. Catalytic Hydrolysis Of Para-Nitrophenyl Acetate By Copolymers Containing Complementary Functional Groups (Hydroxamate And Imidazole). *Macromolecules* **1976,** 9, (1), 15-22.
2. Kunitake, T.; Okahata, Y., Multifunctional Hydrolytic Catalysis.2. Hydrolysis Of Para-Nitrophenyl Acetate By A Polymer Catalyst Which Contains Hydroxamate And Imidazole Functions. *Bioorganic Chemistry* **1975,** 4, (2), 136-148.
3. Lai, K.; Stolowich, N. J.; Wild, J. R., Characterization Of P-S Bond Hydrolysis In Organophosphorothioate Pesticides By Organophosphorus Hydrolase. *Archives Of Biochemistry And Biophysics* **1995,** 318, (1), 59-64.
4. Tago, K.; Yonezawa, S.; Ohkouchi, T.; Hashimoto, M.; Hayatsu, M., Purification and characterization of fenitrothion hydrolase from Burkholderia sp NF100. *Journal Of Bioscience And Bioengineering* **2006,** 101, (1), 80-82.
5. Smith, B. M., Catalytic methods for the destruction of chemical warfare agents under ambient conditions. *Chemical Society Reviews* **2008,** 37, (3), 470-478.
6. Hettich, R.; Schneider, H. J., Cobalt(III) polyamine complexes as catalysts for the hydrolysis of phosphate esters and of DNA. A measurable 10 million-fold rate increase. *Journal Of The American Chemical Society* **1997,** 119, (24), 5638-5647.
7. Kimura, E.; Kodama, Y.; Koike, T.; Shiro, M., Phosphodiester Hydrolysis By A New Zinc(Ii) Macrocyclic Tetraamine Complex With An Alcohol Pendant - Elucidation Of The Roles Of Ser-102 And Zinc(Ii) In Alkaline-Phosphatase. *Journal Of The American Chemical Society* **1995,** 117, (32), 8304-8311.
8. Li, J. Z.; Li, H. B.; Zhou, B. Z.; Zeng, W.; Qin, S. Y.; Li, S. X.; Xie, J. Q., Studies on the reaction kinetics and the mechanism of hydrolysis of bis(4-nitrophenyl)phosphate

(BNPP) by hydroxamic acid complexes containing benzo-15-crown-5. *Transition Metal Chemistry* **2005,** 30, (3), 278-284.
9. Horak, D.; Babic, M.; Mackova, H.; Benes, M. J., Preparation and properties of magnetic nano- and microsized particles for biological and environmental separations. *Journal Of Separation Science* **2007,** 30, (11), 1751-1772.
10. Gupta, A. K.; Gupta, M., Synthesis and surface engineering of iron oxide nanoparticles for biomedical applications. *Biomaterials* **2005,** 26, (18), 3995-4021.